DANMARKS OG GRØNLANDS GEOLOGISKE UNDERSØGELSE RAPPORT 2002/14

Study of Jurassic reservoir quality and diagenesis in the Danish Central Graben, Licenses 4/98, 5/98 and 6/98

Jens Therkelsen, Jan Andsbjerg
and Palle Rubæk Andersen

GEOLOGICAL SURVEY OF DENMARK AND GREENLAND
MINISTRY OF ENVIRONMENT

GEUS

DANMARKS OG GRØNLANDS GEOLOGISKE UNDERSØGELSE RAPPORT 2002/14

Study of Jurassic reservoir quality and diagenesis in the Danish Central Graben, Licenses 4/98, 5/98 and 6/98

Jens Therkelsen, Jan Andsbjerg
and Palle Rubæk Andersen

Released 19.06.2009

GEOLOGICAL SURVEY OF DENMARK AND GREENLAND
MINISTRY OF THE ENVIRONMENT

GEUS

Summary

The sandstones of the Heno Formation occur in the eastern part of the Danish sector of the North Sea Central Graben. The formation consists of back-barrier to lower shoreface deposits.
Cores from the Heno Formation, retrieved from the wells Gert-1, Gert-2, Jeppe-1, Gwen-2, Diamant-1, Ravn-1 and Ravn-2 have been examined in this study.
The Heno Formation, which reach a maximum thickness of c. 160 m in the Gert-1 well, is subdivided into a lower Gert Member (Basal sandstone Unit) and an upper Ravn Member (Heno Formation). Gert Member is cored in the wells Gert-1, Gert-2 and Diamant-1 and Ravn Member in Jeppe-1, Gwen-2, Diamant-1, Ravn-1 and Ravn-2.
The present depth of the Heno Formation differs greatly from well to well. The shallowest burial depth of base Heno Formation is recorded in Diamant-1 (*c*. 3825 m b. msl) and the deepest in Jeppe-1 (*c*. 5000 m b.msl).
The diagenetic main mineral phases, which have an impact on reservoir quality are quartz and carbonate cement and to a lesser extend kaolinite and pyrite. Baryte occur in large amounts in micro-faults and fractures in the Ravn-2 well. Where detrital clay occurs, this is generally Illitized, resulting greatly in reduction of permeability. Secondary porosity is very common and is often a significant contributor to porosity development.
It is believed that only insignificant quartz cement derives from intra-formational sources, and where quartz cement is abundant most silica has been imported into the sandstones from an external source. The wells containing abundant quartz cement are situated relatively close to major faults, which may have acted as substantial fluid conduits, and the fluids are suggested to have been transported via major faults and fractures associated with these.
The majority of carbonate cement occurs in horizons in the shallow marine sandstones, and is related to an early stage of diagenesis. The source for the carbonate cement is local, usually in form of biogenic carbonate. A late stage carbonate cement which occur patchy, has only insignificant influence on permeability. It may derive from internal sources or be a product of fluids flowing along major faults analogue to quartz cement.
Dissolution of predominantly feldspar grains has occurred relatively late in the burial history. In some wells grain dissolution significantly enhances porosity with values up to 13,6% modal volume. The secondary porosity is preserved because pre-developed cement and present-day overpressure in the sandstones support the grain framework and prevents it from collapsing.

Introduction

The overall aim of this project is to evaluate the diagenetic evolution in the sandstones of the Heno Formation in an array of selected wells and to see what impact it makes on the reservoir quality of the sandstones.
In all 236 thin sections constitute the basis for the study. All thin sections were provided from former projects undertaken by Palle Rubæk Andersen at GEUS.
The diagenetic main mineral phases have been tied to the processes and factors, believed to be responsible for their development.
Results presented in tables, figures and microphotographs are found in Appendix 1–3.
Fluid inclusion data have been used (Johannes fabricius, unpublished data), which have been recorded from the wells Gert-1, Ravn-1 and Ravn-2. The inclusions occur in quartz, calcite and baryte cement. However, the literature show that fluid inclusion data may be misleading, especially when they are recorded from carbonate and sulphate minerals such as calcite and baryte (for overview see Emery and Robinson, 1993). Most data will however be presented, as it is believed that they are reliable.

Geological setting

The Middle Jurassic-Upper Jurassic succession in the Danish Central Graben is separated from Lower Jurassic and pre-Jurassic successions by an unconformity formed as a result of Toarcian – Aalenian regional uplift. After the uplift sedimentation resumed in the Danish part of the Central Graben during the Middle Jurassic, with deposition of the sandstone-dominated Bryne and Lulu Formations and the Middle Graben Shale Formation (Michelsen et al., in press). The first marine transgression in the Danish Central Graben occurred during the Callovian-Oxfordian, probably reflecting the onset of domal collapse combined with eustatic sea-level.

During Late Jurassic time the Feda Graben, Heno Plateau and Gertrud Graben became actively subsiding depositional basins, and the depositional area was later extended to the Outer Rough and Ål Basins (Fig. 1). Basin development in the Central Graben was, in addition to the influence of rift tectonics, also strongly influenced by the presence of mobile Zechstein salt. Salt movements had a profound influence on the development of depocentres in the Søgne Basin, Tail End Graben and the Salt Dome Province.

The depositional area began to expand in the late Middle Jurassic as a result of a regional sea-level rise. Accelerating half-graben subsidence during the Callovian – Early Kimmeridgian enhanced the sea-level rise. Several periods of rapid subsidence during the Callovian – Volgian (mainly in the Oxfordian – Early Kimmeridgian and latest Kimmeridgian – Middle Volgian) gave accommodation space to more than four kilometres of marine mud. A break in subsidence in the Late Kimmeridgian, probably related to a change of fault directions, resulted in deposition of shallow marine sandstones on platforms and hanging-wall slopes. The thickest succession of Middle Jurassic deposits occur in the Søgne Basin and the Tail End Graben, along the main boundary fault at the western margin of the Ringkøbing–Fyn High. A thin Middle Jurassic succession occurs across a wider area in the southern and south-eastern part of the Danish Central Graben. Progressively younger Upper Jurassic deposits are found updip on the western hanging-wall slope of the Danish Central Graben.

Rift-related subsidence ceased or slowed down significantly for a period in Late Kimmeridgian time, possibly in relation to a shift in activity from north-south trending to north-west – south-east trending faults (Johannessen et al., 1996; Møller and Rasmussen, in press). The cessation of rift-related subsidence and the associated decrease in accommodation space generation, and possibly an increase in sediment supply, caused the progradation of shallow marine sands of the Late Kimmeridgian Heno Formation in the north-western parts of the Danish Central Graben. Sands that were sourced from the Mid North Sea High prograded towards the east on the Heno Plateau, while sands sourced from the Mandal High prograded towards the west on the Gertrud Plateau and in the Feda Graben (Johannessen et al., 1996).

In the southern part of the Feda Graben, syn-depositional subsidence balanced by a large sediment supply caused the development of an up to 90 m thick succession of aggradational back-barrier sandstones (Andsbjerg and Dybkjær, in press; Johannessen et al., 1996). The back-barrier sandstones are interbedded with mudstones; strong bioturbation and abundant water-escape structures have destroyed primary sedimentary structures. Thin coals and abundant rootlets also occur. The sediments are typically arranged in 3 – 8

metres thick upward coarsening to upward fining units. The backbarrier sandstones are separated from an overlying shoreface succession by a ravinement surface.

On the Heno Plateau, which formed a part of the hanging-wall slope of the Danish Central Graben, a coarsening- to fining upward succession of mainly very fine- to fine-grained sandstones was deposited. The succession is in places more than 100 metres thick and contains one or two distinct pebble conglomerate beds. The sandstones, which normally are completely bioturbated, occur as 2 – 8 metres thick upward coarsening units that were deposited on the lower to middle shoreface. The conglomerate beds represent fluvial gravels that were formed during a fall in sea level and later reworked during a subsequent sea level rise. They thus represent amalgamated sequence boundaries/ravinement surfaces.

In the Danish Central Graben rates of subsidence increased dramatically to a maximum in latest Kimmeridgian – Middle Volgian times (Andsbjerg, 1997; Andsbjerg and Dybkjær, in press; Møller, 1986).

In the Danish Central Graben transgression to the west and southwest of the hanging wall slope continued. A more than 3000 metres thick, strongly asymmetric wedge of marine mudstones of the Farsund Formation was deposited reflecting an average rate of subsidence of approximately 300 m/my centrally in the basin (Britze et al., 1995c; Møller, 1986). Organic-rich shales are associated with the latest Kimmeridgian – Early Volgian maximum flooding surfaces on the western ramp of the Danish Central Graben. These shales probably reflect an updip trapping of clastic sediments and a high rate of organic production in the relatively shallow, nutrition-rich water on the ramp following transgression of the Late Kimmeridgian coastal plain. A wedge of shallow marine sands further updip on the hanging-wall slope in the Outer Rough Basin in the westernmost part of the Danish Central Graben, prograded during the Early to Middle Volgian (Damtoft et al., 1992; Mackertich, 1996).

In Late Volgian – Ryazanian time, the Danish Central Graben broke up into smaller subbasins. Cessation of movements along segments of the eastern boundary fault allowed drainage of new sediment source areas. Turbidite sands and other gravity flow deposits occur both in fans along the eastern boundary fault of the basin and centrally on the basin floor (Damtoft et al., 1992). Intermittent transgressive phases during the otherwise regressive trend caused the deposition of another organic rich shale, the widespread Bo Member (the former ‘hot unit’ equivalent to the most organic rich part of the Mandal Formation; Dybkjær, 1998; Michelsen et al., in press), which is the most important source rock in the Danish Central Graben (Ineson et al., in press).

Late Jurassic rift-related subsidence had created accommodation for nearly 4000 metres of sediment in the deepest parts of the basin (Britze et al., 1995c; Møller, 1986). During the Early Cretaceous the rate of subsidence decreased markedly. Block faulting gradually ceased from the Hauterivian and onwards and gave way to regional subsidence, interrupted by periods of inversion. The resulting thickness of Lower Cretaceous deposits only locally exceeds 800 metres, and in large tracts of the Danish Central Graben the thickness is between 200 and 600 metres (Britze et al., 1995b; Vejbæk, 1986). Relatively slow regional subsidence continued throughout the Late Cretaceous with significant structural inversion influencing the shaping of the depositional basin. The main Upper Cretaceous depocentres are located in three subparallel basins separated by inversion ridges. The maximum thickness of the Chalk Group (Upper Cretaceous plus Danian) is 1500 metres (Britze et al., 1995a). Rates of subsidence began to increase gradually during the Paleo-

gene with high rates of subsidence characterising the Oligocene and the Neogene, when the present day North Sea Basin was shaped. More than 3000 metres thick post-Chalk deposits are mapped in the Danish Central Graben.

Material and methods

From the seven studied wells 236 thin sections, prepared from samples taken from the sandstones of the Heno Formation, have been examined on a conventional polarising light microscope. A subjective estimation of the content of quartz and carbonate cement, clay and distribution of macro-porosity has been performed in all examined thin sections (Tables 1A–G and Fig. 2). Of these 31 thin sections have been point counted and detailed description have been performed (additionally 4 samples were described but not point counted). In each thin section 250 points were recorded. Point counting data can be found in Table 2 and thin section descriptions in Appendix 1. Rock chips from 6 samples (two from Gert-1 and Diamant-1, one from Gert-2 and Ravn-1) were analysed using a scanning electron microscope.

The amount of examined samples for each well is as follows:

In the **Gert-1** well 46 samples have been examined (all back-barrier facies), all taken from the Gert Member. Of these 6 thin sections were point counted and described. The samples are from the depth interval 4920,03 m/ 16141'10''– 4973,24 m/ 16316'5''.

In the **Gert-2** well 14 samples have been examined (3 from Gert Member, 8 from Ravn Member and 2 from the underlying Carboniferous). Of the samples from the Gert Member 1 thin section has been point counted and 2 thin sections described (upper shoreface and back-barrier facies), whereas 1 sample from the Ravn Member has been point counted and described (middle shoreface facies). The 2 samples from the Carboniferous have also been described. The samples are from the depth interval 4817,67 m/ 15806'– 4891,68 m/ 16048'10'.

In the **Jeppe-1** well 25 thin sections have been examined, all taken from the Ravn Member. Of these 6 thin sections were point counted and described (5 from middle shoreface and 1 from lower shoreface facies). The samples are from the depth interval 4939,28 m/ 16205'– 4991,02 m/ 16374'9''.

In the **Gwen-2** well 17 thin sections have been examined, all taken from the Ravn Member. Of these 4 thin sections were point counted and 5 were described (4 from middle–upper shoreface and 1 from lower shoreface facies). The samples are from the depth interval 4237,30 m/ 13901'11''– 4292,73 m/ 14083'9''.

In the **Diamant-1** well 33 samples have been examined (23 Gert Member and 21 from Ravn Member). Of these 5 thin sections have been point counted and described, represented by 2 samples from Gert Member (back-barrier facies) and 3 from Ravn Member (upper shoreface facies). The samples are from the depth interval 3828,05 m/ 12559'3''– 3845,75 m/ 12617'3''.

In the **Ravn-1** well 40 samples have been examined, all taken from the Ravn Member. Of these 6 thin sections were point counted and described (one from lower shoreface and 5 from middle shoreface facies). The samples are from the depth interval 4090,09 m/ 13418'11''– 4152,76 m/ 13624'6''.

In the **Ravn-2** well 33 samples (all from lower shoreface facies) have been examined, all taken from the Ravn Member. Of these 2 thin sections were point counted and described. The samples are from the depth interval 4259,14 m/ 13973'7''– 4279,60 m/ 14040'8''.

Sandstone petrography

Gert-1

Framework grains

The sandstones from the Gert-1 well are quartzarenites (Folk, 1968) (Fig. 3A). However, adjusting for observed dissolution of feldspars in the sandstones, four samples are classified as subarkoses, one as arkose and one remains quartzarenite (Fig. 3B).
Grain size range between fine to medium sand with most samples being fine-grained and grain form varies between subangular to rounded. The sandstones are very well to well sorted (see Table 2).
The framework grains consist of quartz with minor amounts of feldspar (both plagioclase and K-feldspar), minor rock fragments, mica and traces of heavy minerals. Detrital clay matrix is generally rare, but is varying from absent to abundant.
The amount of detrital **quartz** ranges from 47–73% with an average of 62%, but the outline of the original detrital grains is difficult to estimate due to the lack of grain lining clay particles (dust rims) and fluid inclusions in the overgrowths. The majority of the detrital quartz grains are monocrystalline. Polycrystalline grains probably have a metamorphic source. The grains show both uniform and undulose extinction. Contact dissolution/pressure solution textures (irregular grain line contacts) between adjacent quartz grains are seen, however no severe dissolution seems to have occurred. Contacts between quartz and mica have resulted in bending or breaking of the mica and also conformable and straight contacts occur. The later is interpreted as a result of quartz dissolution (cf. Bjørkum, 1996).
Feldspars make up 0–2% (average 0.9%) of the sandstones and consist mainly of K-feldspar. Most observed feldspar grains are totally dissolved; the main contributor of secondary porosity. However, some grains are only weakly effected by dissolution and these occur very immature (Plate 2), showing that they have not experienced long transportation. In a few samples some feldspars seem to have been replaced by kaolinite. Former and present feldspar grains are characterised by having an enclosing clay rim (Plate 1–10).
The sandstones contain 0–1.6% (average 0.7%) **rock fragments**, mainly mudstone clasts and more rarely metamorphic schistose quartz, magmatic grains and chert. The mudstone clasts are in general markedly deformed due to compaction and they occur illitized.
Mica constitutes 0–1.2% (average 0.3%) of the sandstone and is represented exclusively by muscovite. The muscovite often appears bent around quartz grains due to compaction, and is often partially altered to illite.
Heavy minerals such as zircon and rutile are only present in traces. Generally the grains are rounded to well rounded.
Organic matter make up 0–4.8% (average 1.4%) of the sandstones and occur as scattered debris. It is often associated with authigenic pyrite.

Bioclasts are not found in the thin sections.

Diagenetic mineralogy

Authigenic **quartz** ranges from 1.6–22.8% (average 13.9%) of the bulk sample volume. It is ubiquitous in the sandstones except in samples, which have experienced early and total carbonate cementation. Dust rims delimiting the detrital and authigenic quartz are rare, so the overgrowths are distinguished from the detrital grains either by their inclusion-free appearance or the discrete euhedral or syntaxial crystal habit. In some cases quartz overgrowths partially enclose kaolinite and illite crystals, indicating that the formation was synchronous with, or subsequent to formation of kaolinite and illite. Authigenic quartz grows around detrital feldspar grains, which later have been partly dissolved (Plate 5 & 6). Quartz also grows into secondary pore spaces. The overgrowths can be large (up to 400 µm) and develop pyramidal crystal forms. Total occlusion of porosity on a small scale occurs when overgrowths project out from detrital grains into the pores and create interlocking crystal boundaries (Plate 9).

Carbonate cement (0–3.2%, average 1.4%) consists of calcite and dolomite where calcite is the dominating part. The dolomite is commonly growing as a later cement on the surfaces of the calcite crystals. The carbonate cement occur as patchy pore-space filling cement consisting of large rhombic crystals of calcite or patchy, poikilotopic calcite cement. The latter may partly be displacive and therefore an early cement. The carbonate cement fills secondary porosity and partly replaces feldspars. It sometimes surrounds euhedral quartz overgrowths. Illite is also overgrown by carbonate cement.

Kaolinite (0–6.4%, average 1.8%) generally occurs as clustering booklets in primary and secondary pore spaces. The booklets are made up of individual thin pseudohexagonal, euhedral plates, *c.* 10–30 µm across. The clusters of small booklets are often gathered in secondary pores resulting from dissolved feldspar. Kaolinite in primary pore spaces occur overgrown by quartz.

Illite (0-3.2%, average 1.8%) is present in almost all examined samples and occur as dark coloured clay rims on the surfaces of present or former feldspars (Plate 1–10). In the SEM, illitic clay rims generally occurs as a network of tangled threads or dense amorphous crystals (Plate 71–74). The dark colour of the illitic clay rims is resulting from migrating hydrocarbons.

Baryte (0–1.2%, average 0.3%) occur as a scattered and commonly pore occluding cement, which post-dates quartz cement.

Albite (0–0.4%, average <0.1%) is only found in one sample and here in secondary pores in association with feldspar remnants.

Pyrite (0–3.2%, average 1.5%) occur scattered in pore spaces and is commonly associated with organic matter. Pyrite was developed at a very early stage.

Porosity

Total porosity ranges 1.2–18.4% (average 8.9%) and is dominated by secondary porosity, which ranges 0.8–12% (average 5.7%). The secondary porosity is exclusively related to feldspar dissolution.

Gert-2

Framework grains

The sandstones from the Gert-2 well are quartzarenites also when adjusted for observed dissolution of feldspars (Folk, 1968) (Fig. 3A and 3B).
Grain size range between very fine to fine sand and grain form varies between subrounded to rounded. The sandstones are well to moderately sorted (see Table 2).
The framework grains consist of quartz with minor amounts of feldspar (both plagioclase and K-feldspar), minor rock fragments, and traces of mica and heavy minerals. The amount of detrital clay matrix is varying from absent to abundant.
The amount of detrital **quartz** ranges from 63–64%. As for the sandstones in Gert-1 the outline of the original detrital grains is difficult to estimate due to the lack of grain lining clay particles (dust-rims) and fluid inclusions in the overgrowths. The majority of the detrital quartz grains are monocrystalline and polycrystalline grains probably have a metamorphic source. The grains show both uniform and undulose extinction. Contact dissolution/pressure solution textures (irregular grain line contacts) between adjacent quartz grains are in some of the more clay-rich sandstones common (Plate 16). Contacts between quartz and mica have resulted in bending of the mica and also conformable and straight contacts resulting from quartz dissolution occur.
Feldspars have not been recorded in point counting but occur in the sandstones. Most observed feldspar grains are totally dissolved.
The sandstones contain 0.6–1.2% (average 0.9%) **rock fragments**, consisting of mudstone clasts, chert, metamorphic schistose quartz and magmatic grains. The mudstone clasts are in general markedly deformed due to compaction and occur illitized.
Mica is absent or occur as traces in the sandstone and is represented exclusively by muscovite. However, micaceous lamina occurs in a single sample.
Heavy minerals such as zircon and rutile are only present in traces.
Organic matter make up 0–0.8% (average 0.4%) of the sandstones and occur as scattered fine debris and large fragments of woody tissue. It is in general associated with authigenic pyrite, which totally fill out the spaces in the woody tissue fragments.
Traces of **bioclasts** in the form of shell fragments are found in some thin sections.

Diagenetic mineralogy

Authigenic **quartz** ranges from 5.2–17.2% (average 11.2%) of the bulk sample volume. It is the dominating cement in the sandstones except in samples, which have experienced early and total carbonate cementation and where detrital clay is abundant (Plate 13). Dust rims delimiting the detrital and authigenic quartz are rare, so the overgrowths are distinguished from the detrital grains either by their inclusion-free appearance or the discrete euhedral or syntaxial crystal habit. Authigenic quartz grows around detrital feldspar grains, which later have been partly dissolved. Quartz also grows into secondary pore spaces (Plate 14).
Carbonate cement (0–3.6%, average 1.8%) consists of calcite and siderite where calcite is the dominating part. The carbonate cement occur as patchy pore-space filling cement

consisting of large rhombic crystals of calcite or patchy, poikilotopic calcite cement. The latter may partly be displacive and therefore an early cement. Siderite occur as small single rhombs in pore spaces. The carbonate cement fills secondary porosity and sometimes surrounds euhedral quartz overgrowths.

Kaolinite only occur in a few samples as very sporadic clustering booklets in secondary pore spaces resulting from dissolved feldspar. The booklets are made up of individual thin pseudohexagonal, euhedral plates, *c.* 10–30 µm across.

Illite occur as flaky illitized smectitic detrital clay and as delicate spheres and worm-like crystals (Plate 75 & 76). Illite is present in almost all examined samples and is often dark coloured, resulting from migrating hydrocarbons.

Baryte (0–1.6%, average 0.8%) occur as a scattered and commonly pore occluding cement, which post-dates quartz cement (Plate 14).

Pyrite (1.2–26.4%, average 13.8%) occur scattered in pore spaces and is in one sample the dominating cement (Plate 17 & 18). It is commonly associated with organic matter. Pyrite was developed at a very early stage.

Porosity

Total porosity ranges 3.2–5.6% (average 4.4%) and is dominated by primary porosity, which ranges 2.4–3.6% (average 3.0%). The secondary porosity is related to feldspar dissolution.

Jeppe-1

Framework grains

The sandstones from the Jeppe-1 well plot as sublitharenites, Feldspathic litharenites and lithic arkoses (Folk, 1968) (Fig. 3A). When adjusting for observed dissolution of feldspars in the sandstones they are equally divided into Feldspathic litharenites and lithic arkoses (Fig. 3B).

All samples are fine-grained sand except for one where grain size is very fine sand. Grain form varies between angular to rounded and the sandstones are very well to poorly sorted (see Table 2).

The framework grains consist of quartz together with a relatively high amount of feldspar (K-feldspar and subordinate plagioclase), and rock fragments. Mica and detrital clay matrix occurs in minor amount. Heavy minerals, organic matter, bioclasts and glauconitic grains occur in traces.

Quartz (ranging from 40–60% with an average of 47%) is the dominant detrital phase, with a majority of monocrystalline grains. Polycrystalline grains probably have a metamorphic source. The grains show both uniform and undulose extinction. Contact dissolution/pressure solution textures (sutured, long and concavo-convex line contacts) between adjacent quartz grains occurs (Plate 25 & 26). Where quartz and mica are in contact, dissolution may have occurred resulting in conformable and straight contacts.

Feldspars make up 5.6–20% (average 11.6%) of the sandstones and consist mainly of K-feldspar. The feldspar grains occur unaffected to totally dissolved. It is common that the feldspar grains occur with reminiscences of overgrowths, which are now dissolved (Plate 28).
The sandstones contain 7.6–18.8% (average 11.5%) **rock fragments**. These consist mainly of mudstone clasts, metamorphic schistose quartz, magmatic grains and minor chert. The mudstone clasts occur illitized.
Mica constitutes 0–2.8% (average 0.7%) of the sandstone and is represented exclusively by muscovite. Muscovite found outside concretions, occur bent around quartz grains due to compaction. The mica flakes are mostly partially altered and appears swollen.
Heavy minerals such as zircon and rutile are only present in traces. Generally the grains are rounded to well rounded.
Traces of **Organic matter** occur in the sandstones as scattered debris. It is often associated with authigenic pyrite.
Green rounded to well rounded **glauconite grains** occur as traces. The grains may also occur weakly squished due to compaction.
Bioclasts such as shell fragments and calcispheres? occur as traces in the thin sections.

Diagenetic mineralogy

Quartz cement ranges from 0–5.6% (average 2.4%). Quartz overgrowths are commonly small and subhedral but may occur euhedral. Dust rims delimiting the detrital and authigenic quartz are rare. Authigenic quartz grows around euhedral feldspar cement, which later have been partly dissolved (Plate 28). In one sample quartz occur as large overgrowths showing well-develop pyramidal crystal forms, which has replaced and grown into a calcite shell fragment (Plate 32).
Carbonate cement (1.6–43.2%, average 12.8%) consists of calcite and dolomite where calcite is the dominating part. The carbonate cement occur as single crystals in pores, patchy pore-space filling cement consisting of large crystals of calcite (Plate 27,28,30 & 34) or poikilotopic calcite cement. The latter may form concretion horizons and is displacive in nature and therefore an early cement (Plate 23). The carbonate cement fills secondary porosity and may replace feldspars. The pore filling calcite is post-dating quartz overgrowths.
Kaolinite is absent.
Illite is only observed to be present as illitized detrital clay. No SEM work has been done on samples from this well.
Feldspar cement has once been formed on detrital feldspar grains but only the outlines from this cement now occur (Plate 27 &28). The feldspar cement formed as euhedral crystals, which pre-dated quartz cement.
Baryte (0–2%, average 0.5%) occur as a scattered and commonly pore occluding cement, which post-dates quartz cement and feldspar dissolution.
Pyrite (1.6–6.8%, average 3.7%) is an early diagenetic phase and occur scattered in pore spaces as framboids and cubic crystals. It is commonly associated with organic matter. Pyrite was developed at a very early stage.

Porosity

Total porosity ranges 0–10% (average 5.1%) and is dominated by secondary porosity, which ranges 0–8.4% (average 4.2%). The secondary porosity is dominantly related to dissolution of both authigenic and detrital feldspar.

Gwen-2

Framework grains

The sandstones from the Gwen-2 well are sublitharenites and a single sample is litharenite (Folk, 1968) (Fig. 3A). However, adjusting for observed dissolution of feldspars the sandstones become more immature, and are classified both as sublitharenite, feldspathic litharenite and lithic arkose (Fig. 3B).

All samples are fine-grained sand except for one where grain size is very fine sand. Grain form varies between angular to rounded and the sandstones are very well to moderately sorted (see Table 2).

The framework grains consist of quartz together with a relatively high amount of rock fragments and minor feldspar. Mica, organic matter and detrital clay matrix occur in minor amount. Heavy minerals, bioclasts and glauconitic grains occur in traces.

Quartz (ranging from 41.6–51.6% with an average of 47.1%) is the dominant detrital phase, with a majority of monocrystalline grains. Polycrystalline grains probably have a metamorphic source. The grains show both uniform and undulose extinction. Contact dissolution/pressure solution textures (sutured, long and concavo-convex line contacts) between adjacent quartz grains occurs (Plate 42). However, no severe dissolution seems to have occurred. Quartz grains with rounded authigenic quartz overgrowths occur scattered (Plate 38).

Feldspars make up 0.8–4.0% (average 2.6%) of the sandstones and consist mainly of K-feldspar. The feldspar grains occur partially to totally dissolved.

The sandstones contain 2.8–12.0% (average 7.0%) **rock fragments**. The rock fragments consist mainly of mudstone clasts, metamorphic schistose quartz, magmatic grains and minor chert. The mudstone clasts occur illitized.

Mica constitutes 0–2.0% (average 0.4%) of the sandstone and is represented by muscovite. Muscovite found outside concretions, occur bent around quartz grains due to compaction. The mica flakes are commonly partially altered and may appear swollen (Plate 44).

Heavy minerals such as zircon and rutile are only present in traces.

Organic matter (0–0.8%, average 0.2%) occur in the sandstones as scattered debris and coalified woody tissue (Plate 40). It is often associated with authigenic pyrite.

Green rounded to well rounded **glauconite grains** occur scattered in the sandstone. The grains may also occur weakly squished due to compaction.

Bioclasts such as shell fragments occur as traces in the thin sections.

Diagenetic mineralogy

Quartz ranges from 0–14.4% (average 6.7%) in bulk volume. Quartz overgrowths are commonly small and subhedral but may occur euhedral. Total occlusion of porosity on a small scale may occur when overgrowths project out from detrital grains into the pores and create interlocking crystal boundaries. Dust rims delimiting the detrital and authigenic quartz are rare. Quartz cement is both pre- and post-dating feldspar dissolution (euhedral quartz crystals occur in secondary pore spaces).
Carbonate cement (0–40.8%, average 16.6%) consists of calcite. The carbonate cement occur as patchy pore-space filling cement, patchy, poikilotopic cement or concretionary poikilotopic cement (Plate 36–40). The last two cement types are displacive and therefore an early cement. Secondary porosity occur in the carbonate cement. However, delicate calcite rhombs occur in secondary pore spaces.
Kaolinite do not occur.
Illite is only observed to be present as illitized detrital clay. No SEM work has been done on samples from this well.
Baryte occur as delicate needles scattered in pore spaces, which often are secondary pores.
Pyrite (1.6–5.2%, average 3.4%) occur as small single crystals as well as large crystals scattered in pore spaces. The pyrite crystals can form large aggregates as shown in Plate 36. Pyrite is an early cement, seen by its presence in early concretionary, poikilotopic calcite.

Porosity

Total porosity ranges 1.2–21.6% (average 13.3%) and is dominated by secondary porosity, which ranges 1.2–13.6% (average 8.0%). The secondary porosity is primarily related to feldspar dissolution, but also dissolution of metamorphic grain fragments may occur.

Diamant-1

Framework grains

The sandstones from the Diamant-1 well all plot as sublitharenites (Folk, 1968)(Fig. 3A). However, adjusting for observed dissolution of feldspars in the sandstones, two samples are classified as subarkoses, two as sublitharenites and one as feldspathic litharenite (Fig. 3B).
All samples are fine-grained sand except for one where grain size is very fine sand. Grain form varies between subangular to rounded and the sandstones are very well to poorly sorted (see Table 2).
The framework grains are dominated by quartz together with a limited amount of rock fragments. Feldspars are very rare in occurrence. Mica and detrital clay matrix occurs in

minor amount. The content of heavy minerals, organic matter, bioclasts and glauconitic grains are very low.

Quartz (ranging from 57.6–68.0% with an average of 61.4%) is the dominant detrital phase, with a majority of monocrystalline grains. Polycrystalline grains probably have a metamorphic source. Some of the quartz grains occur with conspicuous dust-rims between the detrital grain and overgrowths, and the terminations of the overgrowths rounded (Plate 46). The grains show both uniform and undulose extinction. Contact dissolution/pressure solution textures (sutured, long and concavo-convex line contacts) between adjacent quartz grains are only weakly developed.

Feldspars make up 0–0.4% (average 0.1%) of the sandstones and commonly occur totally dissolved. In carbonate concretions feldspar has probably been replaced by carbonate cement.

The sandstones contain 4.0–11.6% (average 6.6%) **rock fragments**. These consist mainly of metamorphic schistose quartz and magmatic grains, and minor mudstone clasts and chert.

Mica constitutes 0–0.8% (average <0.1%) of the sandstone and is solely represented by muscovite. The mica flakes are often partially or totally altered into kaolinite.

Heavy minerals such as zircon and rutile are only present in traces. Generally the grains are rounded to well rounded.

Organic matter (0–0.8%, average 0.2%) occur in the sandstones as scattered debris. It is often associated with authigenic pyrite.

Green rounded to well rounded **glauconite grains** occur as traces (Plate 50). The grains may also occur weakly squished due to compaction.

Bioclasts such as shell fragments and calcispheres? occur as traces in the thin sections.

Diagenetic mineralogy

Authigenic **quartz** ranges from 0–9.6% (average 3.0%). It is common in the sandstones except in samples, which have experienced early and total carbonate cementation. Dust rims delimiting the detrital and authigenic quartz occur. Some quartz grains occur with very distinctive dust rims, which however is believed to originate from a former sedimentary cycle, due to the occurrence of often well rounded overgrowths (Plate 46). In some cases quartz overgrowths partially enclose kaolinite, indicating that the formation was synchronous with, or subsequent to formation of kaolinite. Quartz grows in some cases around detrital feldspar grains, which later have been partly dissolved and seems also to grow into secondary pore spaces.

Carbonate cement (0–33.2%, average 9.9%) is represented by calcite, dolomite and siderite and is generally the dominating cement in the sandstones. The carbonate cement occur as patchy pore-space filling cement and patchy or concretionary, poikilotopic calcite cement (Plate 45). The poikilotopic calcite cement are displacive and therefore an early cement. Siderite occur scattered as rare small rhombs. The carbonate cements are pre- and post-dating grain dissolution, quartz cementation and kaolinite. The carbonate cements has been described in detail by Andersen (1988).

Kaolinite (0–5.6%, average 2.7%) generally occurs as clustering booklets in primary and secondary pore spaces. The booklets are made up of individual thin pseudohexagonal,

euhedral plates, *c.* 5–10 µm across. Blocky morphology (dickite) is less common but occurs as thick plates in vermiforms or booklets between the kaolinite plates (Plate 77). The clusters of small booklets are often gathered in secondary pores resulting from dissolved feldspar. Mica has been altered into kaolinite. This type of kaolinite is forming large plates and are commonly pore occluding. Kaolinite occurring in primary pore spaces is generally overgrown by quartz and calcite.

Illite occur as illitized smectite, shown by the typical honeycomb structure, which occur on the grain surfaces (Plate 78). Few delicate neoformed laths of illite has delveloped in association with the illitized smectite (Plate 78).

Chert occur as a cement, filling cavities after what is believed to have been calcispheres.

Baryte (0–1.2%, average 0.3%) occur as delicate needles scattered in pore spaces, which often are secondary pores. It is post-dating feldspar dissolution and quartz, and is probably penecontemporaneous with carbonate cement.

Pyrite (0–3.6%, average 1.4%) occur scattered in pore spaces and is often associated with organic matter. Pyrite was developed at a very early stage.

Porosity

Total porosity ranges 0–18.8% (average 10.1%) and is weakly dominated by primary porosity, which ranges 0–8.4% (average 5.5%). The secondary porosity is related to feldspar dissolution and to a lesser extend probably also to dissolution of detrital carbonate.

Ravn-1

Framework grains

The sandstones from the Ravn-1 well all plot as sublitharenites (Folk, 1968) (Fig. 3A). When adjusting for observed dissolution of feldspars in the sandstones four remains sublitharenites, while one sample changes to Feldspathic litharenite and one to subarkose (Fig. 3B).

The sandstone samples are equally divided between very fine-grained and fine-grained sand. Grain form varies between angular to rounded and the sandstones are well to poorly sorted (see Table 2).

The framework grains consist of quartz together with a moderate amount of rock fragments and minor feldspar (mainly K-feldspar). Mica and organic matter occurs in minor amount. The amount of detrital clay matrix is varying from absent to abundant. Heavy minerals and glauconitic grains occur in traces.

Quartz (ranging from 34.0–58.4% with an average of 46.8%) is the dominant detrital phase, with a majority of monocrystalline grains. Polycrystalline grains probably have a metamorphic source. The grains show both uniform and undulose extinction. Contact dissolution/pressure solution textures (sutured, long and concavo-convex line contacts) between adjacent quartz grains occurs.

Feldspars make up 1.2–4.8% (average 2.2%) of the sandstones and consist mainly of K-feldspar. The feldspar grains occur partially to totally dissolved and is often replaced when engulfed in carbonate concretions.
The sandstones contain 4.0–11.2% (average 7.3%) **rock fragments**. These consist mainly of mudstone clasts, metamorphic schistose quartz, magmatic grains and minor chert. The mudstone clasts occur illitized.
Mica constitutes 0–1.2% (average 0.2%) of the sandstone and is represented by muscovite.
Heavy minerals such as zircon, tourmaline and rutile are only present in traces.
Organic matter (0–5.2%, average 1.3%) occur in the sandstones as scattered debris. It is often associated with authigenic pyrite.
Green rounded to well rounded, **glauconite grains** occur as traces (Plate 64).

Diagenetic mineralogy

Quartz cement ranges from 0–9.6% (average 3.6%). It is common in the parts of the sandstones, which have not experienced early and total carbonate cementation and where it have had free space to grow (Plate 59, 60, 65 & 66). The quartz cement generally postdates an early and very common carbonate cement. Dust rims delimiting the detrital and authigenic quartz are rare. Authigenic quartz grows around detrital feldspar grains, which later have been dissolved (Plate 66) and also grow within secondary pore spaces (Plate 56). The overgrowths often develop euhedral crystal forms. Total occlusion of porosity on a small scale occurs when overgrowths project out from detrital grains into the pores and create interlocking crystal boundaries (Plate 9).
Carbonate cement (6.8–50.8%, average 25.1%) is represented by calcite and dolomite and is generally the dominating cement in the sandstones. The carbonate cement occur as patchy pore-space filling cement and patchy or concretionary, poikilotopic calcite cement. The poikilotopic calcite cement may be displacive and therefore an early cement. These cements has been described in detail by Andersen (1988).
Kaolinite has not been observed in the sandstones.
Illite occur primarily as flaky illitized smectitic detrital clay and as neoformed delicate worm-like crystals, which coats pore walls (Plate 79 & 80). The presence of these illite crystals greatly reduce permeability. Illitization is a relatively late diagenetic phase.
Baryte (0–1.2%, average 0.3%) occur as delicate needles scattered in pore spaces, which often are secondary pores. It is post-dating feldspar dissolution and carbonate and quartz cement.
Pyrite (1.2–6.8%, average 2.9%) occur scattered in pore spaces and is commonly associated with organic matter. Pyrite was developed at a very early stage.

Porosity

Total porosity ranges 0–10.4% (average 4.6%) and is weakly dominated by secondary porosity, which ranges 0–6.4% (average 2.6%). The secondary porosity is commonly related to feldspar dissolution.

Ravn-2

Framework grains

The sandstones from the Ravn-2 well are Feldspathic litharenites and subarkoses (Folk, 1968) (Fig. 3A), also when adjusting for observed dissolution of feldspars in the sandstones (Fig. 3B).
The examined samples are fine-grained sand. Grain form varies between angular to subrounded and the sandstones are well to moderately sorted (see Table 2).
The framework grains consist of quartz together with minor feldspar (K-feldspar and subordinate plagioclase), and rock fragments. Mica and organic matter occurs in minor amount. The amount of detrital clay matrix is varying from absent to abundant. Heavy minerals and glauconitic grains occur in traces.
Quartz (average of 46.4%) is the dominant detrital phase, with a majority of monocrystalline grains. Polycrystalline grains probably have a metamorphic source. The grains show both uniform and undulose extinction. Contact dissolution/pressure solution textures (sutured, long and concavo-convex line contacts) between adjacent quartz grains occurs
Feldspars make up 5.6–7.2% (average 6.4%) of the sandstones and consist mainly of K-feldspar. The feldspar grains occur unaffected to totally dissolved.
The sandstones contain 2.0–10.0% (average 6.0%) **rock fragments**. These consist mainly of mudstone clasts, metamorphic schistose quartz, magmatic grains and minor chert. The mudstone clasts occur illitized.
Mica constitutes 0–0.4% (average 0.1%) of the sandstone and is solely represented by muscovite. The mica flakes may occur partially altered and appear swollen.
Heavy minerals such as zircon and rutile are only present in traces.
Organic matter (0–0.8%, average 0.4%) occur in the sandstones as scattered debris. It is often associated with authigenic pyrite.
Green rounded to well rounded **glauconite grains** occur as traces. The grains may also occur weakly squished due to compaction.

Diagenetic mineralogy

Authigenic **quartz** ranges from 13.2–17.2% (average 15.2%) of the bulk sample volume. It is locally occluding parts of the sandstones (Plate 67–69). Dust rims delimiting the detrital and authigenic quartz are rare. Large pyramidal quartz crystals has commonly developed in micro-fractures in the sandstones. These crystals are generally engulfed by baryte cement, filling the fractures. Authigenic quartz grows around what is believe to have been detrital feldspar grains, which later have been dissolved and also grows into secondary pore spaces (Plate 68). Total occlusion of porosity on a small scale occurs when overgrowths project out from detrital grains into the pores and create interlocking crystal boundaries. Quartz cement is post-dating and relatively early carbonate cement and is predating a late carbonate cement. It is pre- and post-dating detrital grain dissolution.
Carbonate cement (5.6–15.2%, average 10.4%) consists of calcite and dolomite. The dolomite is commonly growing as single rhombs, which may occur zoned and overgrown

by quartz. The carbonate cement occur as patchy pore-space filling cement consisting of large rhombic crystals of calcite or patchy, poikilotopic calcite cement. The latter may partly be displacive and therefore an early cement. The carbonate cement partly replaces detrital feldspar and quartz. It sometimes surrounds euhedral quartz overgrowths. As with quartz, large calcite crystals has commonly developed in micro-fractures in the sandstones, and they are generally engulfed by baryte cement, which fills the fractures.
No **kaolinite** has been observed.
Illite is only observed to be present as illitized detrital clay. No SEM work has been done on samples from this well.
Baryte (0–0.4%, average 0.2%) occur as delicate needles scattered in pore spaces, which often are secondary pores (Plate 68). It is filling micro-fractures, which is very common in the samples. It occur as a relatively late diagenetic phase, both post- and pre-dating carbonate and quartz cement. it post-dates feldspar dissolution.
Pyrite (2.8–6.8%, average 4.8%) occur scattered in pore spaces and is commonly associated with organic matter (Plate 70). Pyrite was developed at a very early stage.

Porosity

Total porosity ranges 3.2–6.0% (average 4.6%) and is equally shared by secondary and primary porosity. The secondary porosity is generally related to feldspar dissolution.

DISCUSSION

In the following the paragenetic sequences showing the diagenetic main phases will be presented for the individual examined wells. Further the diagenetic phases, which have an effect on the reservoir quality will be presented, and the possible processes and sources for their development will be discussed.

Paragenetic sequence

The simplified paragenetic sequences for the sandstones in the examined wells are shown in figure 4A–G, which illustrates the inferred main mineral phases in relation to time and burial. The diagenetic processes involve reactions between pore water and mineral phases where unstable minerals are dissolved and more stable mineral phases are precipitated. The involved processes and phases will be related to possible source material, temperature, pore water chemistry and fluid flows.
Roughly the diagenetic phases can be related to the following phases in the basin evolution: 1) sedimentation, burial (and meteoric flushing restricted to Gert-1, Diamant-1 and subordinately Gert-2); 2) fast burial, overpressure build up, increasing temperature; 3) hot fluid pulses probably related to pressure release along old, deeply rooted faults.

Facies related diagenesis

Varying amounts of pyrite are preserved in the sandstones. It is found both in the shoreface sandstones and in the back-barrier sandstones. Pyrite is generally accepted to be an early diagenetic mineral, mainly related to marine or brackish environments (e.g. Berner, 1981; Berner and Raiswell, 1984).

Quartz cement

In the literature it is indicated that quartz cement in clastic rocks can derive locally from kaolinization of feldspars, replacement of smectite/illite and kaolinite by illite, intergranular pressure solution, stylolitisation, and dissolution of detrital quartz (Houseknecht, 1988; McBride, 1989; Sibley and Blatt, 1976). Furthermore, the silica can be transported into the formation by fluid flows from other parts of the basin (McBride, 1989).

The main part of the quartz cement in the Upper Jurassic sandstones appears to have developed at a relatively late stage during deep burial (mesodiagenetic). This is suggested by quartz cement overgrowing early kaolinite and illite/illitized kaolinite and by syntaxial quartz crystals growing into secondary pore spaces. Fluid inclusion data from Gert-1 show that onset of quartz cementation began at an average temperature of 101°C (Johannes Fabricius, unpublished data).

Many models of quartz cementation are based on studies from the US Gulf Coast and the North Sea, areas with deep basins and rapid subsidence. Fluid inclusion data from these areas have shown that the most significant phases of quartz precipitation occur at temperatures ranging from 60–100°C and at temperatures >100°C. Quartz cementation shows a systematic increase in relation to depth in these basins and it has been concluded that quartz cementation is only important in depths exceeding 2–3 km, where diffusion from pressure dissolution along grain contacts and stylolites are the sources (Bjørlykke and Egeberg, 1993; McBride, 1989; Walderhaug, 1994). In the present study quartz is both pre- and post-dating illite, which indicate that quartz is a late stage cement when it is known that illite forms at ≈120°C – ≈140°C (Bjørlykke and Aagaard, 1992; Ehrenberg and Nadeau, 1989). The pressure dissolution model is not the most adequate to be used to explain the quartz cementation found in the Jurassic sandstones of the Heno Formation. No conspicuous signs of severe pressure solution have been observed. However, it can be hard to discern an overgrowth and the actual detrital grain when dust-rims are rare, and it has not been possible to do any cathodoluminescence analysis in the present study to solve the problem. But from the presence of dust-rims in a few samples with high amounts of quartz cement, it has been deduced that pressure dissolution was generally not important for the quartz cementation, and has surely not been severe enough to account for the observed volumes of quartz cement in some of the samples. This implies that the silica was derived mainly from intra-formational mineral transformations and/or was imported into the sandstone formations from an unknown source.

Dissolution of feldspar associated with kaolinitization and illitization of detrital clay is considered as the main source when looking for internal silica. No opaline skeletal grains are found, so silica contribution from these can be excluded.

One internal source of silica could be from dissolution and kaolinitization of feldspar grains in the sandstone, although this produces little diagenetic quartz. According to Haszeldine

et al. (1984) dissolution of 10% feldspar grains would form only 2% quartz cement in the rock. Illitization of kaolinite would also contribute with silica in a limited amount. However, the sandstones with high secondary porosity clearly show that the quartz cementation predates the dissolution of feldspar, so therefore this process can not be the source for quartz to develop, except for the minor amount of syntaxial quartz crystals which occur in the secondary pores.

Due to the very low solubility of silica, immense amounts of water are required for quartz to precipitate in the amounts recorded in the studied sandstones. Extensive fluid flow in sandstone formations are provided either by meteoric flushing (e.g. Bjørlykke, 1983), recirculation by heat induced convection (e.g. Bjørlykke et al., 1988; Wood and Hewett, 1982) or by introduction of extra-formational fluids. McBride (1989) concluded that the amount of quartz cement derived from silica in meteoric water in sandstone formations is relatively small. If kaolinite has been formed from K-feldspar during flushing of meteoric pore water it is most likely that silica has been removed through the process (Bath et al., 1987; Bjørlykke and Egeberg, 1993). Further it is likely that the low temperatures at shallow depth can prevent quartz precipitation during meteoric water flushing, albeit that the pore water is supersaturated with respect to quartz (Bjørlykke and Egeberg, 1993; Blatt, 1979). This is seen in the North Sea Brent Group which has experienced extensive meteoric flushing and feldspar dissolution, but is showing little evidence of quartz cementation at shallow depth (Bjørlykke and Egeberg, 1993). As noted above, early kaolinite and feldspar dissolution occur in some of the studied sandstones, but no evidence of early quartz is found. It is therefore assumed that the same conditions as described from the Brent Group sandstones have dominated in the Heno formation during the first events of burial. Quartz dissolution at the contacts between mica and quartz is, according to Bjørkum (1996), a process which occurs at low pressures and insignificant overburden load, i.e., at the same time as meteoric flushing. The dissolved silica has not re-precipitated due to the low temperature but has probably been transported out of the system.

The conclusion of these observations is that intra-formational sources have had only an insignificant influence on the amount of quartz cementation in the sandstones.

Another model used to explain the formation of quartz cement is based on fluid inclusions, CL petrography and isotope data from associated illite. The data indicate that quartz cementation is episodic and related to heating and rifting events, and the flow of hot fluids along fault planes (Burley et al., 1989; Glasmann et al., 1989; Gluyas et al., 1993; Lee et al., 1985), and the model involves import of silica from outside the sandstone formations.

The conclusion that only insignificant quartz cement derives from intra-formational sources, show that where quartz cement is abundant (as in Gert-1, Ravn-2 and to some extend in Gwen-2 and Gert-2) most silica has been imported into the sandstones from an external source. The problem is from where the silica is fed and under which circumstances. Not many data are presently available to bring forth a definitive conclusion but some suggestions will be presented in the following. As mentioned above, fluid inclusion data from Gert-1 has shown that onset of quartz cementation began at an average temperature of 101°C (Johannes Fabricius, unpublished data). The trapped fluids have salinities as high as 20–25 eq. wt.% NaCl, which may indicate that they derive from deeply circulating solutions, maybe from the evaporite-containing Triassic and Permian sediments. The fluids, which probably were highly pressured, were transferred from the deeper parts of the basin into the Jurassic sandstones, where mixing with less saline fluids and cooling of the invading

fluids resulted in quartz precipitation (cf. Burley et al., 1989). Also silica-rich fluids expelled from overpressured, down-thrown Upper Jurassic mudstones may have contributed.
The wells containing abundant quartz cement are situated relatively close to major faults (see Fig. 1), which may have acted as substantial fluid conduits, and the fluids are suggested to have been transported via major faults. These events may have occurred as pulses of relatively highly saline hot fluid flow escaped from overpressured, deeper formations. This means that precipitation of quartz was not necessarily a continuous process, reflecting increased burial, but rather relates to short-lived events of faulting and fluid migration along fault plans.
The movement of hot fluids from the faults into the sandstone formations may have contributed to the establishment of a thermal convection flow due to the great changes in temperature of the pore water close to the fault zone (Bjørlykke et al., 1988). To generate a high flux of water to transport silica, the formation must not alone have a high inclination with parallel isotherms, but also be relatively thick and have a high permeability. The studied sandstones are relatively thick and have good lateral continuity and transmissivity. As a result of faulting and block rotation the inclination has probably been sufficient and permeability has at the actual time been higher than present. The flow velocity is a function of the slope of the isotherms and the thickness of the bed (Bjørlykke et al., 1988). The relatively large thickness of the beds and presence of especially hot fluid introduction through faults giving sloping isotherms, makes it possible that thermal convection could have had some influence on silica transport and quartz precipitation in the sandstone formations. However, this is only the case for the sandstones where there is no interbedding of fine-grained material to interrupt the convection flow.
In sandstones containing relatively high amounts of detrital clay, the quartz cement is commonly poorly developed. This is due to the lack of pore space for the crystals to grow freely into.
Quartz cement may, although it reduce the porosity, locally be a help to preserve permeability as it enclose clay minerals and produce smooth grain surfaces. However, where the quartz cement is abundant it may close pore throats and severely reduce permeability.

Carbonate cement

The marine sandstone is characterised by the presence of several lateral carbonate cemented horizons. The high minus cement porosity and the presence of floating quartz grains indicate that cementation took place pre-compactional. This concretionary carbonate pre-dates quartz cementation since there is a lack of quartz overgrowths within the cemented horizons, thus confirming the early diagenetic origin.
Sources for carbonate cemented horizons in shallow marine sandstones have been discussed by Walderhaug and Bjørkum (1998). They concluded that transport of significant amount of calcite into a sandstone from an external source can normally be disregarded as being of any importance and the source for the calcite cement is local, usually in form of biogenic carbonate (Walderhaug and Bjørkum, 1998). This is inferred to be the primary source in this case, but Calcium may also have been supplied from replaced feldspars.
The patchy carbonate cement occur with fluid inclusions, which have shown homogenization temperatures of 96°C in the Gert-1 well and 115°C in the Ravn-1 well (Johannes Fabricius, unpublished data). Recorded salinities are >25 eq. wt.% NaCl. Calcite filled veins

also occur in samples in the same wells, and in Gert-1 two populations of homogenization temperatures has been observed to occur with average temperatures around 55°C and 101°C. Salinities is in the range 20–25 eq. wt.% NaCl. In Ravn-1 homogenization temperature is around 107°C and salinities >25 eq. wt.% NaCl. Except from the recorded homogenization temperature around 55°C, which is difficult to explain, these data indicate that the patchy carbonate cement and calcite filled veins are late stage phases. Values are in the same range as what were seen in the fluid inclusions found in the quartz cement in Gert-1.

The source of carbonate cement under burial conditions often remains problematic, but can derive internally from the sandstones and externally from fluids intruding from deeper parts of the basin or interbedded strata. The most likely sources are from dissolution of carbonate, illitization of smectite (release of Ca, Mg and Fe) (Boles and Franks, 1979) and Ca from dissolution of feldspar (Morad et al., 1990). However, as the fluid inclusion analysis show, some of the carbonate may as well derive from hot fluids migrating along faults, brought up from deeper formations. Triassic and Permian sediments found in the area are made up of carbonates, which could have contributed as a source for the carbonate cement in the sandstones.

The concretionary very early carbonate cement may locally destroy porosity and severely reduce permeablity. However, the reservoir quality of the entire sandstone body may remain good, if the concretionary horizons occur as discontinuous laterally isolated bodies which do not completely obstruct flow, neither vertically nor laterally. However, if the horizons are continuous over significant lateral distances, they may have a profound impact on reservoir quality. The Intergranular carbonate cement is totally occluding pore spaces, but its patchy occurrence makes it not a significant component for reduction in permeability.

Kaolinite formation

Kaolinite occurs mostly as clustering booklets with some vermiform aggregates in pore spaces in the sandstones, but also as pore-filling, tight masses in association with altered mica. The booklet kaolinites contain minor dickite (Plate 77).

The common distribution of kaolinite in fluvial and near-shore sandstones suggests that kaolinite is formed in meteoric pore waters (Bjørlykke, 1984; Hurst and Irwin, 1982). It is believed that some meteoric water flushing of the sandstones has occurred during the first period of subsidence in the Jurassic. Introduction of meteoric water into the sandstones may have been aided by a meteoric head from the elevated subaerial parts of the basin. The meteoric flushing may to a certain degree, have contributed to the formation of early, diagenetic kaolinite by dissolution of K-feldspar and alteration of mica (Bjørlykke, 1984; Bjørlykke et al., 1992; Glasmann, 1992; Khanna et al., 1997). There are no signs of early quartz cement, which could be related to K-feldspar dissolution. This shows that silica have been removed by the meteroic water (cf. Bath et al. (1987).

Partial replacement of kaolinite by dickite has been observed to take place with increasing burial depth and temperature (Kantorowicz, 1984; Smithson, 1954). The burial diagenetic transformation of kaolinite into dickite occurs at temperatures between ≈80°C and ≈120°C (Ehrenberg et al., 1993; McAulay et al., 1994; Morad et al., 1994).

Illite formation

Illite has formed from smectite and from transformation of detrital clay. Some pores have illitic pore linings and pore bridgings between individual grains. The honeycomb texture of the illite is smectitic (Plate 78), suggesting that authigenic smectite was diagenetically altered into illite (Pollastro, 1985; Wilson and Pittman, 1977). The transformation of smectite into illite is affected by temperature, the duration of time at elevated temperature, composition of the original smectite and K activity in the pore fluids (Chang et al., 1986; Ramseyer and Boles, 1986; Srodon, 1984). The transformation begins at temperatures of ~50°C (Srodon, 1984).
Generally extensive illitization occurs mainly by replacement of earlier authigenic kaolinite accompanied by dissolution of K-feldspar in the reaction:

Kaolinite + K-feldspar = Illite + quartz + H_2O

This implies that both kaolinite and K-feldspar, or some other potassium-containing mineral is needed to form illite. If K^+ is not available, kaolinite can remain stable up to 200°C, where after it transforms to pyrophyllite (Velde, 1984). In the studied sandstones it is inferred that detrital K-feldspar has been present in sufficient amounts for illite to form as it is still present in small amounts in some samples and it is further inferred that feldspar dissolution in some areas was contemporaneous with illitization. However, It seems that kaolinite, when present has not been transformed into illite or only weakly transformed. The reason for this is unclear.
Illite probably began to form during increased burial and temperature, but the growth may have been “boosted” when pulses of hot fluid was introduced to the sandstones, analogue to the process of quartz and carbonate cement formation discussed above. These fluids may be an alternative potassium source as it has been suggested for the Middle Jurassic Brent Group reservoirs by Jourdan et al. (1987).
Illite has a relatively minor effect on total porosity but severely reduce permeability. The reason for this is that the illitic fibres and laths strongly increase the relative surface area: volume ratio of the pore spaces and make the surfaces of the pores rough. In sandstones with relatively high content of detrital clay, illitization will contribute severely to the reduction of permeability.

Baryte

Bayte occur as patchy pore filling (often poikilotopic) cement and as single needle-shaped crystals in mostly secondary pore spaces. In Ravn-2 baryte is very often filling microfaults/fractures. In the baryte veins euhedral quartz and calcite crystals occur, which indicate that baryte post-dates these. Fluid inclusions in the baryte veins have been analysed and show such varying temperatures as 70°C, 123°C and 153°C, while salinites are inferred to be significantly higher than 25 eq. wt.% NaCl and possibly as high as 45 eq. wt.% NaCl (Johannes Fabricius, unpublished data). Petrographic studies show that baryte generally is a late cement, often contemporaneous with or post-dating quartz precipitation, and mostly post-dating grain dissolution. Baryte is not exactly the most reliable mineral for fluid inclusion analysis as it occur with cleavages and low mechanical strength, which may re-

sult in stretching or leakage of the inclusions (Emery and Robinson, 1993). However, the fact that baryte is contemporaneous with or post-dates quartz precipitation, which is a late stage cement, makes the recorded high temperatures more reliable.
Ravn-2 is situated very close to a major fault zone, which probably also is the reason why the sandstones are severely micro-faulted and fractured. Particularly for this well is it believed that fluids have migrated up from deeper formations via the fault planes and fractures where baryte has precipitated from solutions rich in Barium and sulphate. Both the Barium and the sulphate are believed to derive from Triassic or Permian evaporites and the very high salinities in the fluid inclusions support this. These sediments are probably also the source for baryte found in the other wells. However, feldspars can contain Barium and can be a source for baryte. This may be the reason why baryte often occurs in secondary pore spaces in the sandstones in all wells.

Grain dissolution: Porosity enhancement

The majority of dissolution of detrital grains (primarily feldspar) occur at a relatively late stage in the diagenetic sequence. Pressure in the sandstones has build up relatively fast and the sandstones is in a state of overpressure. During renewed burial of the sandstones in Late Jurassic – Cretaceous time and since rapid subsidence began in Oligocene the overburden of thick mudstones acted as an impermeable seal. This seal prevented pore fluid from escaping from the sandstones. It also contributed to the build up of overpressure due to relatively rapid burial and subsequent disequilibrium compaction and secondarily as a result of temperature increase, water release due to mineral transformation and possibly hydrocarbon generation (cf. review by Swarbrick and Osborne (1998). Overpressure in the sandstone, which rules at the present time (See Fig. 5), will have led to a decrease in the stress at contacts between detrital grains (effective stress), inhibiting further significant compaction and preventing severe pressure solution (Osborne and Swarbrick, 1999).
However, overpressure leak-off may have occurred in relation to faulting as discussed above. This means that fluid flow related to overpressure leak-off may have removed elements from dissolved feldspars out of the system (cf. Wilkinson et al. (1997).

Reservoir quality

Permeability and porosity analysis show, in general, low permeability and medium porosity values. Permeability ranges roughly from 0.01 mD to 1200 mD with the highest frequency in the 0–10 mD range and porosity ranges from 2% to 30% with maximum frequency in the 10–20% range.

Going through the diagenetic sequence, it can be seen that the first mineral phase, which has had an effect on reservoir quality, was the early, diagenetic carbonate cement in the marine sandstones. The carbonate cemented horizons which, could due to their lateral extension, thickness and total occlusion of the pore spaces, work like barriers to upward migrating hydrocarbons. However, if the horizons actually are lensoid bodies with limited extension, they would not have this effect. The more scattered and patchy pore space scale occurrence of carbonate cement has only minor effects on porosity and permeability.

The formation of kaolinite and illite contributes to abundant microporosity but gives no significant increase in pore volume. Actually, substantial amounts of kaolinite and illite create a serious reduction in permeability and, thus, accordingly in reservoir quality. However, kaolinite is not a common cement in the wells except from Diamant-1. Illite occur as illitization of detrital clay and neoformed minute fibres or threads and is believed to be an important component, for the reduction in permeability in the wells. The largest influence on reservoir quality must be ascribed to the periods of faulting, and resulting overpressure leak-off. The severe cementation by quartz in some wells is often seen as greatly decreasing permeability and porosity by occlusion of intergranular pores. At the same time, illitization was accelerated due to the increase in temperature, resulting in low permeability. Secondary porosity is generally dominating over primary porosity, which makes grain dissolution an important contribution to retain or enhance reservoir quality in the sandstones. However, the secondary porosity may occur in severely cemented areas, where connectivity between the pore spaces is poor.

Conclusions

Quartz and carbonate and to a lesser extend kaolinite, baryte and pyrite are the cements which occur in the sandstones and have an impact on the reservoir quality. Detrital clay is generally Illitized, which may result greatly in reduction of permeability. Secondary porosity is very common and is often a significant contributor to porosity development.

Where quartz cement is abundant most silica has been imported into the sandstones from an external source. The wells containing abundant quartz cement are situated relatively close to major faults, which may have acted as substantial fluid conduits, and the fluids are suggested to have been transported via major faults and fractures associated with these.

The majority of carbonate cement occurs in horizons and is related to an early stage of diagenesis with the source being biogenic carbonate. A late stage carbonate cement may derive from internal sources or be a product of fluids flowing along major faults analogue to quartz cement.

Dissolution of predominantly feldspar grains has in some wells significantly enhances porosity. However, the grain dissolution occurred relatively late in the burial history, often post-dating quartz and carbonate cement, and the occlusion of pore throats and pore spaces by these cements before the occurrence of grain dissolution may retain low permeability, albeit porosity is enhanced. The secondary porosity is preserved because predeveloped cement and present-day overpressure in the sandstones support the grain framework and prevents it from collapsing.

No clear trends in diagenesis related to sedimentary environment, grain size or sorting seems to be present. However, it is believed that the sandstones in wells located close to major and deeply rooted faults may experience a larger impact of diagenetic processes as a result of enhanced input of (hot) fluids, which may contribute to severe cementation and to some extend grain dissolution. The sandstone reservoirs close to these faults are therefore in danger of being of relatively low quality.

References

Andersen, P. R., 1988, Upper Jurassic sandstones. Part 2: Diagenetic alterations based on isotope studies. CENBAS sub-project B, Geological Survey of Denmark, p. 78.

Andsbjerg, J., 1997, Sedimentology and sequence stratigraphy of Middle Jurassic deposits, Danish and Norwegian Central Graben, Part 1, 2, 3 and 4: Unpublished Ph.D Thesis thesis, University of Copenhagen, 165 p.

Andsbjerg, J., and K. Dybkjær, in press, Jurassic sequence stratigraphy of the Danish Central Graben, *in* F. Surlyk, and J. R. Ineson, eds., The Jurassic of Denmark and Greenland, Geology of Denmark Survey Bulletin.

Bath, A. H., A. E. Mildowsky, and G. E. Strong, 1987, Fluid flow and diagenesis in the East Midland Triassic sandstone aquifer, *in* J. C. Goff, and B. P. J. Williams, eds., Fluid flow in Sedimentary Basins and Aquifers, Geological Society, London, p. 127-140.

Berner, R. A., 1981, Authigenic mineral formation resulting from organic matter decomposition in modern sediments: Fortschritte der Mineralogie, p. 117-135.

Berner, R. A., and R. Raiswell, 1984, C/S method for distinguishing freshwater from marine sedimentary rocks: Geology, v. 12, p. 365-368.

Bjørkum, P. A., 1996, How important is pressure in causing dissolution of quartz in sandstones?: Journal of Sedimentary Research, v. 66, p. 147-154.

Bjørlykke, K., 1983, Diagenetic reactions in sandstones, *in* A. Parker, and B. W. Sellwood, eds., Sediment Diagenesis. Proceedings, NATO Advanced Study Institute: Series C: Mathematical and Physical Sciences, Reidel Publ. Co., Reading, UK, p. 169-213.

Bjørlykke, K., 1984, Formation of secondary porosity. How important is it?, *in* D. A. McDonald, and R. C. Surdam, eds., Clastic Diagenesis, American Association of Petroleum Geologists, p. 285-292.

Bjørlykke, K., and P. K. Egeberg, 1993, Quartz cementation in sedimentary basins: American Association of Petroleum Geologists Bulletin, v. 77, p. 1538-1548.

Bjørlykke, K., A. Mo, and E. Palm, 1988, Modelling of thermal convection in sedimentary basins and its relevance to diagenetic reactions: Marine and Petroleum Geology, v. 5, p. 338-351.

Bjørlykke, K., T. Nedkvitne, M. Ramm, and G. C. Saigal, 1992, Diagenetic processes in the Brent Group (Middle Jurassic) reservoirs of the North Sea; an overview, *in* A. C. Morton, R. S. Haszeldine, M. R. Giles, and S. Brown, eds., Geology of the Brent Group, London, Geological Society Special Publications, 61, p. 263-287.

Bjørlykke, K., and P. Aagaard, 1992, Clay minerals in North Sea sandstones, *in* D. W. Houseknecht, and E. D. Pittman, eds., Origin, diagenesis, and petrophysics of clay minerals in sandstones: SEPM, Special Publication 47, p. 65-80.

Blatt, H. B. K., 1979, Diagenetic processes in sandstones, *in* P. A. Scholle, and P. R. Schluger, eds., Aspects of diagenesis, SEPM Special Publication 26, p. 141-157.

Boles, J. R., and S. G. Franks, 1979, Clay diagenesis in Wilcox sandstones of southwest Texas: implications of smectite diagenesis on sandstones cementation: Journal of Sedimentary Petrology, v. 49, p. 55-70.

Britze, P., P. Japsen, and C. Andersen, 1995a, Geological map of Denmark. 1:200,000. The Danish Central Graben. Base Chalk and the Chalk Group (two-way travel time

and depth, thickness and interval velocity): Geological Survey of Denmark, Map series, v. 48, p. 7.

Britze, P., P. Japsen, and C. Andersen, 1995b, Geological map of Denmark. 1:200,000. The Danish Central Graben. Base Cretaceous and the Cromer Knoll Group (two-way travel time and depth, thickness and interval velocity): Geological Survey of Denmark, Map series, v. 49, p. 7.

Britze, P., P. Japsen, and C. Andersen, 1995c, Geological map of Denmark. 1:200,000. The Danish Central Graben. Base Upper Jurassic and the Upper Jurassic (two-way travel time and depth, thickness and interval velocity): Geological Survey of Denmark, Map series, v. 50, p. 7.

Burley, S. D., J. Mullis, and A. Matter, 1989, Timing diagenesis in the Tartan Reservoir (UK North Sea): constraints from combined cathodoluminescence microscopy and fluid inclusion studies: Marine and Petroleum Geology, v. 6, p. 98-120.

Chang, H., F. T. MacKenzie, and J. Schoonmaker, 1986, Comparisons between the diagenesis of dioctahedral and trioctahedral smectite, Brazilian offshore basins: Clays and Clay Minerals, v. 34, p. 407-423.

Damtoft, K., L. H. Nielsen, P. N. Johannessen, E. Thomsen, and P. R. Andersen, 1992, Hydrocarbon plays in the Danish central Trough, *in* A. M. Spencer, ed., Generation, accumulation and production of Europe's hydrocarbons II, EAPG Special Publications, p. 35-58.

Dybkjær, K., 1998, Palynological dating of the Mandal Formation (uppermost Jurassic - lowermost Cretaceous, Norwegian Central Graben) and correlation to organic rich shales in the Danish sector: Marine and Petroleum Geology, v. 15, p. 495-503.

Ehrenberg, S. N., and P. H. Nadeau, 1989, Formation of diagenetic illite in sandstones of the Garn Formation, Haltenbanken area, Mid-Norwegian continental shelf.: Clay Minerals, v. 24, p. 233-253.

Ehrenberg, S. N., P. Aagaard, M. J. Wilson, A. R. Fraser, and D. M. L. Duthie, 1993, Depth-dependent transformation of kaolinite to dickite in sandstones of the Norwegian Continental shelf: Clay Minerals, v. 28, p. 325-352.

Emery, D., and A. Robinson, 1993, Inorganic geochemistry: applications to petroleum geology: Oxford, Blackwell Scientific Publications, 254 p.

Folk, R. L., 1968, Petrology of Sedimentary Rocks: Austin, Hemphill Book Store, 170 p.

Glasmann, J. R., 1992, The fate of feldspar in Brent Group reservoirs, North Sea; a regional synthesis of diagenesis in shallow, intermediate, and deep burial environments, *in* A. C. Morton, R. S. Haszeldine, M. R. Giles, and S. Brown, eds., Geology of the Brent Group, London, Geological Society Special Publications, 61, p. 329-350.

Glasmann, J. R., R. A. Clark, S. Larter, N. A. Briedis, and P. D. Lundegard, 1989, Diagenesis and hydrocarbon accumulation, Brent Sandstones (Jurassic), Bergen High, North Sea: American Association of Petroleum Geologists, v. 73, p. 1341-1360.

Gluyas, J. G., A. G. Robinson, and S. M. Grant, 1993, Geochemical evidence for a temporal control on sandstone cementation, *in* A. D. Horbury, and A. G. Robinson, eds., Diagenesis and Basin Development, American Association of Petroleum Geologists Studies in Geology 36, p. 23-33.

Haszeldine, R. S., I. M. Samson, and C. B. K. Cornford, 1984, Quartz diagenesis and convective fluid movement; Beatrice Oilfield, UK North Sea: Clay Minerals, v. 19, p. 391-402.

Houseknecht, D. W., 1988, Intergranular pressure solution in four quartzose sandstones: Journal of Sedimentary Petrology, v. 58, p. 228-246.

Hurst, A., and H. Irwin, 1982, Geological modelling of clay diagenesis in sandstones: Clay Minerals, v. 17, p. 5-22.

Ineson, J. R., J. Bojesen-Koefod, K. Dybkjær, and L. H. Nielsen, in press, Volgian - Ryazanian "hot shales" of the Farsund Formation in the Danish Central Graben, North Sea: stratigraphy, facies and geochemistry, *in* F. Surlyk, and J. R. Ineson, eds., The Jurassic of Denmark and Greenland; Geology of Denmark Survey Bulletin, Geological Survey of Denmark and Greenland.

Johannessen, P. N., K. Dybkjær, and E. S. Rasmussen, 1996, Sequence stratigraphy of Upper Jurassic sandstones in the northern part of the Danish Central Trough, North Sea: Marine and Petroleum Geology, v. 13, p. 755 - 770.

Jourdan, A. P., M. Thomas, O. Brevart, P. Robson, F. Sommer, and M. Sullivan, 1987, Diagenesis as the control of the Brent sandstone reservoir properties in the greater Alwyn area (East Shetland Basin), *in* J. Brooks, and K. W. Glennie, eds., Petroleum geology of north west Europe, Graham & Trotman, p. 951-961.

Kantorowicz, J., 1984, Nature, origin and distribution of authigenic clay minerals from Middle Jurassic Ravenscar and Brent Group sandstones: Clay Minerals, v. 19, p. 359-375.

Khanna, M., G. C. Saigal, and K. Bjørlykke, 1997, Kaolinitization of Upper Triassic-Lower Jurassic sandstones of the Tampen Spur area, North Sea; implications for early diagenesis and fluid flow, *in* I. P. Montaneez, J. M. Gregg, and K. L. Shelton, eds., Basin-wide diagenetic patterns; integrated petrologic, geochemical, and hydrologic considerations, SEPM Special Publication No. 57, p. 253-268.

Lee, M., J. L. Aronson, and S. M. Savin, 1985, K/Ar dating of the time of gas emplacement in Rotliegendes sandstone, Netherlands: American Association of Petroleum Geologists Bulletin, v. 69, p. 1381-1385.

Mackertich, D., 1996, The Fife Field, UK Central North Sea: Petroleum Geoscience, v. 2, p. 373-380.

McAulay, G. E., S. D. Burley, A. E. Fallick, and N. J. Kusznir, 1994, Palaeohydrodynamic fluid flow regimes during diagenesis of the Brent Group in the Hutton-NW Hutton reservoirs: constraints from oxygen isotope studies of authigenic kaolin and reverse flexural modelling: Clay Minerals, v. 29, p. 609-626.

McBride, E. F., 1989, Quartz cement in sandstones: a review: Earth-Science Reviews, v. 26, p. 69-112.

Michelsen, O., L. H. Nielsen, P. N. Johannessen, J. Andsbjerg, and F. Surlyk, in press, Jurassic lithostratigraphy and depositional development onshore and offshore Denmark, *in* F. Surlyk, and J. R. Ineson, eds., The Jurassic of Denmark and Greenland. Geology of Denmark Survey Bulletin, Geological Survey of Denmark and Greenland.

Morad, S., H. Ben Ismail, L. F. De ros, I. S. Al-Aasm, and N.-E. Serrhini, 1994, Diagenesis and formation water chemistry of Triassic reservoir sandstones from southern Tunisia: Sedimentology, v. 41, p. 1253-1272.

Morad, S., M. Bergan, R. Knarud, and J. P. Nystuen, 1990, Albitization of detrital plagioclase in Triassic reservoir sandstones from Snorre filed, Norwegian North Sea: Journal of Sedimentary Petrology, v. 60, p. 411-425.

Møller, J. J., 1986, Seismic structural mapping of the Middle and Upper Jurassic in the Danish Central Trough: Geological Survey of Denmark, Series A, v. 13, p. 37.

Møller, J. J., and E. S. Rasmussen, in press, Middle Jurassic - Early Cretaceous rifting of the Danish Central Graben, *in* F. Surlyk, and J. R. Ineson, eds., The Jurassic of Denmark and Greenland. Geology of Denmark Survey Bulletin.

Osborne, M. J., and Swarbrick, R. E., 1999, Diagenesis in North Sea HPHT clastic reservoirs - consequences for porosity and overpressure prediction: Marine and Petroleum Geology, v. 16, p. 337-353.

Pollastro, R. M., 1985, Mineralogical and morphological evidence for the formation of illite at the expense of illite/smectite: Clays and Clay Minerals, v. 33, p. 265-274.

Ramseyer, K., and J. R. Boles, 1986, Mixed-layer illite/smectite minerals in Tertiary sandstones and shales, San Joaquin Basin, California: Clays and Clay Minerals, v. 34, p. 115-124.

Sibley, D. F., and H. Blatt, 1976, Intergranular pressure solution and cementation of the Tuscarora orthoquartzite: Journal of sedimentary Petrology, v. 46, p. 881-896.

Smithson, F., 1954, The petrography of dickitic sandstones in north Wales and northern England: Geological Magazine, v. 91, p. 177-188.

Srodon, J., 1984, Mixed-layer illite-smectite in low-temperature diagenesis: data from the Miocene of the Carpathian foredeep: Clay Minerals, v. 19, p. 205-215.

Swarbrick, R. E., and M. J. Osborne, 1998, Mechanisms that generate abnormal pressure: an overview, *in* B. E. Law, G. F. Ulmishek, and V. I. Slavin, eds., Abnormal pressures in hydrocarbon environments, AAPG Memoir 70, p. 13-34.

Vejbæk, O. V., 1986, Seismic stratigraphy and tectonic evolution of the Lower Cretaceous in the Danish Central Trough: Geological Survey of Denmark, Series A, v. 11, p. 46.

Velde, B., 1984, Transformations of clay minerals, *in* B. Duran, ed., Thermal phenomena in sedimentary basins, Internationale Collequim Bordeaux, June 7-10 1983, p. 11-116.

Walderhaug, O., 1994, Temperatures of quartz cementation in Jurassic sandstones from the Norwegian Continental Shelf - evidence from fluid inclusions: Journal of Sedimentary Research, v. 64A, p. 311-323.

Walderhaug, O., and P. A. Bjørkum, 1998, Calcite cement in shallow marine sandstones: growth mechanisms and geometry, *in* S. Morad, ed., Carbonate Cementation in Sandstones, Special Publication of the International Association of Sedimentologists, p. 179-192.

Wilkinson, M., D. Darby, R. S. Haszeldine, and G. D. Couples, 1997, Secondary porosity generation during deep burial associated with overpressure leak-off; Fulmar Formation, United Kingdom Central Graben: AAPG Bulletin, v. 81, p. 803-813.

Wilson, M. D., and E. D. Pittman, 1977, Authigenic clays in sandstones: recognition and influence on reservoir properties and paleoenvironmental analysis: Journal of Sedimentary Petrology, v. 47, p. 3-31.

Wood, J. R., and T. A. Hewett, 1982, Fluid convection and mass transfer in porous sandstones - a theoretical model: Geochimica et Cosmochimica Acta, v. 46, p. 1707-1713.

APPENDIX 1: TABLES

In Tables 1A–G the estimated content of quartz and carbonate cement, total clay and macro-porosity is shown. The content of quartz and carbonate cement, and total clay is shown by the figures **0**, **1**, **2** and **3**, which respectively stand for: **Absent**, **rare**, **common** and **abundant**.
The estimation of macro-porosity is shown in the following manner:

No porosity = 0
Very low porosity = 0.5
Low porosity = 1.0
Low–medium porosity = 1.5
Medium porosity = 2.0
Medium–high porosity = 2.5
High porosity = 3.0

The value 0 is typically encountered in carbonate concretions where visible porosity is zero and the value 3.0 often occur in relatively clay-free samples with a measured Helium porosity around 30%.

Table 2 show the results of the petrographic modal analysis.

Gert-1

Sample No.	Depth (m b.KB)	Depth (ft)	Depth (in)	Member	"Environment"	Quartz cem.	Carb. cem.	Clay content	Est. Porosity
4450	4920,03	16141	10	Gert	Back-barrier	3	2	1	1
4451	4921,40	16146	4	Gert	Back-barrier	3	2	0	2
4453	4922,22	16149	0	Gert	Back-barrier	0	3	0	0
4454	4922,27	16149	2	Gert	Back-barrier	0	3	0	0
3962	4922,32	16149	4	Gert	Back-barrier	3	2	1	1,5
4455	4922,52	16150	0	Gert	Back-barrier	0	3	0	0
4456	4922,65	16150	5	Gert	Back-barrier	3	3	1	1
4457	4922,80	16150	11	Gert	Back-barrier	2	2	2	1
3964	4927,32	16165	9	Gert	Back-barrier	3	2	0	1,5
3965	4928,21	16168	8	Gert	Back-barrier	3	2	0	2
4458	4931,89	16180	9	Gert	Back-barrier	3	2	0	2
4459	4931,99	16181	1	Gert	Back-barrier	3	1	0	1,5
4460	4934,33	16188	9	Gert	Back-barrier	3	1	1	1,5
4461	4934,56	16189	6	Gert	Back-barrier	0	3	0	0
4462	4934,76	16190	2	Gert	Back-barrier	3	3	1	1
4463	4934,79	16190	3	Gert	Back-barrier	0	3	0	0
4464	4934,86	16190	6	Gert	Back-barrier	0	3	0	0
4465	4934,99	16190	11	Gert	Back-barrier	0	3	0	0
4466	4936,08	16194	6	Gert	Back-barrier	3	2	1	1,5
4467	4938,09	16201	1	Gert	Back-barrier	3	2	1	1,5
4044	4938,85	16203	7	Gert	Back-barrier	3	2	0	1,5
3960	4940,99	16210	7	Gert	Back-barrier	3	1	1	1
3959	4941,29	16211	7	Gert	Back-barrier	3	2	1	2
3958	4941,90	16213	7	Gert	Back-barrier	2	2	1	2,5
3957	4942,48	16215	6	Gert	Back-barrier	3	1	1	1
4469	4944,29	16221	5	Gert	Back-barrier	0	3	0	0
4470	4950,97	16243	4	Gert	Back-barrier	3	2	2	1,5
4471	4951,30	16244	5	Gert	Back-barrier	0	3	0	0
4472	4951,55	16245	3	Gert	Back-barrier	0	0	3	0,5
4047	4953,53	16251	9	Gert	Back-barrier	3	1	1	1,5
4048	4954,96	16256	5	Gert	Back-barrier	3	2	1	2
4049	4958,00	16266	5	Gert	Back-barrier	3	2	2	1,5
4473	4958,99	16269	8	Gert	Back-barrier	3	2	1	1
4474	4959,15	16270	2	Gert	Back-barrier	3	3	1	0,5
4051	4959,17	16270	3	Gert	Back-barrier	0	3	0	0,5
4475	4959,22	16270	5	Gert	Back-barrier	0	3	0	0
4476	4959,35	16270	10	Gert	Back-barrier	0	3	0	0
4477	4959,63	16271	9	Gert	Back-barrier	0	3	0	0
4478	4959,83	16272	5	Gert	Back-barrier	0	3	0	0
4479	4961,08	16276	6	Gert	Back-barrier	3	2	1	1
4480	4967,68	16298	2	Gert	Back-barrier	1	1	3	1
4056	4969,56	16304	4	Gert	Back-barrier	3	2	2	1
4481	4969,66	16304	8	Gert	Back-barrier	3	2	1	0,5
4482	4969,94	16305	7	Gert	Back-barrier	3	3	2	0,5
4483	4970,48	16307	4	Gert	Back-barrier	0	3	2	0
4484	4973,24	16316	5	Gert	Back-barrier	2	0	3	1

Table 1A. Shows information from the examined samples in the Gert-1 well. Samples marked by yellow have been described in detail and point counted.

Gert-2

Sample No.	*Depth (m b. KB)*	*Depth (ft)*	*Depth (in)*	*Member*	*"Environment"*	Quartz cem.	Carb. cem.	Clay content	Est. Porosity
2689	4817,67	15806	0	Ravn	Middle shoreface	3	2	3	1
2688	4821,05	15817	1	Ravn	Lower shoreface	1	1	3	1
2691	4821,78	15819	6	Ravn	Lower shoreface	1	2	3	1
2690	4823,38	15824	9	Ravn	Lower shoreface	0	0	3	0
2692	4826,74	15835	9	Ravn	Lower shoreface	0	0	3	0
2697	4828,46	15841	5	Ravn	Lower shoreface	0	0	3	0
2693	4832,45	15854	6	Ravn	Lower shoreface	0	0	3	0
2694	4834,86	15862	5	Ravn	Lower shoreface	0	0	3	0
4057	4869,10	15974	9	Ravn	Upper shoreface	0	3	0	1
2695	4870,48	15979	3	Ravn	Upper shoreface	1	1	3	1
2696	4873,73	15989	11	Gert	Back-barrier	2	1	2	1
2685	4877,36	16001	10	Carboniferous		2	1	2	2
2686	4883,53	16022	1	Carboniferous		0	0	3	0
2687	4891,68	16048	10	Carboniferous		3	0	1	0,5

Table 1B. Shows information from the examined samples in the Gert-2 well. Samples marked by yellow have been described in detail and point counted.

Jeppe-1

Sample No.	Depth (m)	Depth (ft)	Depth (in)	Member	"Environment"	Quartz cem.	Carb. cem.	Clay content	Est. Porosity
4255	4939,28	16205	0	Ravn	Middle shoreface	0	3	1	0
4257	4940,04	16207	6	Ravn	Middle shoreface	2	2	2	1
4258	4941,01	16210	8	Ravn	Middle shoreface	0	3	1	0
4259	4941,05	16210	10	Ravn	Middle shoreface	0	3	1	0
4260	4941,67	16212	10	Ravn	Middle shoreface	2	2	2	1,5
4261	4943,74	16219	7	Ravn	Middle shoreface	2	2	2	1,5
4262	4945,81	16226	5	Ravn	Middle shoreface	2	2	2	1,5
4263	4947,53	16232	1	Ravn	Middle shoreface	1	3	1	0,5
4264	4947,80	16232	11	Ravn	Middle shoreface	2	3	2	2
4265	4949,40	16238	2	Ravn	Middle shoreface	3	2	2	1,5
4266	4953,13	16250	5	Ravn	Middle shoreface	1	3	1	0
4267	4953,16	16250	6	Ravn	Middle shoreface	2	2	2	2
4268	4953,74	16252	5	Ravn	Middle shoreface	2	2	2	2
4269	4957,15	16263	7	Ravn	Middle shoreface	1	3	1	0
4270	4957,57	16265	0	Ravn	Middle shoreface	2	2	2	2
4271	4957,91	16266	1	Ravn	Middle shoreface	1	3	1	0
4272	4961,72	16278	7	Ravn	Middle shoreface	1	3	1	0
4273	4961,84	16279	0	Ravn	Middle shoreface	2	2	2	2
4274	4964,08	16286	4	Ravn	Middle shoreface	2	2	2	2
4275	4971,77	16311	7	Ravn	Middle shoreface	2	2	2	2
4276	4976,89	16328	5	Ravn	Middle shoreface	1	3	3	0
4277	4985,33	16356	1	Ravn	Lower shoreface	1	2	3	0,5
4278	4987,26	16362	5	Ravn	Lower shoreface	1	2	3	0,5
4279	4988,45	16366	4	Ravn	Lower shoreface	1	2	3	0,5
4280	4991,02	16374	9	Ravn	Lower shoreface	1	2	3	0,5

Table 1C. Shows information from the examined samples in the Jeppe-1 well. Samples marked by yellow have been described in detail and point counted.

Gwen-2

Sample No.	*Depth (m)*	*Depth (ft)*	*Depth (in)*	*Member*	*"Environment"*	Quartz cem.	Carb. cem.	Clay content	Est. Porosity
3612	4237,30	13901	11	Ravn	Middle-upper shoreface	0	3	1	0,5
3614	4239,08	13907	9	Ravn	Middle-upper shoreface	0	0	3	0
3615	4240,76	13913	3	Ravn	Middle-upper shoreface	0	0	3	0
3411	4244,57	13925	9	Ravn	Middle-upper shoreface	1	0	3	1,5
3412	4245,41	13928	6	Ravn	Middle-upper shoreface	2	1	1	3
3618	4248,56	13938	10	Ravn	Middle-upper shoreface	1	2	2	1,5
3607	4249,01	13940	4	Ravn	Middle-upper shoreface	2	2	2	1,5
3608	4250,87	13946	5	Ravn	Middle-upper shoreface	0	3	0	0,5
3415	4252,57	13952	0	Ravn	Middle-upper shoreface	2	1	3	1,5
3416	4254,83	13959	5	Ravn	Middle-upper shoreface	3	1	1	2,5
3613	4256,46	13964	9	Ravn	Middle-upper shoreface	2	1	2	2,5
3616	4260,32	13977	5	Ravn	Middle-upper shoreface	0	3	1	0,5
3617	4260,65	13978	6	Ravn	Middle-upper shoreface	1	1	1	3
3609	4272,48	14017	4	Ravn	Lower shoreface	0	3	3	1
3610	4278,40	14036	9	Ravn	Lower shoreface	0	0	3	0
3611	4286,55	14063	6	Ravn	Lower shoreface	0	2	3	0
3619	4292,73	14083	9	Ravn	Lower shoreface	0	1	3	0

Table 1D. Shows information from the examined samples in the Gwen-2 well. Samples marked by yellow have been described in detail and point counted.

Diamant-1

Sample No.	Depth (m)	Depth (ft)	Depth (in)	Member	"Environment"	Quartz cem.	Carb. cem.	Clay content	Est. Porosity
3564	3828,05	12559	3	Ravn	Upper shoreface	0	3	0	0
3563	3828,09	12559	4	Ravn	Upper shoreface	0	3	0	0
3565	3828,71	12561	5	Ravn	Upper shoreface	1	2	2	3
3465	3829,32	12563	5	Ravn	Upper shoreface	1	2	2	3
3525	3829,60	12564	4	Ravn	Upper shoreface	1	2	0	3
3788	3831,06	12569	1	Ravn	Upper shoreface	1	2	0	3
3466	3831,77	12571	5	Ravn	Upper shoreface	1	3	1	0
3789	3832,25	12573	0	Ravn	Upper shoreface	2	2	0	3
3568	3832,27	12573	1	Ravn	Upper shoreface	1	2	0	3
3790	3832,55	12574	0	Ravn	Upper shoreface	1	3	0	0,5
3467	3833,10	12575	9	Ravn	Upper shoreface	1	2	2	1
3782	3834,22	12579	6	Ravn	Upper shoreface	2	1	1	2
3574	3834,75	12581	2	Ravn	Upper shoreface	2	1	1	2
3785	3835,13	12582	5	Gert	Back-barrier/lagoon	1	2	2	0,5
3575	3835,97	12585	2	Gert	Back-barrier/lagoon	2	1	1	2
3845	3836,11	12585	8	Gert	Back-barrier/lagoon	1	2	1	2,5
3576	3836,20	12585	11	Gert	Back-barrier/lagoon	2	1	0	2,5
3578	3837,16	12589	1	Gert	Back-barrier/lagoon	0	0	3	0
3579	3837,71	12590	11	Gert	Back-barrier/lagoon	2	2	1	1,5
3846	3837,96	12591	9	Gert	Back-barrier/lagoon	2	2	2	2,5
3581	3838,09	12592	2	Gert	Back-barrier/lagoon	1	0	3	1
3580	3838,13	12592	3	Gert	Back-barrier/lagoon	1	0	3	1
3523	3838,37	12593	1	Gert	Back-barrier/lagoon	1	1	1	3
3780	3838,71	12594	2	Gert	Back-barrier/lagoon	2	1	1	2
3582	3839,59	12597	1	Gert	Back-barrier/lagoon	0	0	3	0
3583	3839,96	12598	4	Gert	Back-barrier/lagoon	0	0	3	0
3584	3840,92	12601	5	Gert	Back-barrier/lagoon	0	0	3	0
3585	3840,93	12601	6	Gert	Back-barrier/lagoon	0	0	3	0
3847	3841,51	12603	5	Gert	Back-barrier/lagoon	0	0	3	0
3586	3841,53	12603	5	Gert	Back-barrier/lagoon	0	0	3	0
3587	3842,01	12605	0	Gert	Back-barrier/lagoon	0	0	3	0
3588	3844,47	12613	1	Gert	Back-barrier/lagoon	0	0	3	0
3589	3845,75	12617	3	Gert	Back-barrier/lagoon	0	0	3	0

Table 1E. Shows information from the examined samples in the Diamant-1 well. Samples marked by yellow have been described in detail and point counted.

Ravn-1

Sample No.	Depth (m)	Depth (ft)	Depth (in)	Member	"Environment"	Quartz cem.	Carb. cem.	Clay content	Est. Porosity
3802	4090,09	13418	11	Ravn	Lower shoreface	0	1	3	0,5
3803	4093,69	13430	9	Ravn	Lower shoreface	0	3	0	0
3804	4094,25	13432	7	Ravn	Lower shoreface	0	2	3	0,5
3805	4098,49	13446	6	Ravn	Lower shoreface	0	3	0	0
3806	4105,44	13469	3	Ravn	Lower shoreface	0	2	3	0,5
3807	4112,57	13492	8	Ravn	Lower shoreface	1	2	3	0,5
3808	4113,04	13494	3	Ravn	Middle shoreface	1	3	3	0,5
3809	4113,28	13495	0	Ravn	Middle shoreface	0	3	0	0
3810	4113,44	13495	6	Ravn	Middle shoreface	0	3	0	0
3811	4114,25	13498	2	Ravn	Middle shoreface	0	1	3	0,5
3812	4114,55	13499	2	Ravn	Middle shoreface	2	3	0	2
3813	4114,80	13500	0	Ravn	Middle shoreface	0	3	0	0
3814	4115,03	13500	9	Ravn	Middle shoreface	0	3	0	0
3470	4115,25	13501	6	Ravn	Middle shoreface	2	3	0	1
3815	4115,70	13502	11	Ravn	Middle shoreface	2	2	2	2,5
3471	4115,90	13503	7	Ravn	Middle shoreface	2	2	3	1
3816	4116,38	13505	2	Ravn	Middle shoreface	1	1	2	2
3817	4119,38	13515	0	Ravn	Middle shoreface	1	2	2	1
3818	4119,80	13516	5	Ravn	Middle shoreface	1	1	1	1,5
3472	4120,57	13518	11	Ravn	Middle shoreface	2	2	1	1
3473	4122,88	13526	6	Ravn	Middle shoreface	2	1	1	1,5
3819	4123,00	13526	11	Ravn	Middle shoreface	1	1	2	2,5
3820	4124,68	13532	5	Ravn	Middle shoreface	0	3	0	0
3821	4125,05	13533	8	Ravn	Middle shoreface	0	3	0	0
3822	4125,38	13534	9	Ravn	Middle shoreface	3	3	1	1,5
3823	4125,70	13535	9	Ravn	Middle shoreface	1	2	2	1,5
3824	4128,52	13545	0	Ravn	Lower shoreface	0	0	3	0
3825	4129,05	13546	9	Ravn	Lower shoreface	0	3	0	0
3826	4132,80	13559	1	Ravn	Middle shoreface	1	2	2	1,5
3827	4135,31	13567	3	Ravn	Middle shoreface	1	2	2	2
3474	4135,55	13568	1	Ravn	Middle shoreface	1	1	3	1
3828	4136,64	13571	8	Ravn	Middle shoreface	0	3	1	0
3829	4137,16	13573	4	Ravn	Middle shoreface	1	2	2	2,5
3830	4140,88	13585	7	Ravn	Middle shoreface	3	1	0	2
3831	4142,15	13589	9	Ravn	Middle shoreface	3	1	2	2
3832	4142,88	13592	2	Ravn	Middle shoreface	3	2	2	1,5
3833	4145,04	13599	3	Ravn	Middle shoreface	3	3	1	1
3834	4151,07	13619	0	Ravn	Lower shoreface	0	3	0	0
3835	4152,40	13623	4	Ravn	Lower shoreface	0	0	3	0
3836	4152,76	13624	6	Ravn	Lower shoreface	2	2	2	1,5

Table 1F. Shows information from the examined samples in the Ravn-1 well. Samples marked by yellow have been described in detail and point counted.

Ravn-2

Sample No.	Depth (m)	Depth (ft)	Depth (in)	Member	"Environment"	Quartz cem.	Carb. cem.	Clay content	Est. Porosity
4281	4259,14	13973	7	Ravn	Lower shoreface	0	3	1	0
4282	4259,44	13974	6	Ravn	Lower shoreface	0	1	3	0
4283	4259,74	13975	6	Ravn	Lower shoreface	0	2	3	0
4284	4260,10	13976	8	Ravn	Lower shoreface	2	2	2	1
4285	4260,31	13977	5	Ravn	Lower shoreface	1	3	2	0,5
4286	4260,87	13979	3	Ravn	Lower shoreface	0	3	2	0
4287	4261,00	13979	8	Ravn	Lower shoreface	1	3	2	0
4288	4261,53	13981	5	Ravn	Lower shoreface	2	2	2	1
4289	4262,43	13984	4	Ravn	Lower shoreface	3	2	3	1
4290	4262,87	13985	10	Ravn	Lower shoreface	0	1	3	0
4291	4263,31	13987	3	Ravn	Lower shoreface	2	3	0	0
4292	4263,48	13987	10	Ravn	Lower shoreface	1	3	0	0,5
4293	4263,83	13988	11	Ravn	Lower shoreface	3	1	3	1
4294	4263,91	13989	2	Ravn	Lower shoreface	1	2	3	0,5
4295	4264,99	13992	9	Ravn	Lower shoreface	2	1	1	0,5
4296	4265,36	13994	0	Ravn	Lower shoreface	2	1	2	2
4297	4266,03	13996	2	Ravn	Lower shoreface	1	1	2	1,5
4298	4266,21	13996	9	Ravn	Lower shoreface	1	2	2	1
4299	4266,41	13997	5	Ravn	Lower shoreface	1	3	1	1
4300	4266,49	13997	8	Ravn	Lower shoreface	1	3	1	1
4301	4270,28	14010	1	Ravn	Lower shoreface	1	3	1	1
4302	4270,51	14010	10	Ravn	Lower shoreface	1	3	1	1
4303	4271,02	14012	6	Ravn	Lower shoreface	1	1	3	1
4304	4271,25	14013	3	Ravn	Lower shoreface	2	2	2	1,5
4305	4272,88	14018	8	Ravn	Lower shoreface	3	1	1	1
4306	4273,01	14019	1	Ravn	Lower shoreface	3	1	1	0,5
4307	4273,66	14021	2	Ravn	Lower shoreface	3	1	1	1
4308	4273,81	14021	8	Ravn	Lower shoreface	3	2	1	2
4309	4274,30	14023	4	Ravn	Lower shoreface	2	2	2	2
4310	4274,74	14024	9	Ravn	Lower shoreface	2	2	2	2
4311	4276,75	14031	4	Ravn	Lower shoreface	1	2	2	2
4312	4277,78	14034	9	Ravn	Lower shoreface	1	2	2	2
4313	4279,60	14040	8	Ravn	Lower shoreface	2	2	3	1

Table 1G. Shows information from the examined samples in the Ravn-2 well. Samples marked by yellow have been described in detail and point counted.

APPENDIX 2: FIGURES

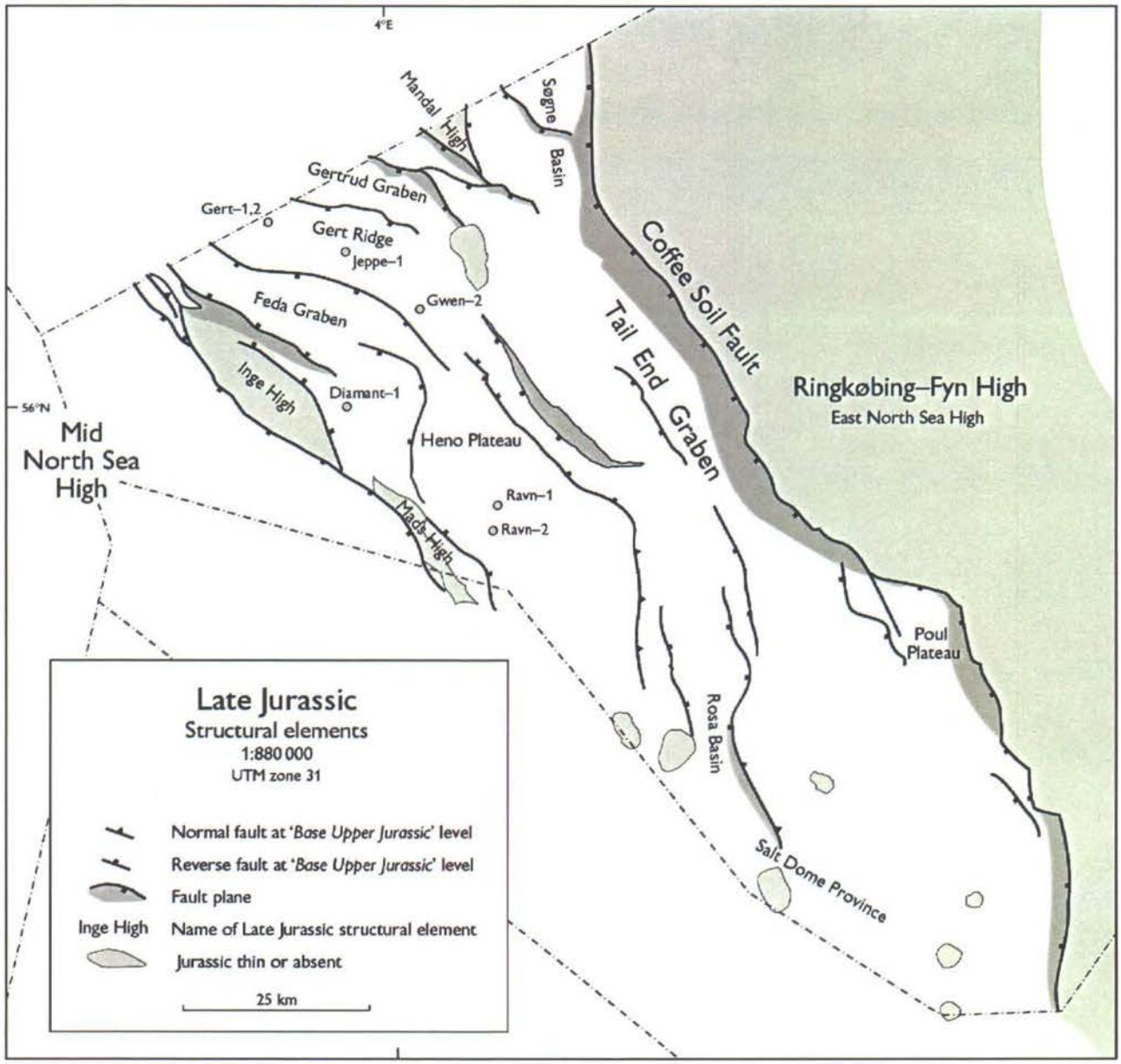
4°E
56°N
Mandal High
Søgne Basin
Gertrud Graben
Gert–1,2
Gert Ridge
Jeppe–1
Gwen–2
Feda Graben
Inge High
Diamant–1
Mid North Sea High
Heno Plateau
Ravn–1
Ravn–2
Mads High
Coffee Soil Fault
Tail End Graben
Ringkøbing–Fyn High
East North Sea High
Poul Plateau
Rosa Basin
Salt Dome Province
Late Jurassic
Structural elements
1:880 000
UTM zone 31
Normal fault at 'Base Upper Jurassic' level
Reverse fault at 'Base Upper Jurassic' level
Fault plane
Inge High
Name of Late Jurassic structural element
Jurassic thin or absent
25 km

Fig.01

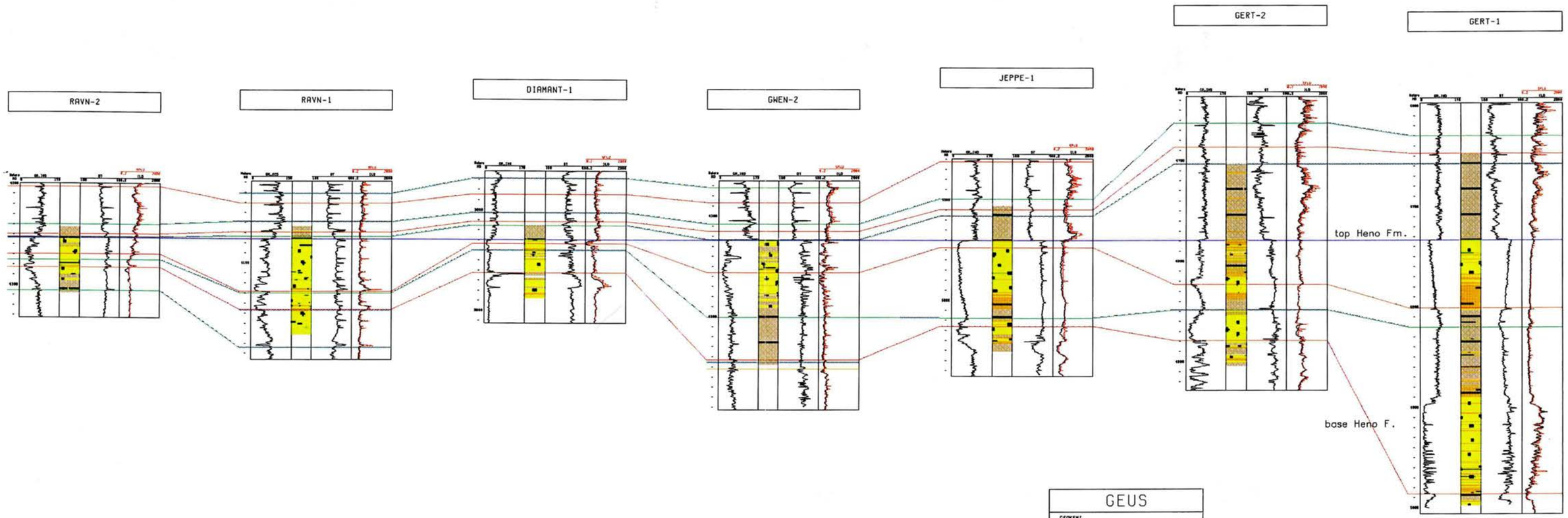

GEUS

GEOKEMI

Danish Central Graben

1:4000	1:3948	YE = 0.985
METERS	METERS	
JTH.J	03.01.2002	

Figure 2

Log panel. all project wells S - N

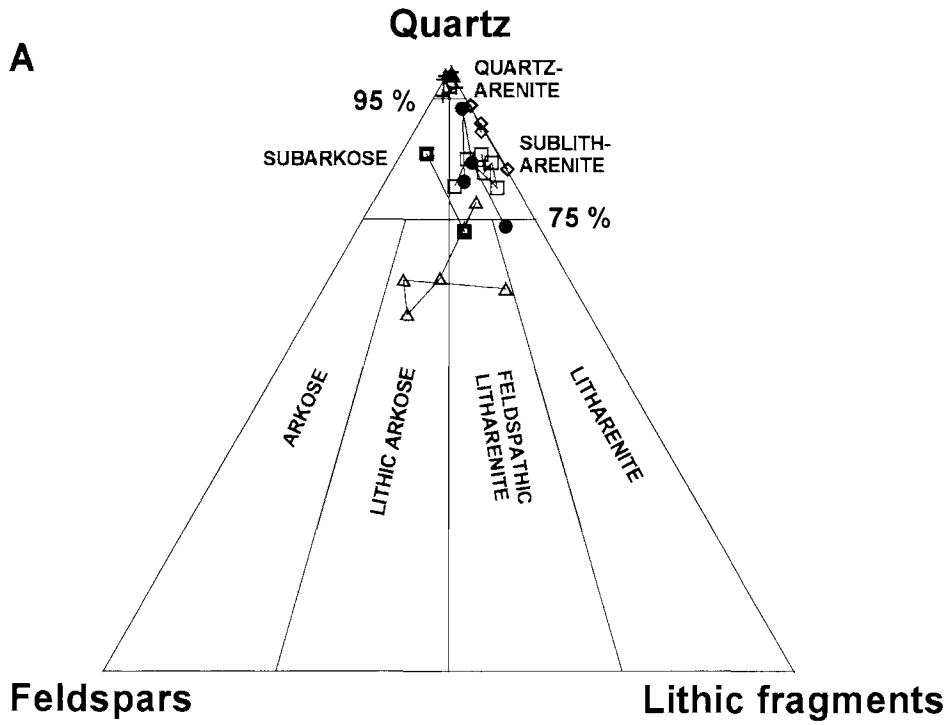

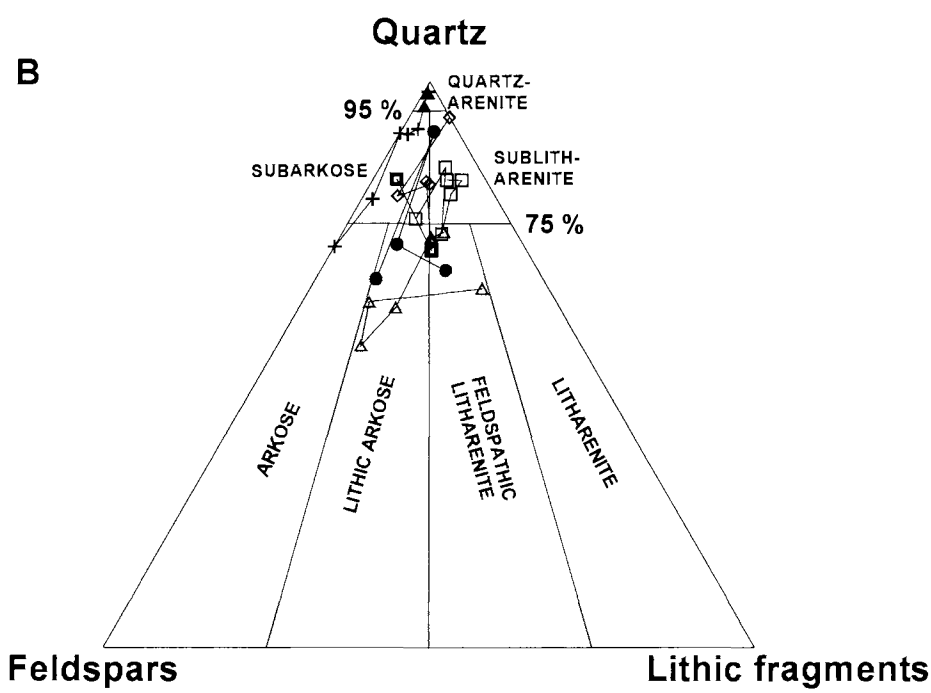

Figure 3. Detrital composition of the Upper Jurassic sandstones from Diamant-1(◇), Gert-1(+), Gert-2(▲), Gwen-2 (●), Jeppe-1(Δ), Ravn-1 (□) and Ravn-2 (◘)(after Folk, 1968). Figure 3A shows the present sandstone composition and 3B shows the corrected and estimated original sandstone composition. The correction is carried out, by assuming secondary porosity and kaolinite as former feldspars, and thus adding these to the content of feldspar.

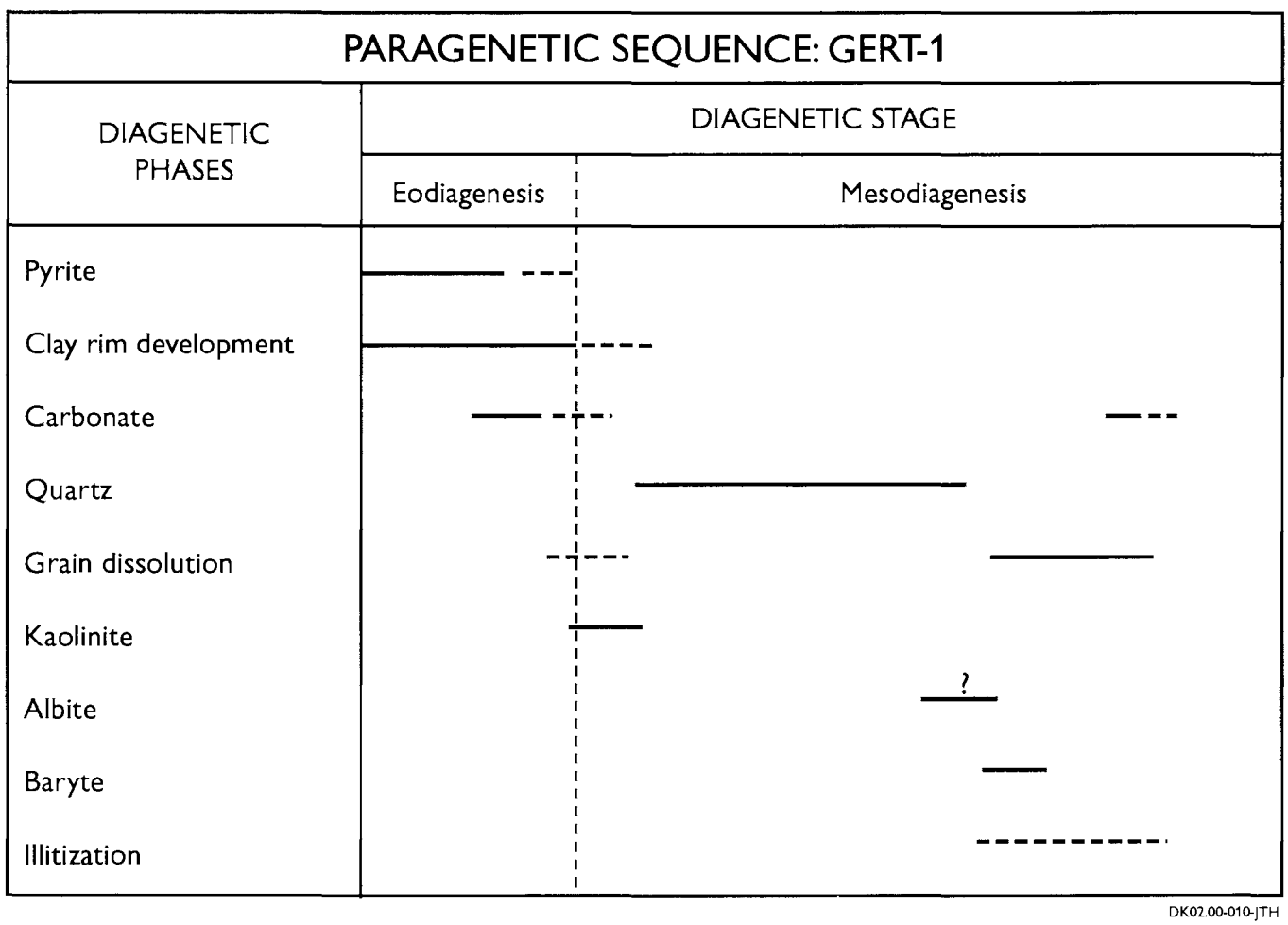

Figure 4A. Paragenetic sequence for the sandstones in well Gert-1.

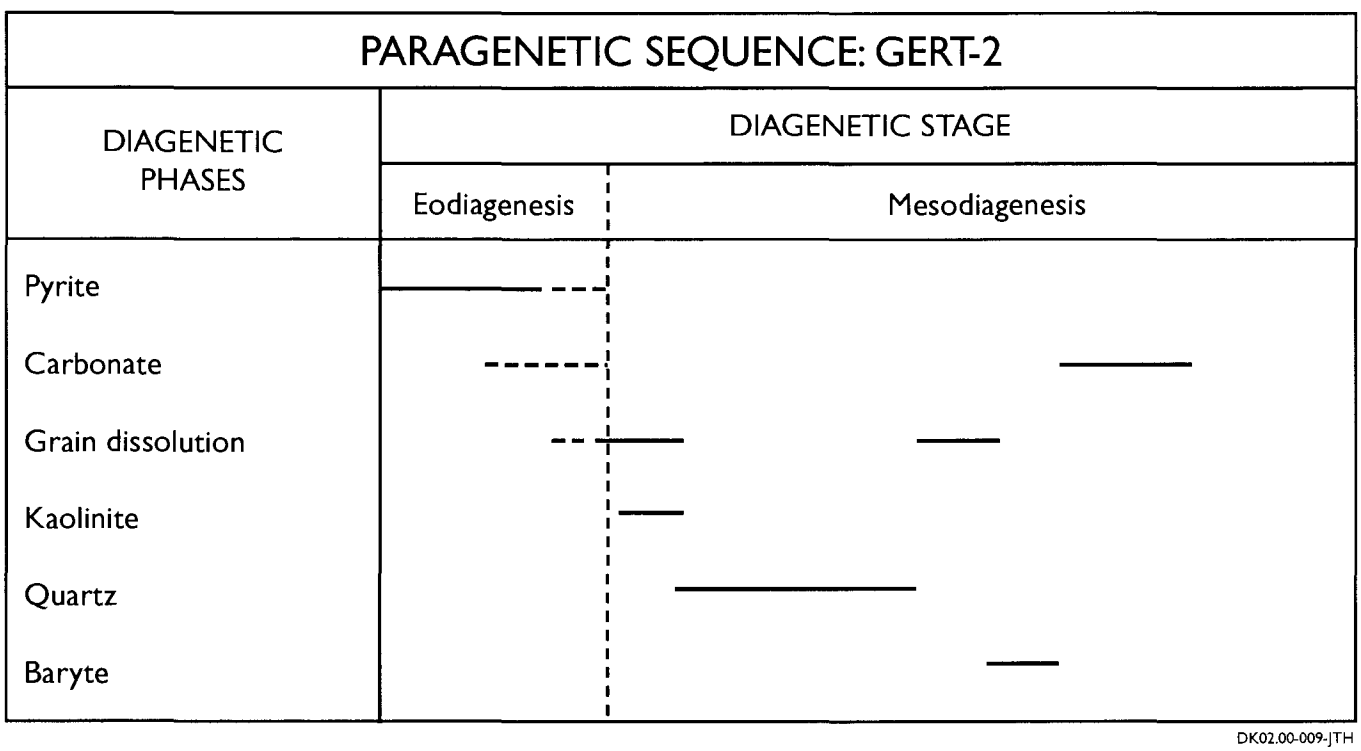

Figure 4B. Paragenetic sequence for the sandstones in well Gert-2.

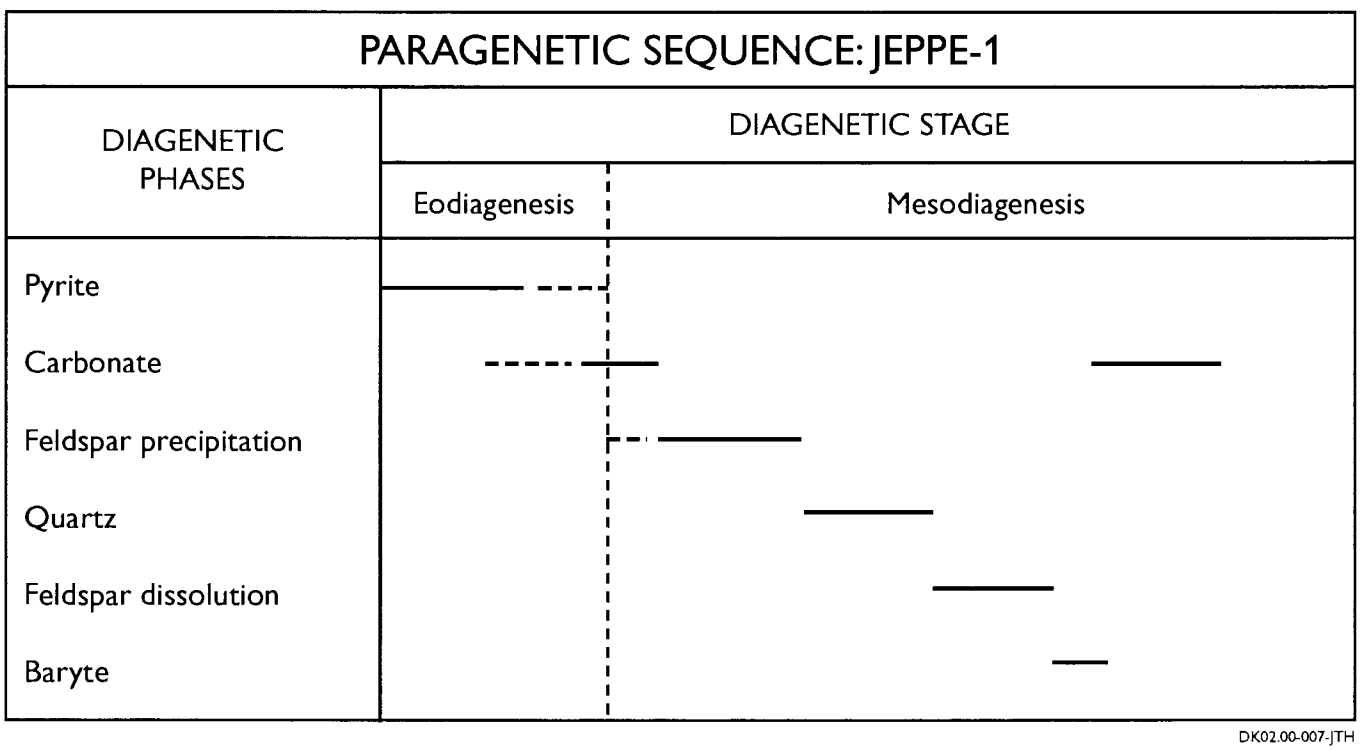

Figure 4C. Paragenetic sequence for the sandstones in well Jeppe-1.

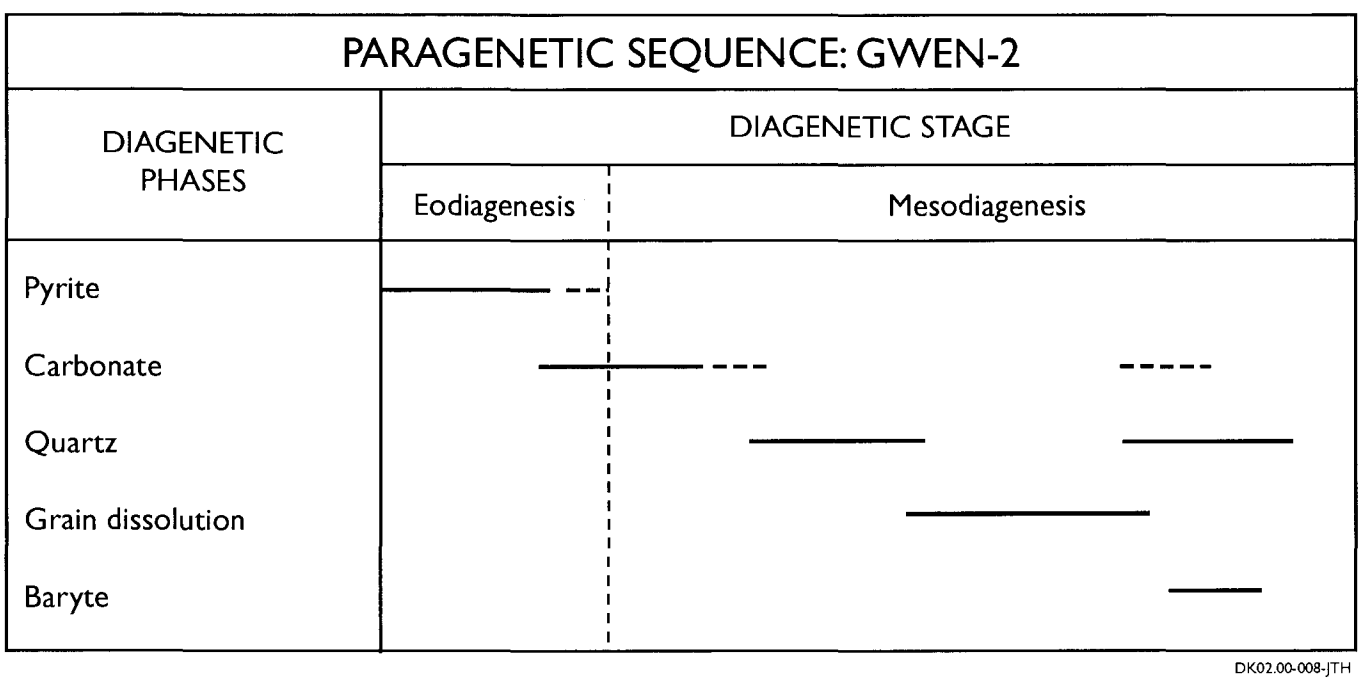

Figure 4D. Paragenetic sequence for the sandstones in well Gwen-2.

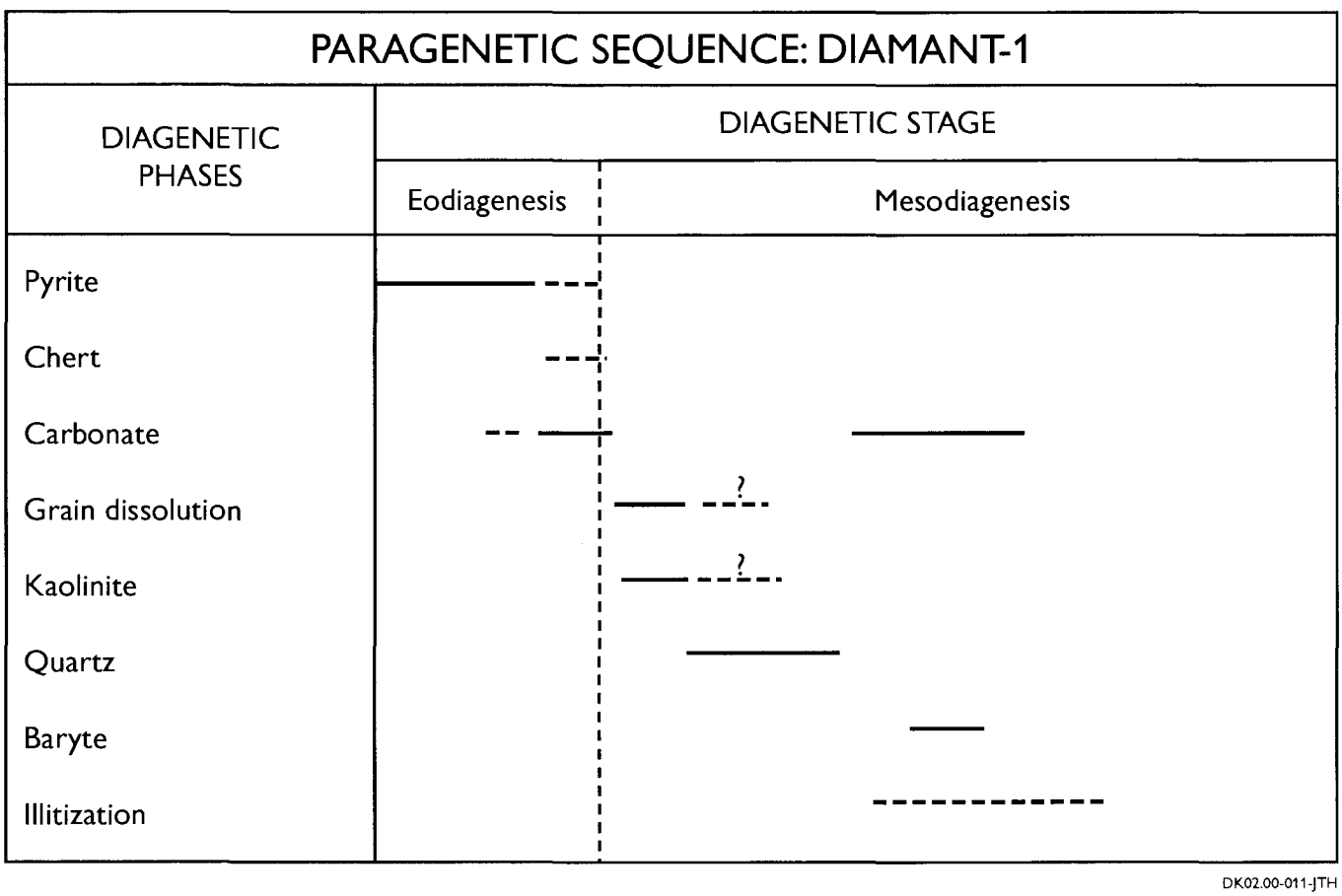

Figure 4E. Paragenetic sequence for the sandstones in well Diamant-1.

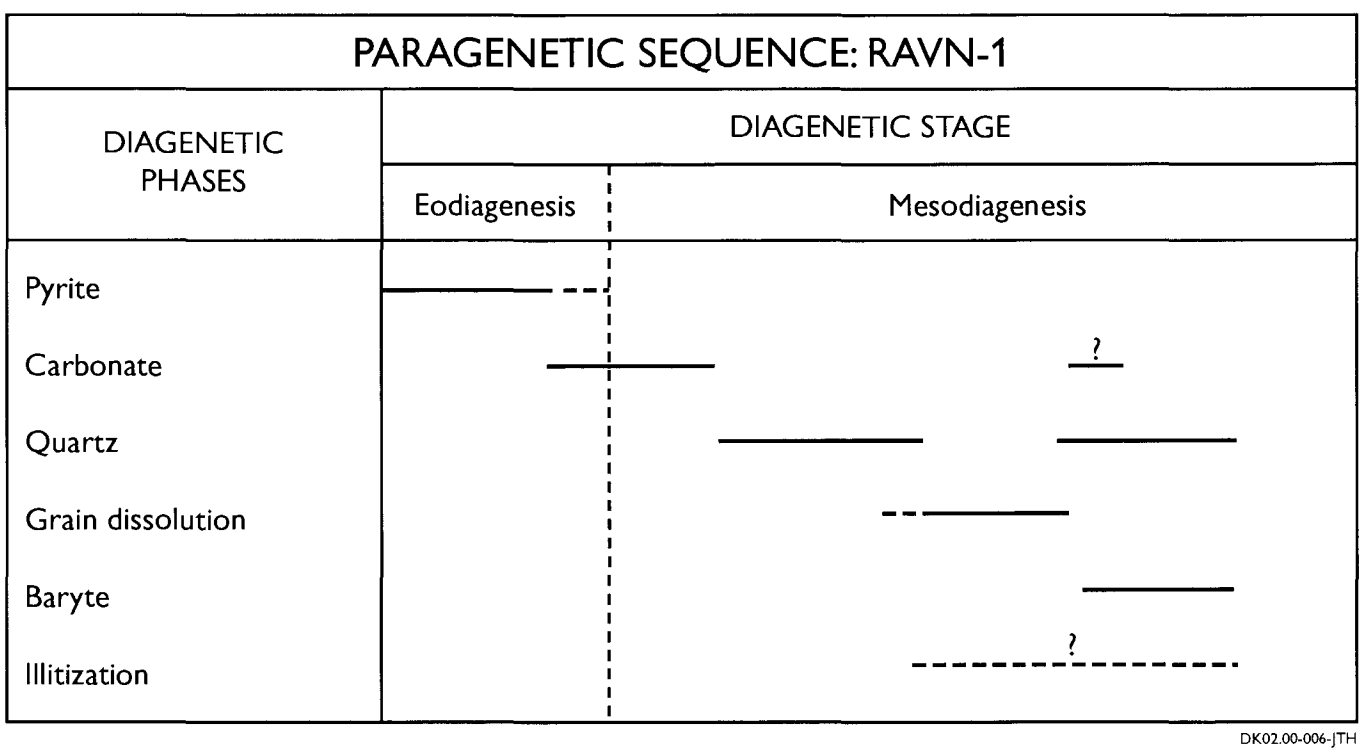

Figure 4F. Paragenetic sequence for the sandstones in well Ravn-1.

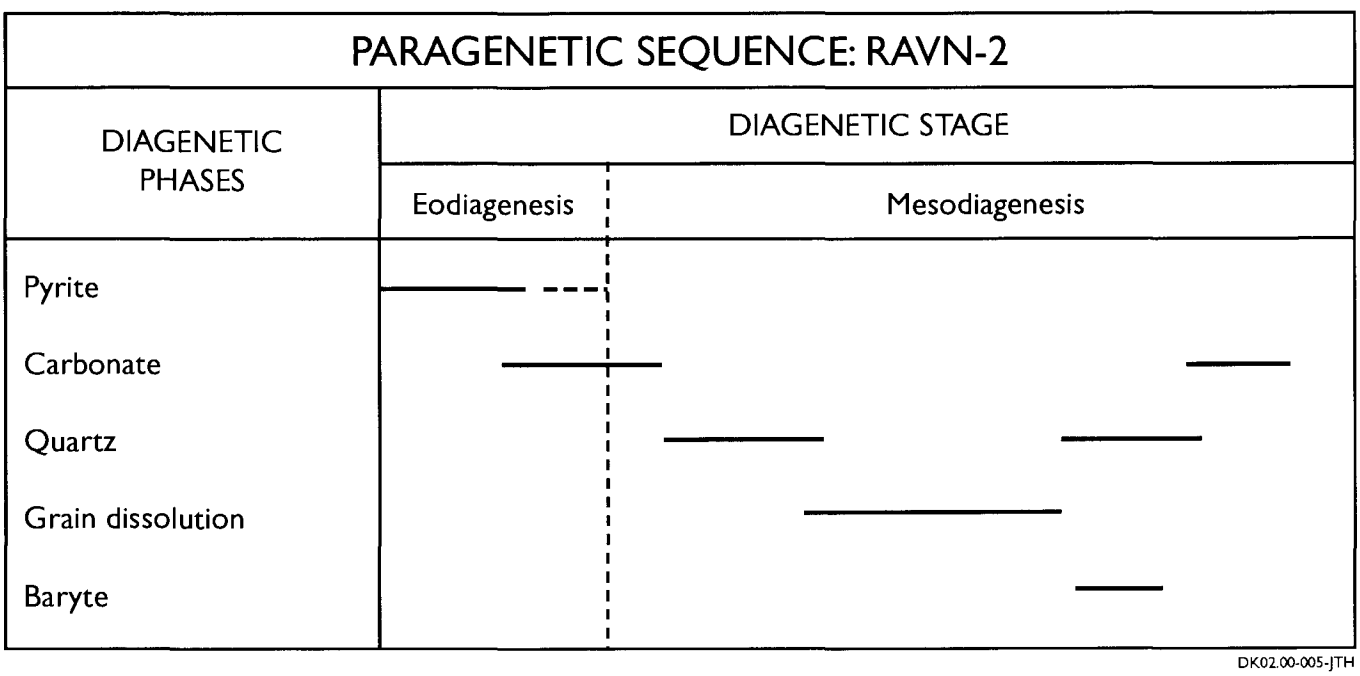

Figure 4G. Paragenetic sequence for the sandstones in well Ravn-2.

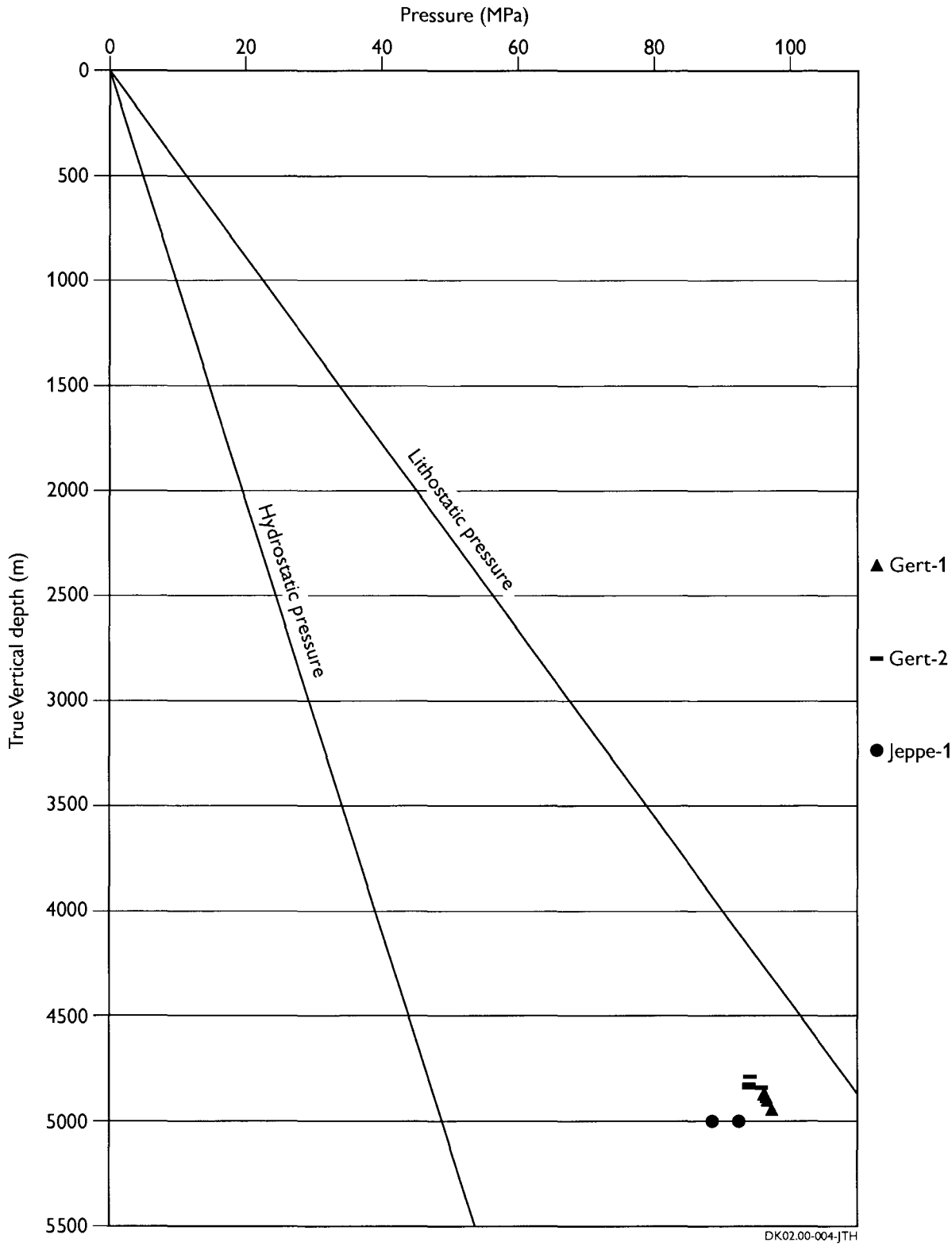

Figure 5. Pressure conditions (RTF data) for 3 of the examined wells, which shows that the sandstones are at the present in a state of high overpressure.

APPENDIX 3: PLATES

Thin section photomicrographs
Well: GERT-1 Depth: 4921.4m

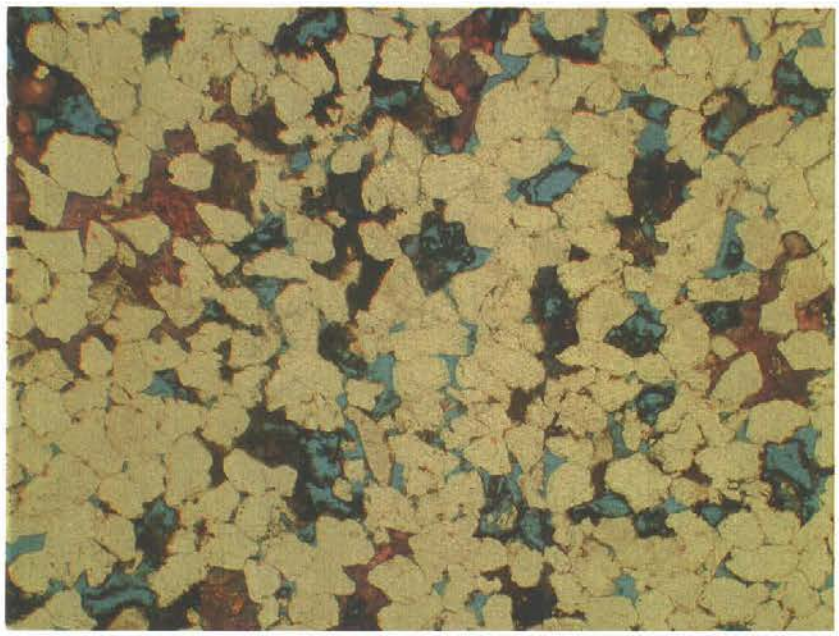

Plate 1. This general view displays a very well to well sorted, fine-grained quartzarenite, showing widespread quartz cementation, scattered calcite cement (coloured red) and relative high porosity dominated by secondary pores (outlined by dark-stained clay-rims). Field of view 3.4 x 2.6mm, PPL, Alizarin Red S stained.

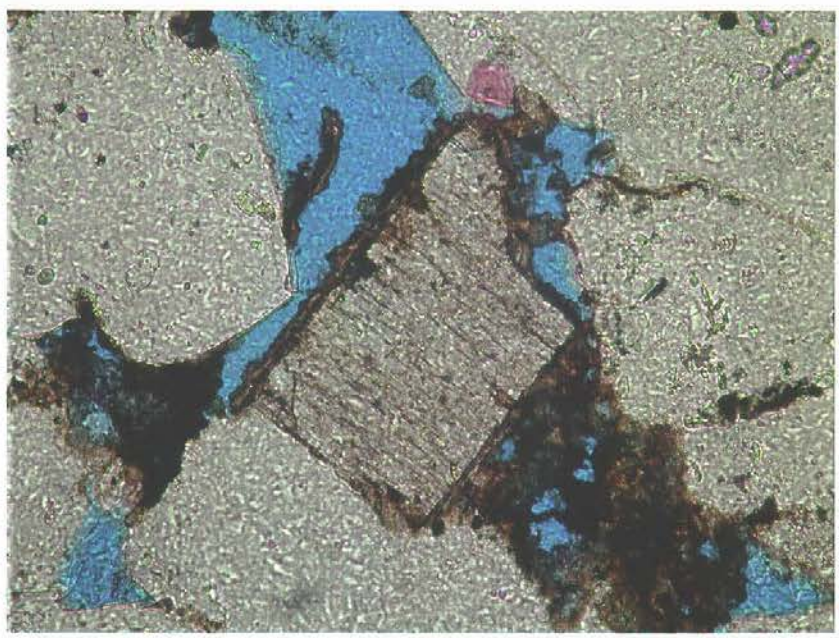

Plate 2. This detailed view shows one of the few non-dissolved detrital feldspar grains, which occurs in the sample. The grain occurs with a typical dark-stained clay-rim. As illustrated in plate 1 are these clay-rims widespread in the sample, and are actually ghosts marking the presence of former detrital feldspars. Field of view 0.5 x 0.4mm, PPL, Alizarin Red S stained.

Thin section photomicrographs
Well: GERT-1 Depth: 4927.32m

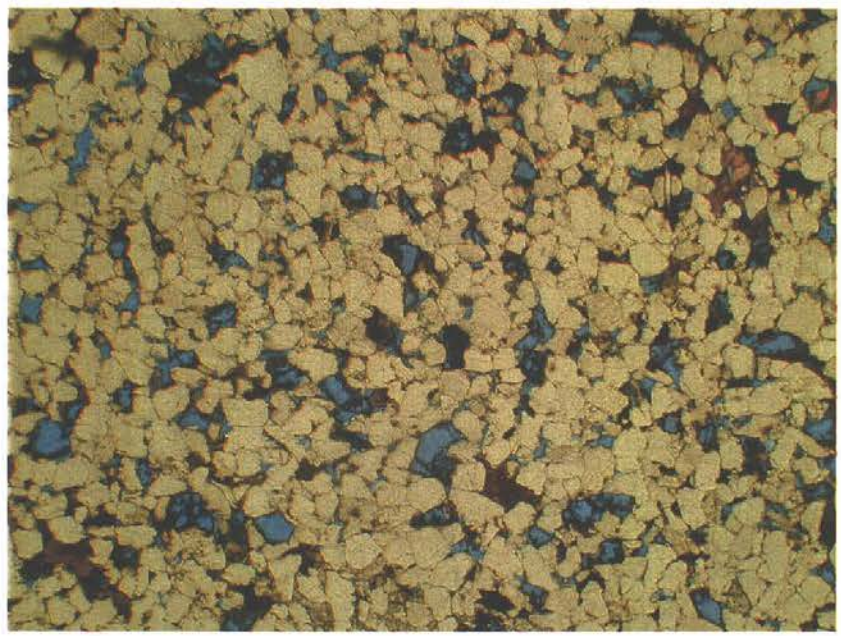

Plate 3. This general view displays a well sorted medium-grained quartzarenite, showing widespread quartz cementation, scattered calcite cement (coloured red), scattered baryte (lowest centre of photo), scattered pyrite and relative high macro-porosity dominated by secondary pores (outlined by dark-stained clay-rims). Field of view 5.6 x 4.2mm, PPL, Alizarin Red S stained.

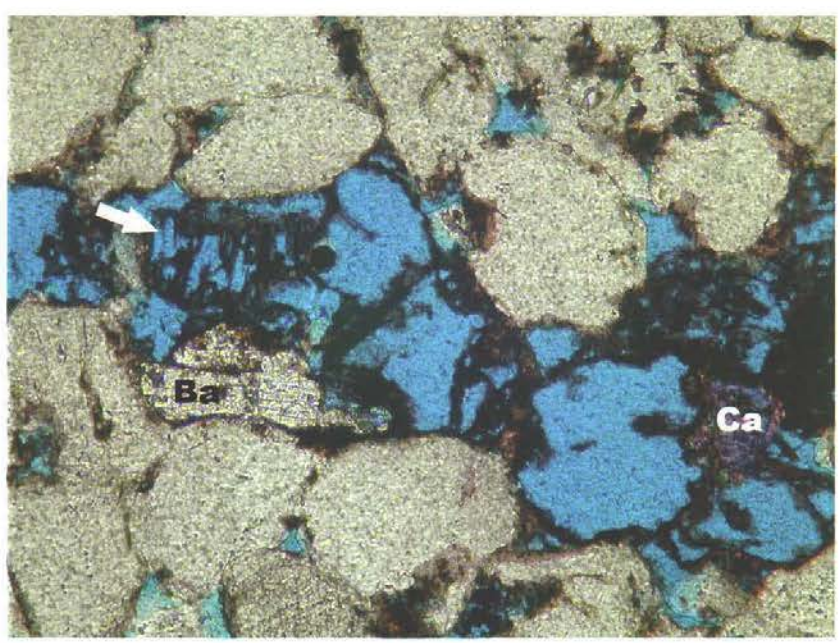

Plate 4. This detailed view shows dissolved detrital feldspar grains, where the former detrital feldspars are outlined by the dark-stained clay-rims. Indication of fracturing of the former feldspar grains is shown by clay filled cracks (white arrow). Also seen are quartz cement, baryte cement (Ba) and calcite cement (Ca). Field of view 1.0 x 0.8mm, PPL, Alizarin Red S stained.

Thin section photomicrographs
Well: GERT-1 Depth: 4940.99m

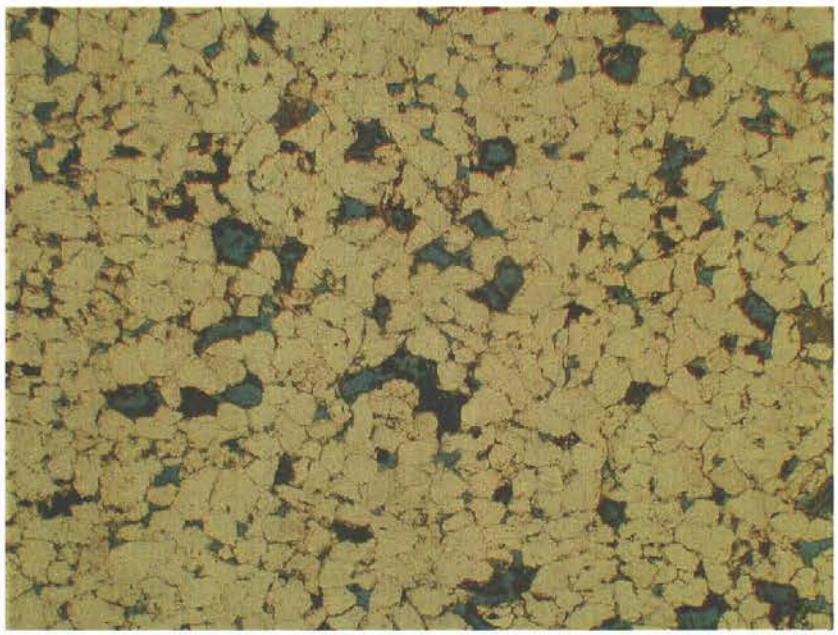

Plate 5. This general view displays a very well to well sorted fine-grained quartzarenite, showing severe quartz cementation, scattered pyrite and low macro-porosity dominated by secondary pores (outlined by dark-stained clay-rims). Note the very low interconnectivity between the secondary pores. Field of view 4.1 x 3.0mm, PPL.

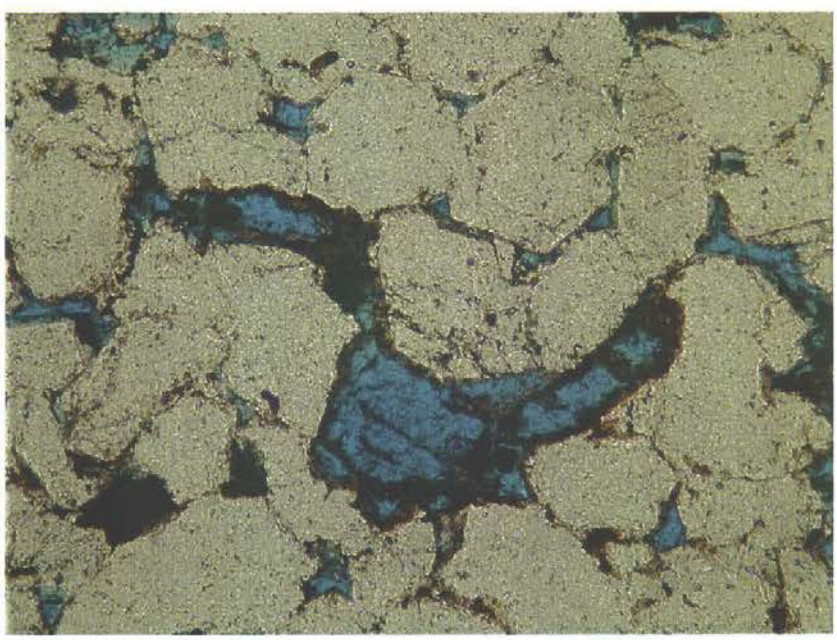

Plate 6. This detailed view shows severe quartz cementation, wherein secondary pores after dissolved detrital feldspar grains occur. Dust-rims occur between quartz overgrowths and the detrital grain. The remaining primary pores are very small and badly connected. Note that the feldspar dissolution is post-dating quartz cement. Field of view 1.0 x 0.8mm, PPL.

Thin section photomicrographs
Well: GERT-1 Depth: 4958.0m

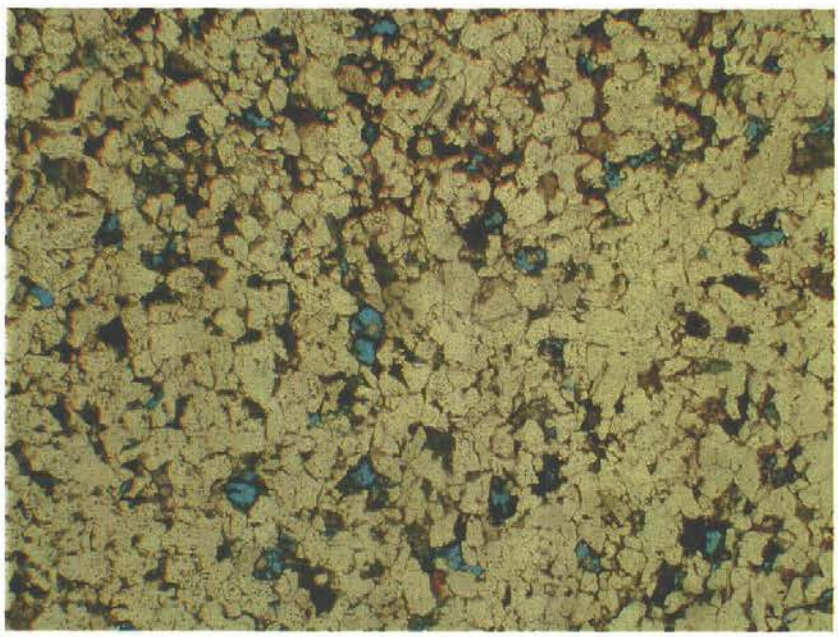

Plate 7. This general view displays a well sorted fine-grained quartzarenite, showing severe quartz cementation, scattered pyrite, organic matter, brownish clayey matrix and low macro-porosity dominated by secondary pores (outlined by dark-stained clay-rims). Note the very low interconnectivity between the secondary pores. Field of view 3.1 x 2.3mm, PPL.

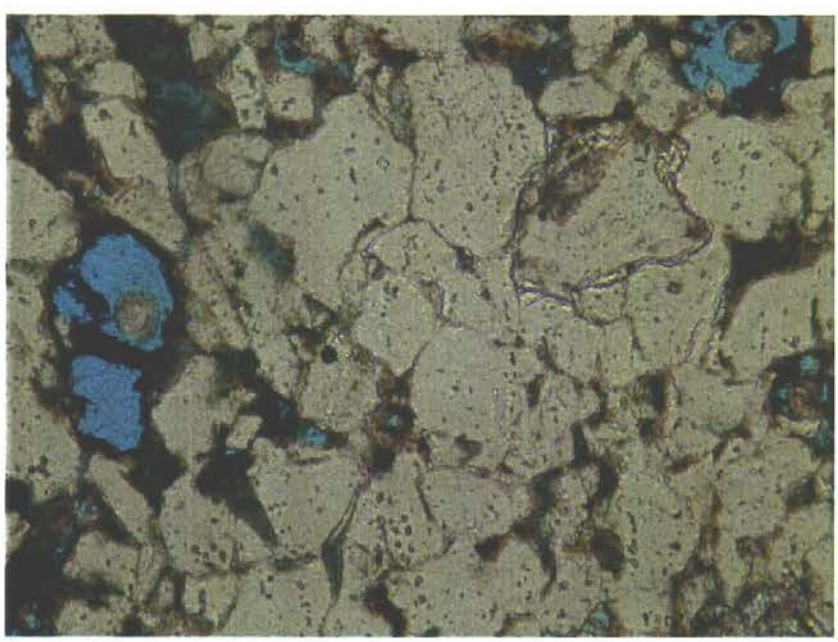

Plate 8. This detailed view shows severe quartz cementation, wherein secondary pores after dissolved detrital feldspar grains occur. Note that quartz cement both pre- and post-dates the feldspar dissolution (delicate quartz crystals are growing within secondary pore spaces. Field of view 1.0 x 0.8mm, PPL.

Thin section photomicrographs
Well: GERT-1 Depth: 4961.08m

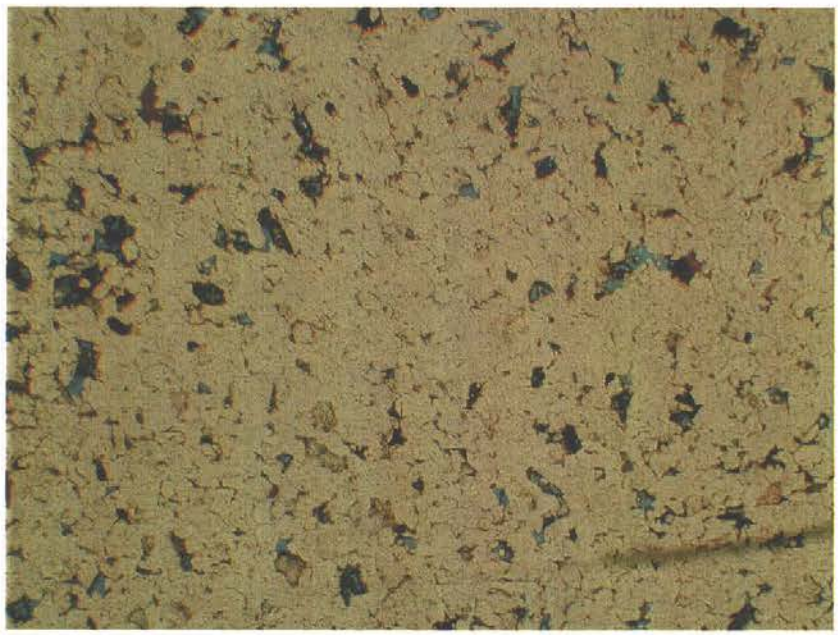

Plate 9. This general view displays a well sorted fine-grained quartzarenite, showing pore occluding quartz cement, rare calcite cement (coloured red), and low macro-porosity dominated by secondary pores (outlined by dark-stained clay-rims). Interconnectivity between pores is very low. Field of view 4.4 x 3.3mm, PPL, Alizarin Red S stained.

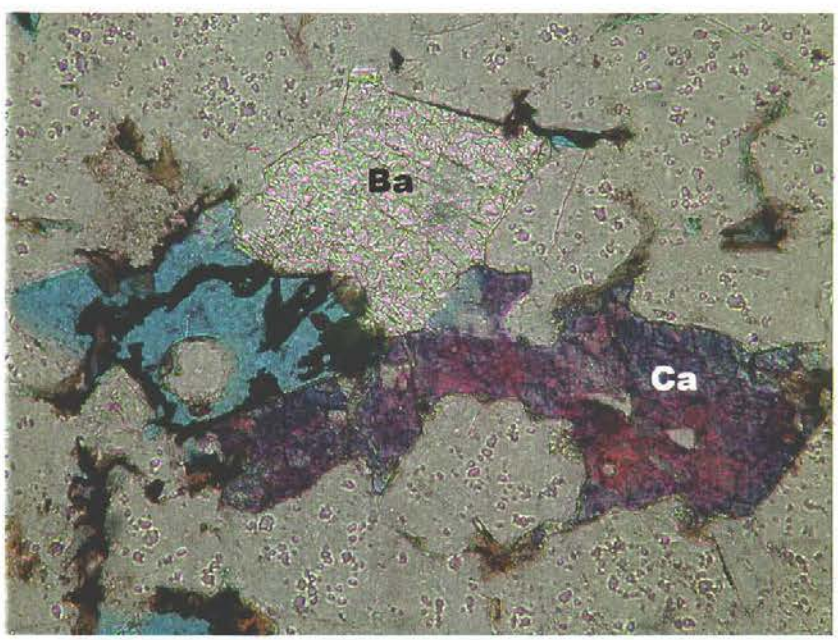

Plate 10. This detailed view shows secondary pore after dissolved detrital feldspar grain, quartz cement, baryte cement (Ba) and calcite cement (Ca). Note that baryte post-dates quartz cement and feldspar dissolution and pre-dates calcite. Field of view 0.5 x 0.4mm, PPL, Alizarin Red S stained.

Thin section photomicrographs
Well: GERT-1 Depth: 4973.24m

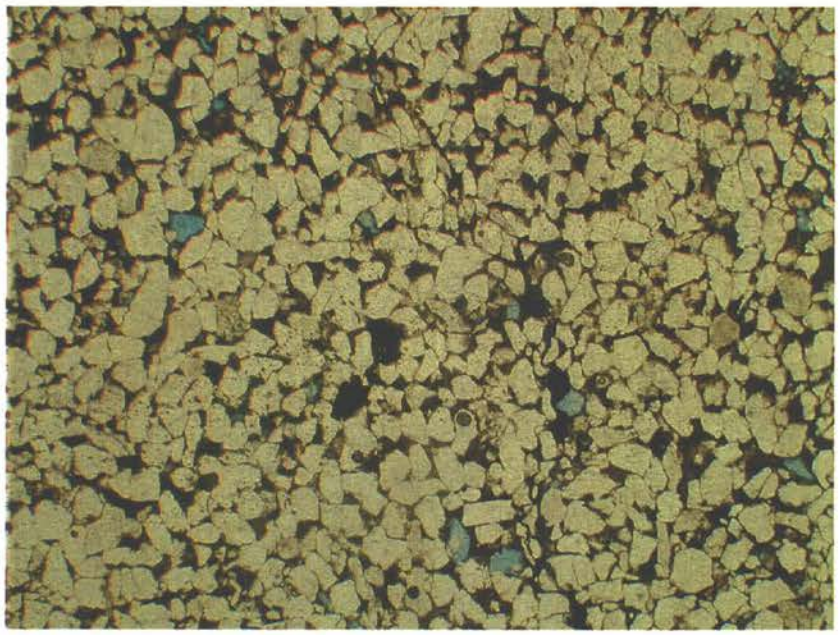

Plate 11. This general view displays a well sorted, fine-grained quartzarenite, showing some quartz cementation, organic matter, scattered pyrite, widespread dark detrital clayey matrix and low macro-porosity dominated by secondary pores. Note the more or less non-existing or very low interconnectivity between the secondary pores. Field of view 4.1 x 3.0mm, PPL.

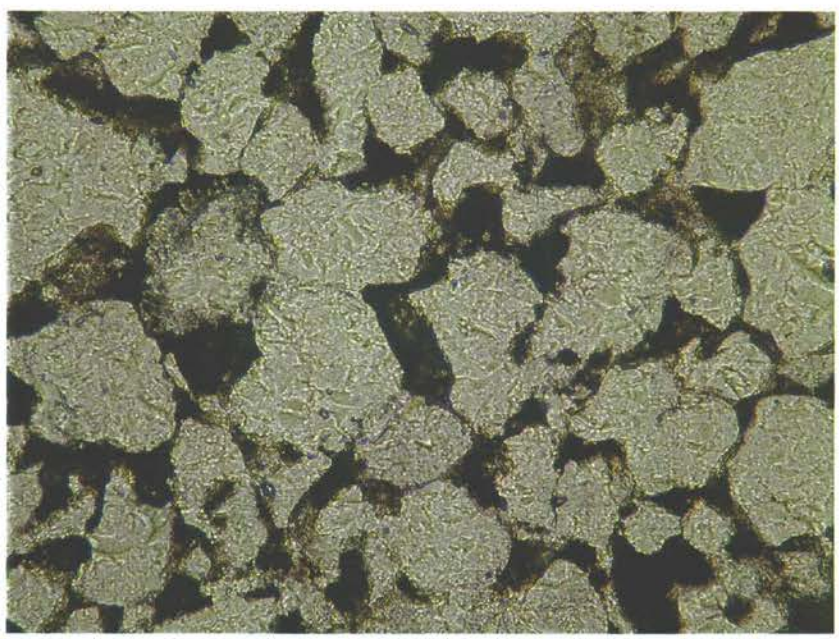

Plate 12. Widespread dark detrital clay, which is filling pore spaces, inhibits development of significant quartz cement. No macro-porosity is present in primary pore spaces and permeability is very low. Field of view 1.0 x 0.7mm, PPL.

Thin section photomicrographs
Well: GERT-2 Depth: 4817.67m

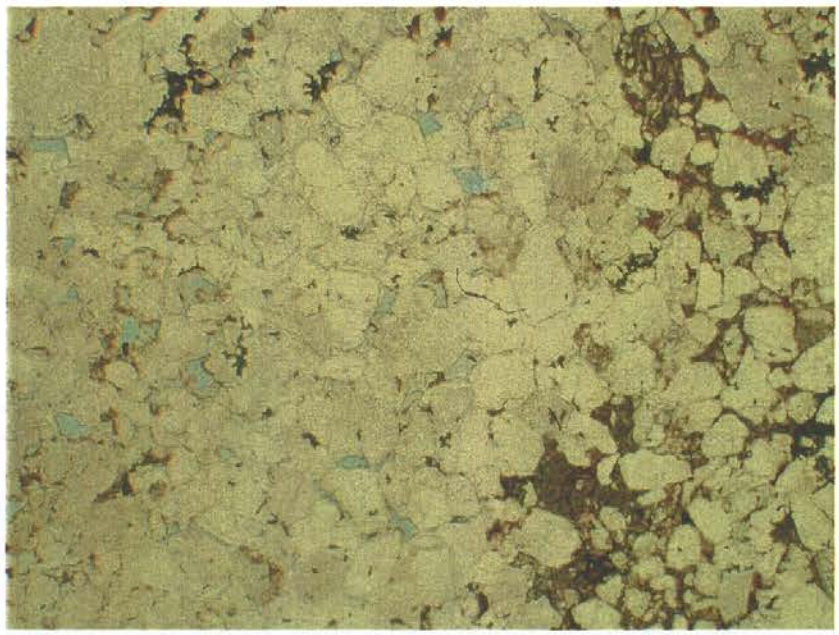

Plate 13. This general view displays a well to moderately sorted fine-grained quartzarenite, showing severe quartz cementation (on the left-hand side), with low macro-porosity (both primary and secondary). On the right-hand side brownish detrital clay is filling the pore spaces. Note the very low interconnectivity between pores in the quartz cemented area. Field of view 4.4 x 3.3mm, PPL.

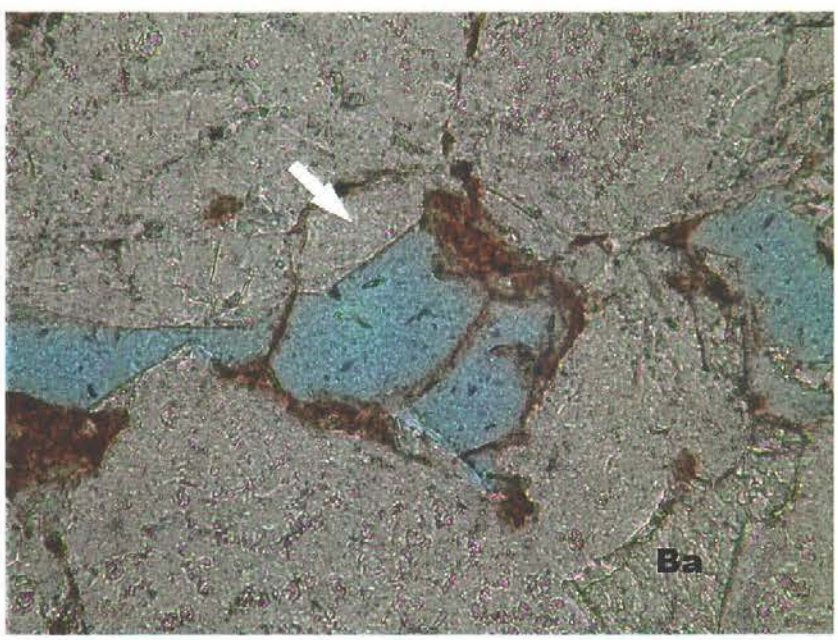

Plate 14. This detailed view shows severe quartz cementation, wherein secondary pores after dissolved detrital feldspar grains occur. Note that quartz cement both pre- and post-dates the feldspar dissolution (quartz crystal is growing within secondary pore spaces; white arrow). Baryte (Ba) occurs as a post-quartz pore filling cement. Field of view 0.4 x 0.3mm, PPL.

Thin section photomicrographs
Well: GERT-2 Depth: 4870.48m

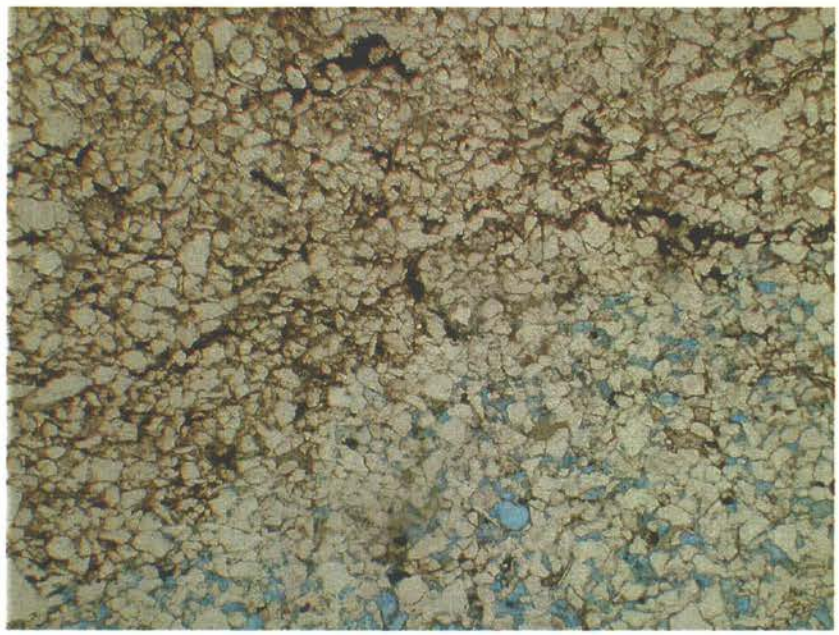

Plate 15. This general view displays a moderately sorted very fine-grained quartz wacke, showing weak quartz cementation (in the lower clay free zone), scattered pyrite and high macro-porosity (both primary and secondary) with good interconnectivity between pores. In the upper clay-rich part side brownish detrital clay, organic matter and pyrite is filling the pore spaces, with no macro-porosity to be present as a result. Field of view 4.7 x 3.5mm, PPL.

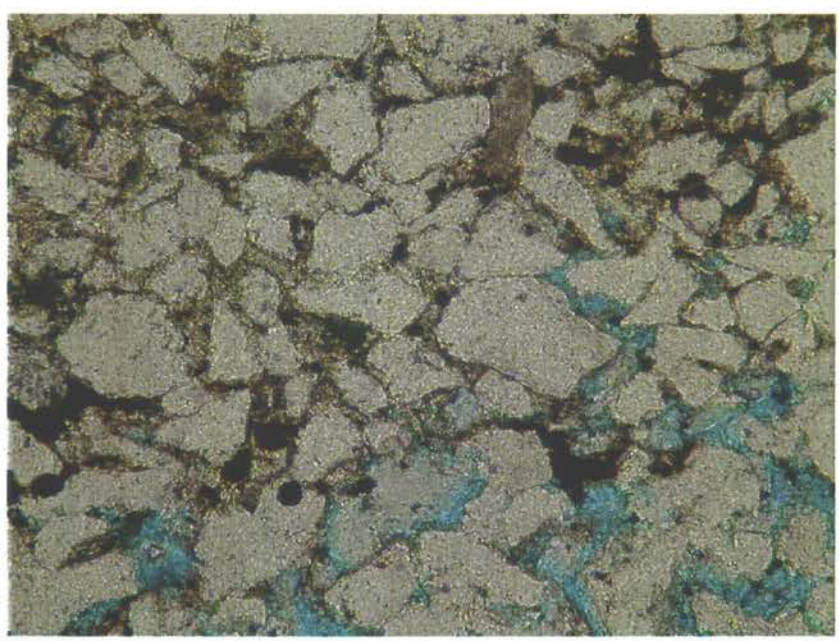

Plate 16. Close up of the boarder-area between clay-filled and clay-free pore spaces. Pyrite and organic matter occur in the pore spaces. Note the presence of long and concavo-convex point contacts, especially in the clay-filled area, which hamper interconnectivity between pores even more. Field of view 0.9 x 0.7mm, PPL.

Thin section photomicrographs
Well: GERT-2 Depth: 4873.73m

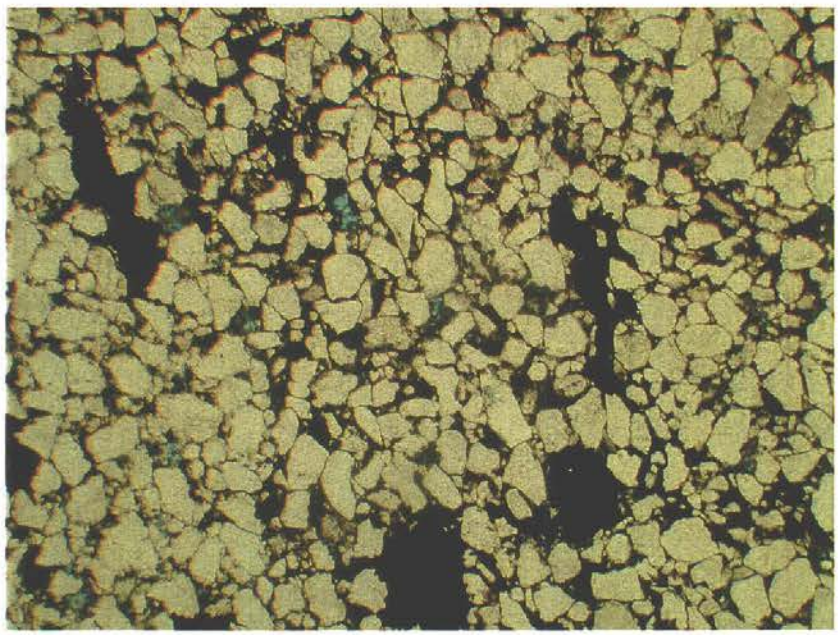

Plate 17. This general view displays a moderately sorted fine-grained quartzarenite, dominated by pyritized organic matter, weak quartz cementation, dark brownish detrital clay and very low macro-porosity. Very low interconnectivity between pores. Field of view 4.2 x 3.2mm, PPL.

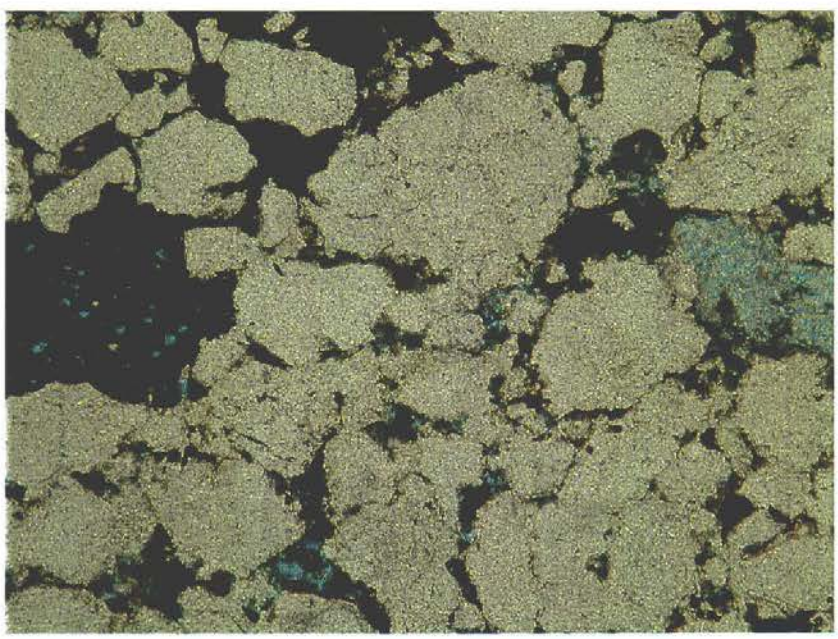

Plate 18. This detailed view shows on the left-hand side pyritized woody tissue, where some of the cell-cavities have preserved porosity. On the right-hand side a secondary pore contains kaolinite booklets. Field of view 1.3 x 1.0mm, PPL.

Thin section photomicrographs
Well: GERT-2 Depth: 4877.36m

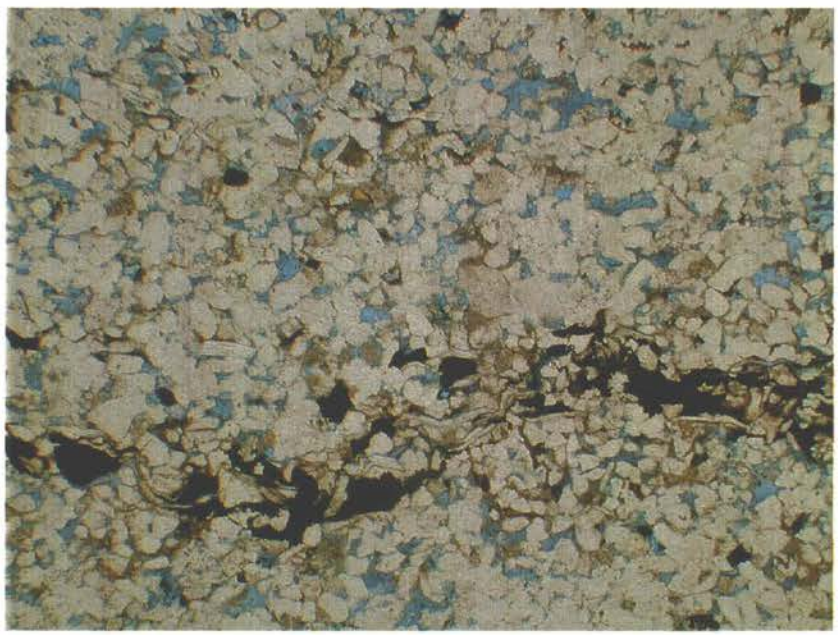

Plate 19. This general view displays a well sorted fine-grained quartzarenite, containing a lamina consisting of mica, organic matter and pyrite. Outside the lamina pore interconnectivity is good, while the lamina may work as a barrier for upward flowing fluids. Field of view 4.5 x 3.4mm, PPL.

Plate 20. This detailed view shows a close-up of the lamina, where mica occurs both bended and unaffected. Contacts between mica and quartz are often conform, showing dissolution of quartz. Note concavo-convex contacts between quartz grains in the lamina and quartz cement in the upper part of the photography. Field of view 1.0 x 0.7mm, PPL.

Thin section photomicrographs
Well: GERT-2 Depth: 4891.68m

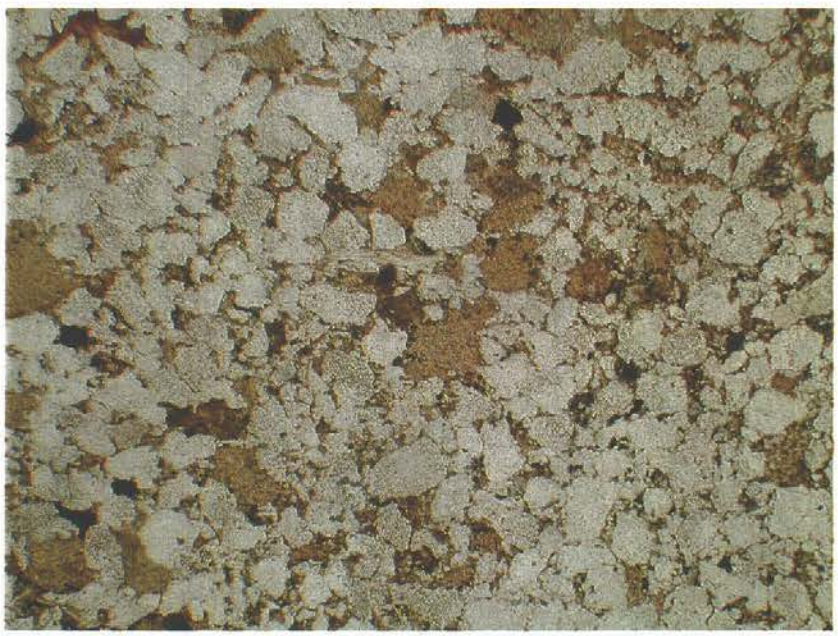

Plate 21. This general view displays a well to moderately sorted medium-grained quartzarenite, containing abundant brownish kaolinite booklets, which are totally in-filling oversized (secondary) pore spaces. Note the occurrence of quartz cement. Macro-porosity is very low and permeability is considerably reduced. Field of view 5.3 x 4.0mm, PPL.

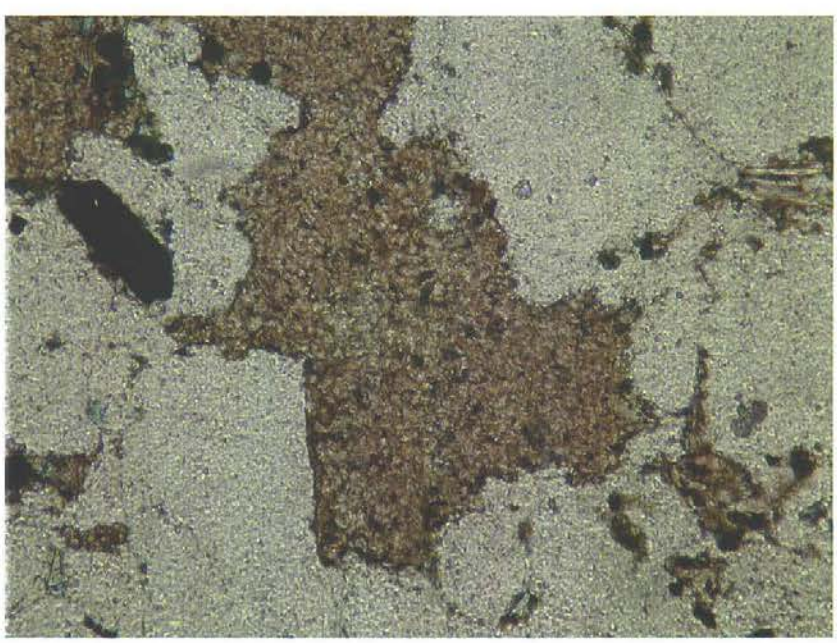

Plate 22. This detailed view illustrates the abundance and densely packed nature of the kaolinite booklets in secondary pore spaces. Note that quartz is overgrowing the kaolinite. Field of view 1.0 x 0.8mm, PPL.

Thin section photomicrographs
Well: JEPPE-1 Depth: 4939.28m

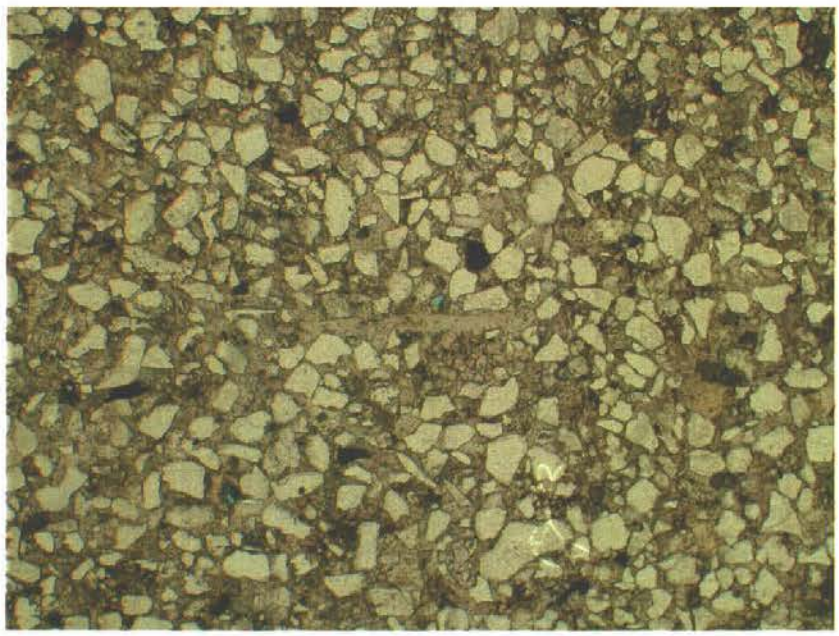

Plate 23. This general view displays a moderately sorted fine-grained feldspathic litharenite, showing total carbonate cementation. Note that the detrital grains are often "floating" in the carbonate cement. A few small secondary pores (coloured blue) occur. Field of view 4.3 x 3.3mm, PPL.

Plate 24. This detailed view shows a secondary pore, which occur in the pore occluding carbonate cement. The pore space is now partially filled by carbonate cement. Field of view 0.7 x 0.5mm, PPL.

Thin section photomicrographs
Well: JEPPE-1 Depth: 4940.04m

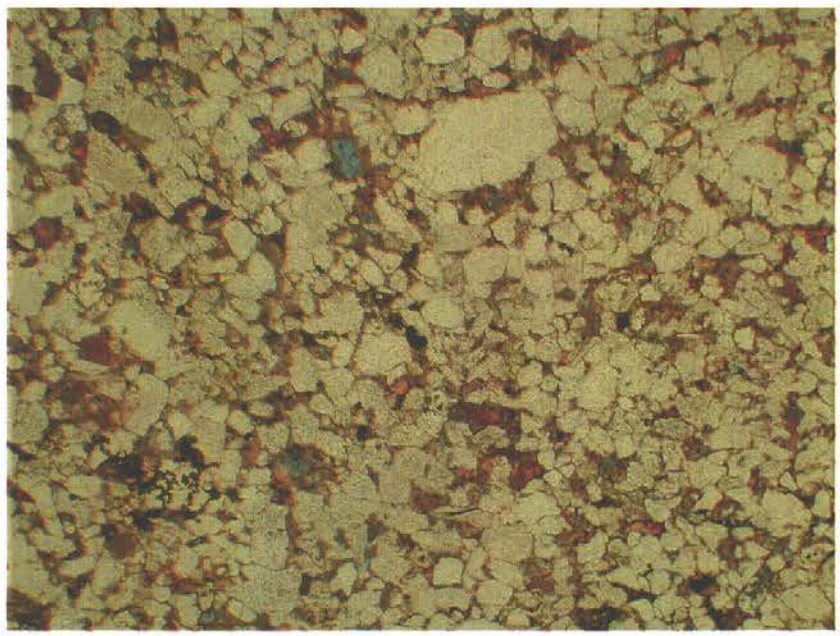

Plate 25. This general view displays a moderately to poorly sorted fine-grained sublitharenite, showing carbonate cementation (red and mauve), detrital clay and scattered secondary porosity. Numerous long, sutured and concavo-convex point contacts together with the detrital clay and carbonate cement hamper interconnectivity between pores. Field of view 4.5 x 3.4mm, PPL, Alizarin Red S stained.

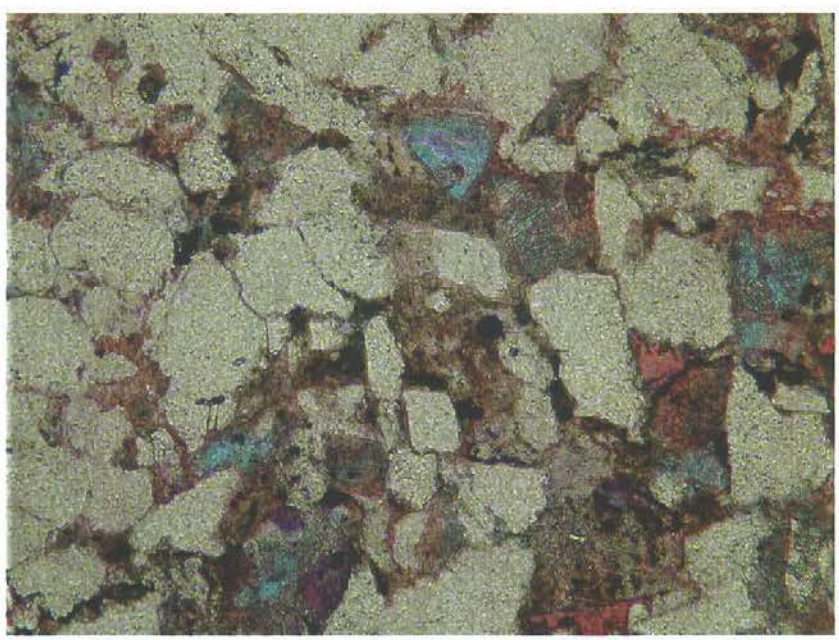

Plate 26. This detailed view illustrates dissolution contacts between detrital quartz grains and the presence of secondary porosity due to dissolution of feldspar grains. Field of view 0.9 x 0.7mm, PPL, Alizarin Red S stained.

Thin section photomicrographs
Well: JEPPE-1 Depth: 4949.40m

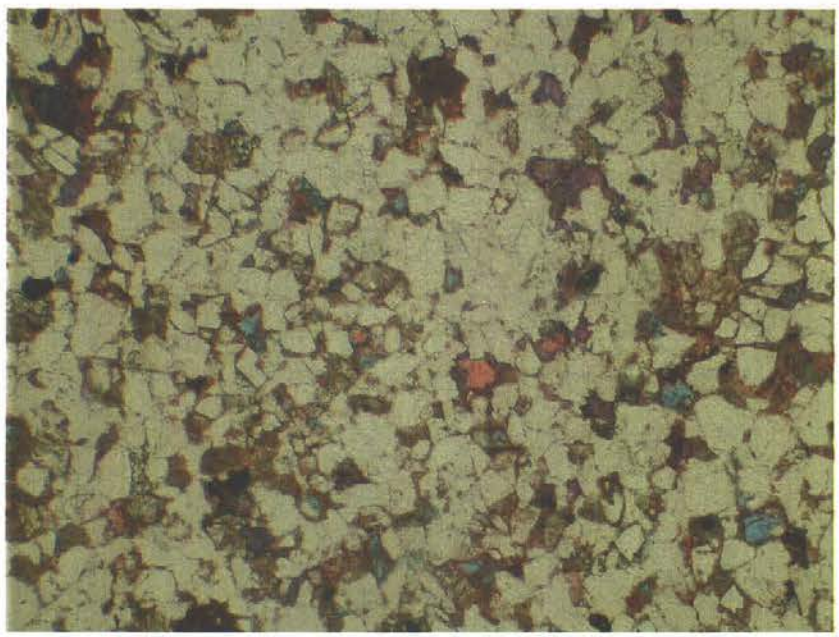

Plate 27. This view illustrates a well to moderately sorted fine-grained lithic arkose, showing carbonate cementation (red and mauve), quartz cement and totally and partially dissolved detrital feldspar grains (secondary pores). Interconnectivity between pores is very low. Field of view 2.8 x 2.1mm, PPL, Alizarin Red S stained.

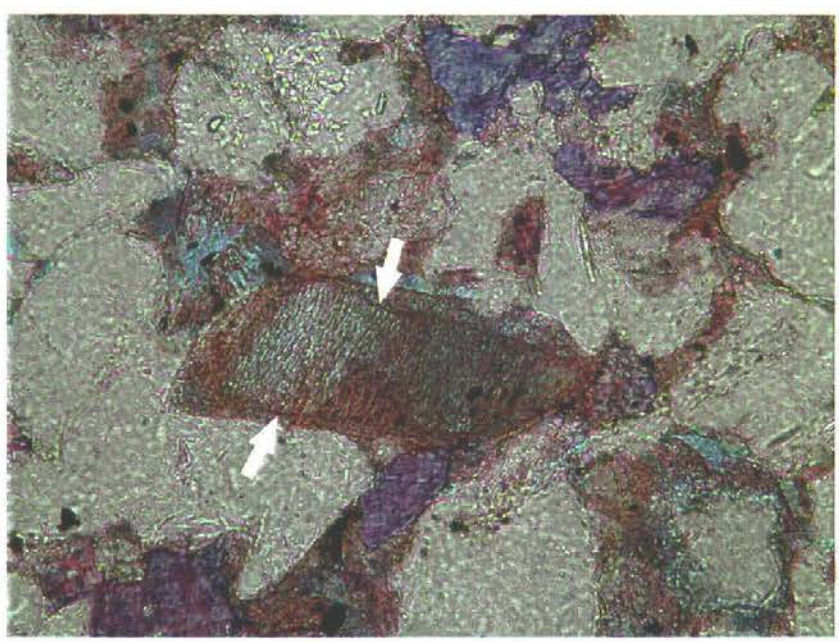

Plate 28. This detailed view shows remnants after a now partially dissolved feldspar grain. The outlines of the original detrital grain is shown by the two white arrows and it is seen that the grain has been overgrown by an euhedral cement. The euhedral cement pre-dates the surrounding quartz cement. Field of view 0.5 x 0.3mm, PPL, Alizarin Red S stained.

Thin section photomicrographs
Well: JEPPE-1 Depth: 4957.57m

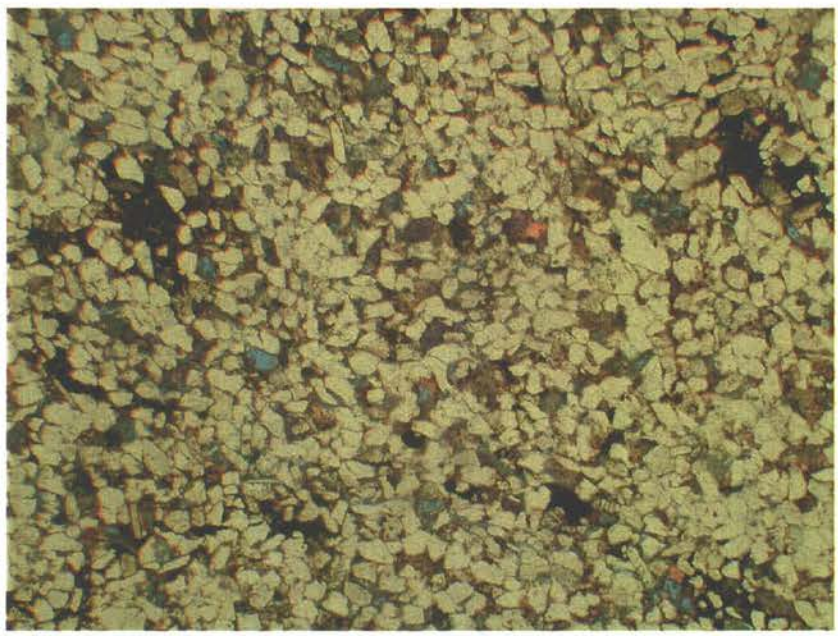

Plate 29. This view illustrates a very well to well sorted fine-grained lithic arkose, showing carbonate cementation (red and mauve), quartz cement, mudstone clasts, pyrite and totally and partially dissolved detrital feldspar grains (secondary pores). Interconnectivity between pores is very low. Field of view 4.2 x 3.2mm, PPL, Alizarin Red S stained.

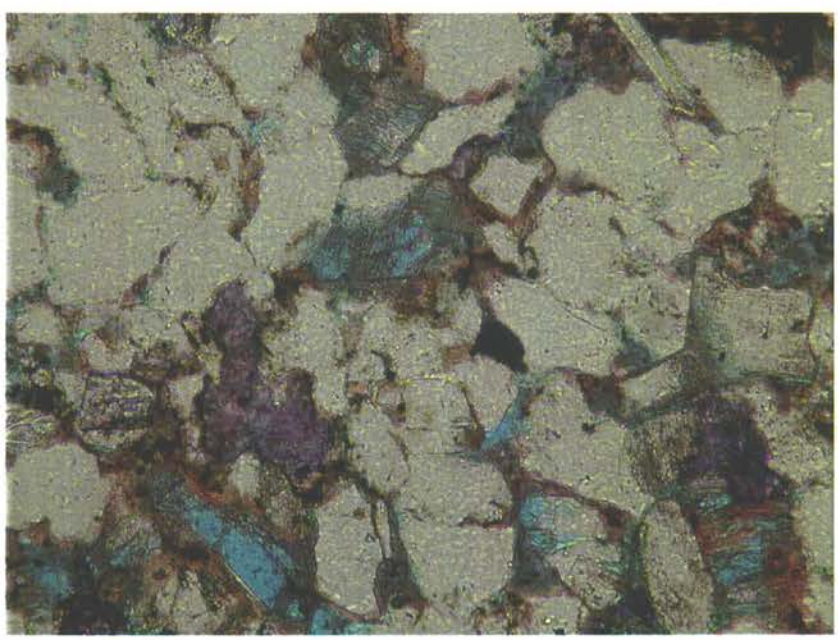

Plate 30. This detailed view illustrates the distribution of carbonate cement (mauve) and weakly to totally dissolved feldspar grains. Field of view 0.9 x 0.7mm, PPL, Alizarin Red S stained.

Thin section photomicrographs
Well: JEPPE-1 Depth: 4971.77m

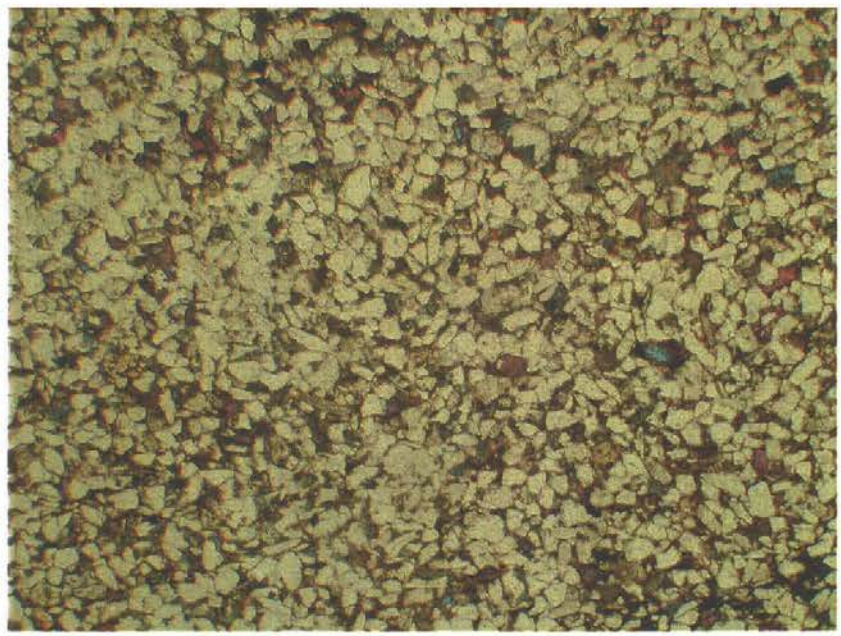

Plate 31. This view illustrates a well sorted fine-grained lithic arkose, showing carbonate cementation (red), quartz cement, pyrite and totally and partially dissolved detrital feldspar grains (secondary pores). Interconnectivity between pores is very low. Field of view 4.1 x 3.0mm, PPL, Alizarin Red S stained.

Plate 32. Syntaxial quartz has grown into a shell fragment and replaced the calcite. Note the presence of abundant calcite inclusions in the quartz crystals (arrowed). Field of view 1.1 x 0.8mm, XPL, Alizarin Red S stained.

Thin section photomicrographs
Well: JEPPE-1 Depth: 4991.02m

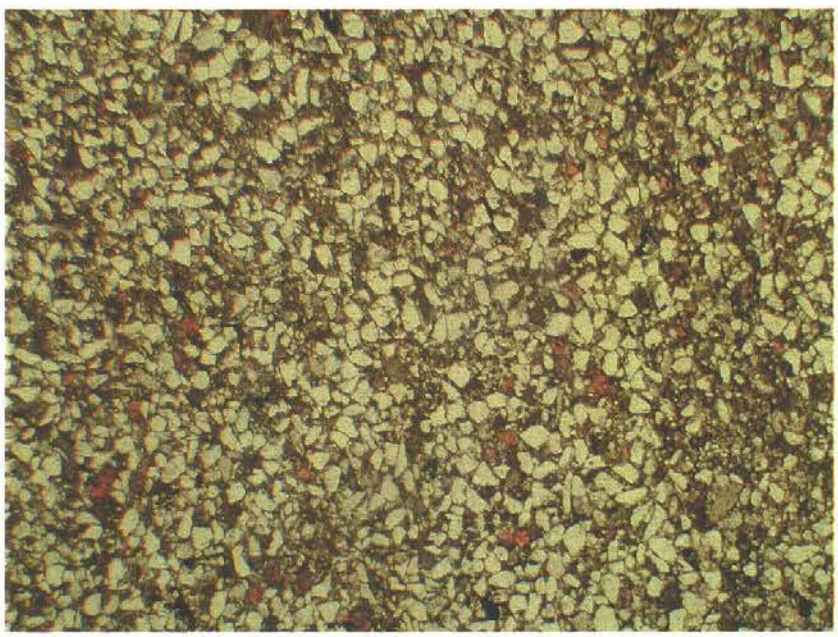

Plate 33. This general view displays a moderately to poorly sorted very fine-grained feldspathic litharenite, showing carbonate cement (coloured red) and scattered pyrite, rare glauconite pellets and detrital clay in pore spaces. Macro-porosity and permeability is very low. Field of view 4.4 x 3.3mm, PPL, Alizarin Red S stained.

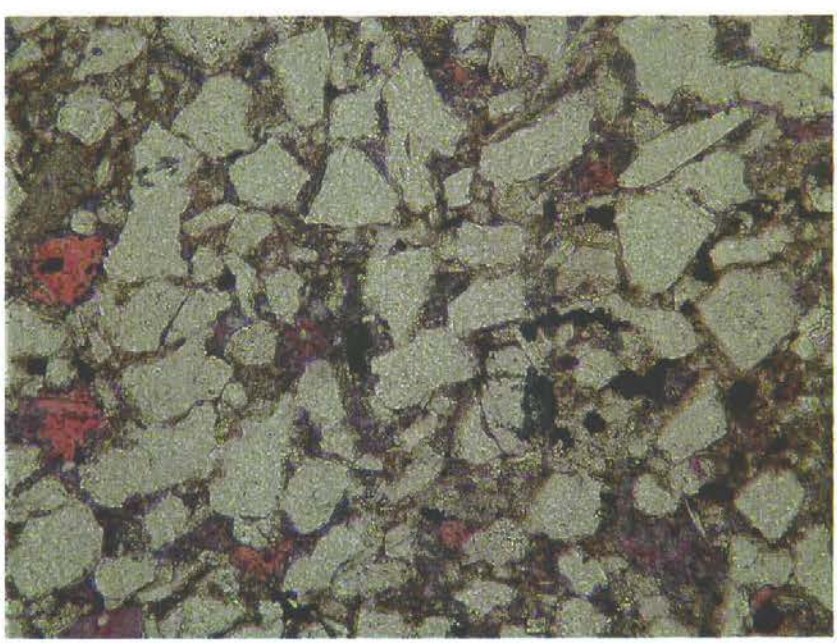

Plate 34. This detailed view illustrates the distribution of carbonate cement and detrital clay, which results in very low macro-porosity and permeability. Field of view 1.0 x 0.7mm, PPL, Alizarin Red S stained.

Thin section photomicrographs
Well: GWEN-2 Depth: 4245.41m

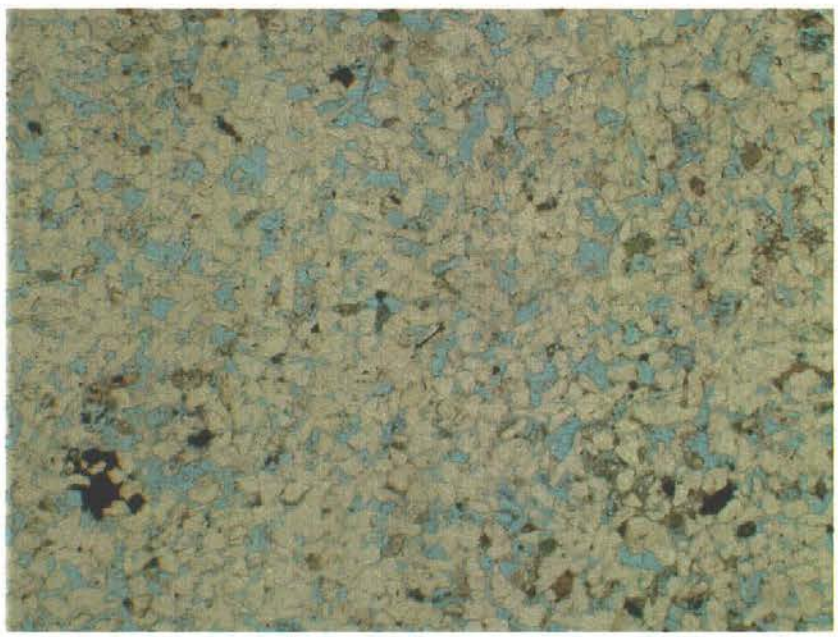

Plate 35. This general view displays a well sorted fine-grained sublitharenite, showing high macro-porosity and relatively good interconnectivity between pores. The porosity is considerably enhanced by secondary porosity. Field of view 4.2 x 3.2mm, PPL.

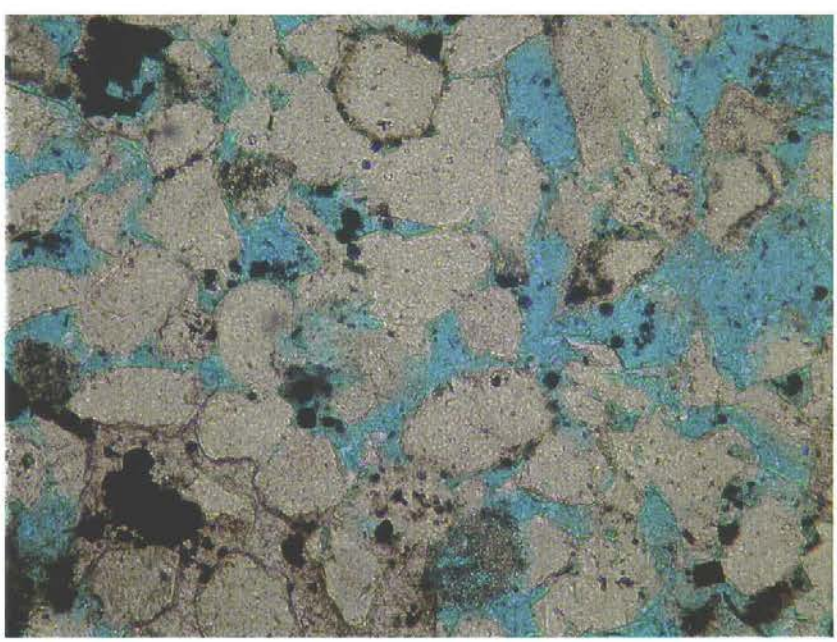

Plate 36. This view illustrates grain dissolution resulting in enhanced porosity. On the lower left patchy poikilotopic carbonate cement occur incorporating pyrite and at the top centre quartz cement is present. Note the occurrence of scattered pyrite in the pore spaces. Field of view 1.0 x 0.8mm, PPL.

Thin section photomicrographs
Well: GWEN-2 Depth: 4250.87m

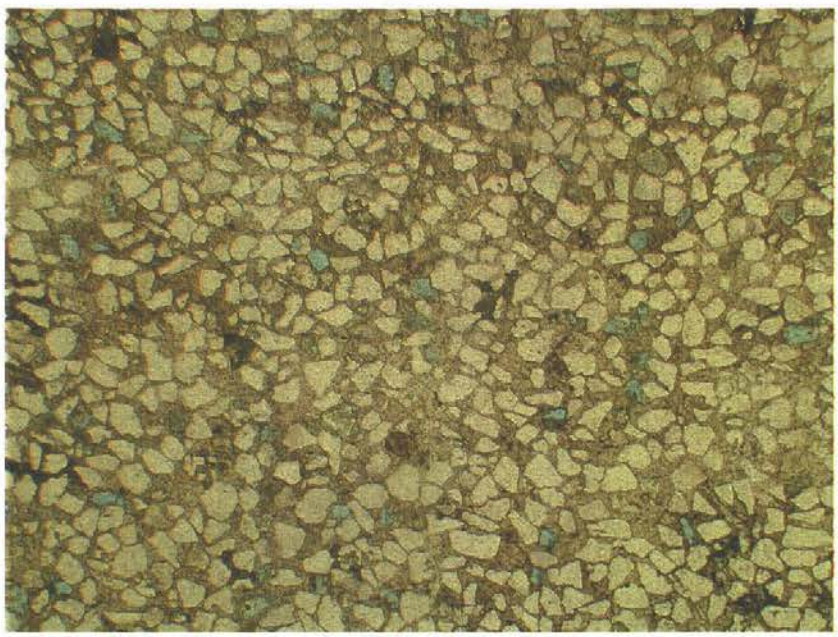

Plate 37. This general view displays a very well sorted fine-grained sublitharenite, showing total poikilotopic carbonate cementation. Note that the detrital grains are "floating" in the carbonate cement and that secondary pores (coloured blue) occur. Field of view 4.4 x 3.2mm, PPL.

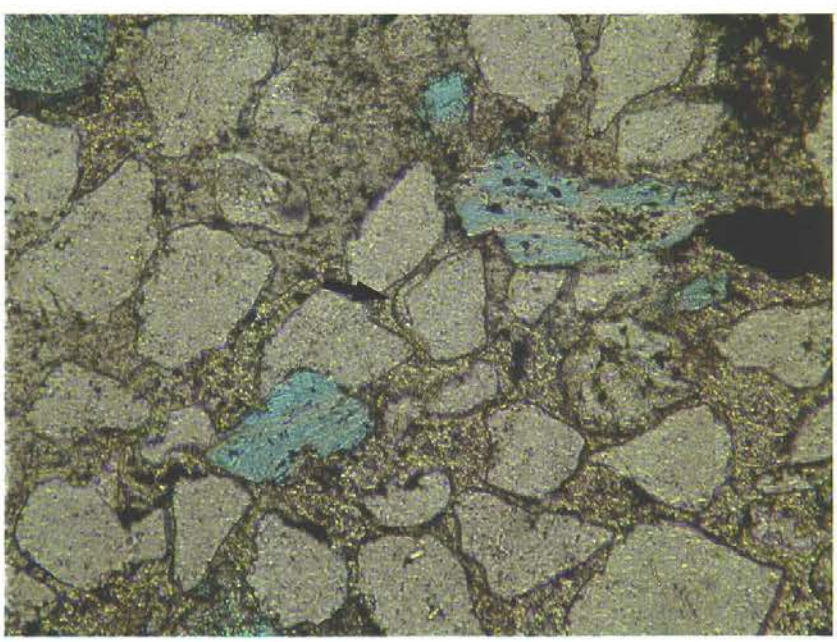

Plate 38. This detailed view shows secondary pores after dissolution of detrital grains. In the pores mica occurs as a residuum. The former grains may have been metamorphic rock fragments, where only the mica resisted dissolution. Note rounded overgrowth on detrital quartz (arrowed). Field of view 0.9 x 0.7mm, PPL.

Thin section photomicrographs
Well: GWEN-2 Depth: 4260.32m

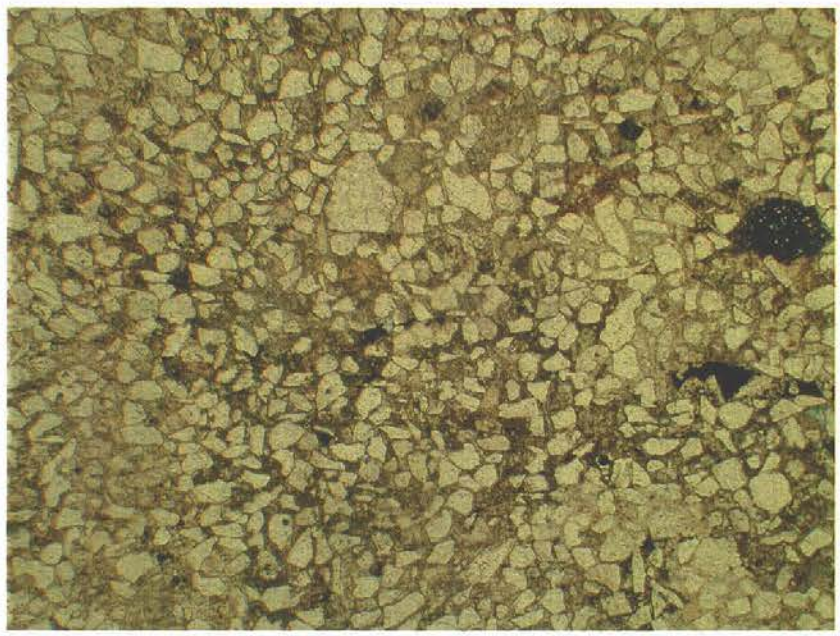

Plate 39. This general view displays a well sorted fine-grained sublitharenite, showing total poikilotopic carbonate cementation. Note that the detrital grains are "floating" in the carbonate cement or has tangential point contacts. Field of view 4.2 x 3.2mm, PPL.

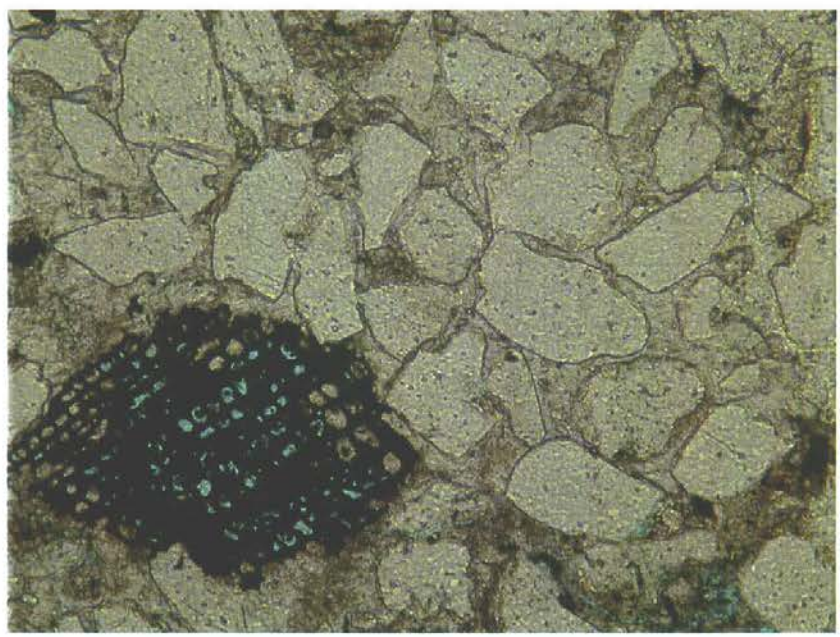

Plate 40. This detailed view shows on the left-hand side woody tissue, where some of the cell-cavities have preserved porosity. Note that the woody tissue has not been deformed, which show that the surrounding carbonate, is a pre-compaction cement. Field of view 1.0 x 0.8mm, PPL.

Thin section photomicrographs
Well: GWEN-2 Depth: 4260.65m

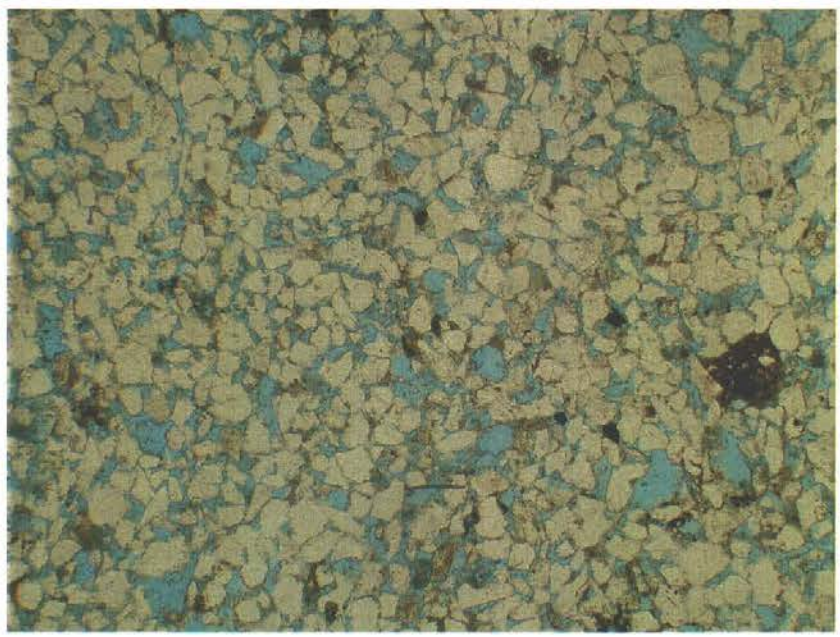

Plate 41. This general view displays a well to moderately sorted fine-grained sublitharenite, showing high macro-porosity and relatively good interconnectivity between pores. The porosity is considerably enhanced by secondary porosity. Note scattered pyrite and mudclasts. Field of view 4.1 x 3.0mm, PPL.

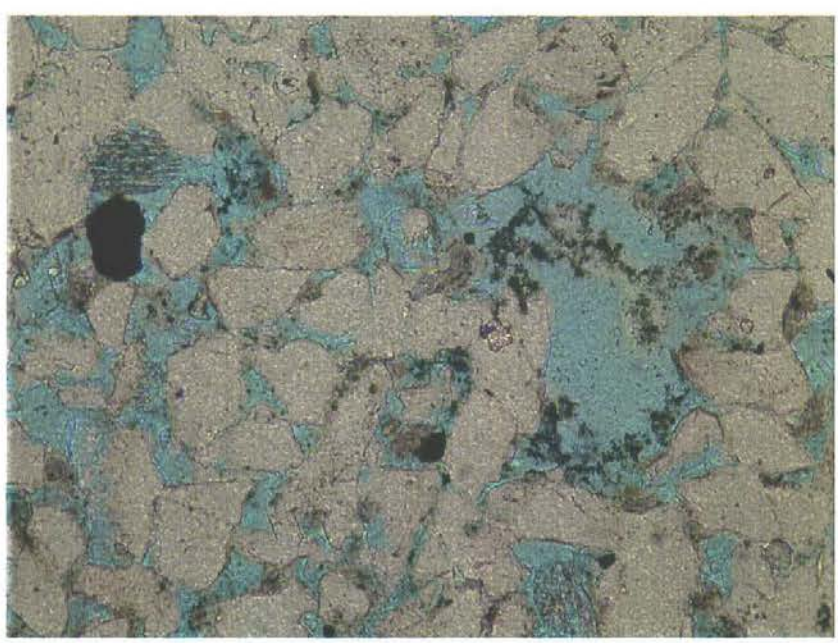

Plate 42. This detailed view shows how oversized pores resulting from grain dissolution enhance porosity. Note the occurrence of straight and concavo-convex point contacts between quartz grains and minor quartz cement. Field of view 1.2 x 0.9mm, PPL.

Thin section photomicrographs
Well: GWEN-2 Depth: 4272.48m

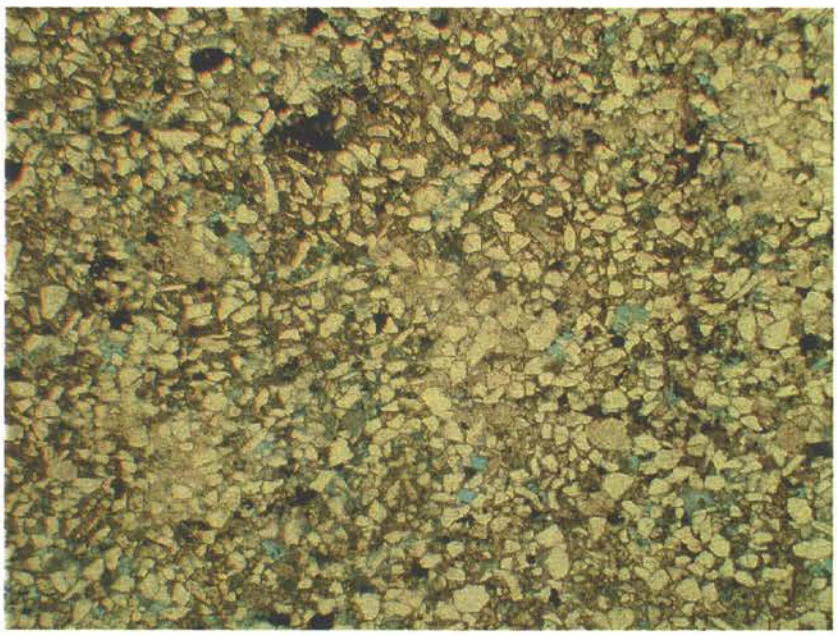

Plate 43. This general view displays a well to moderately sorted very fine-grained litharenite, showing poikilotopic carbonate cement containing pyrite and detrital clay and mudclasts. Note that the detrital grains are "floating" in the carbonate cement and that secondary pores (coloured blue) occur. Field of view 4.2 x 3.2mm, PPL.

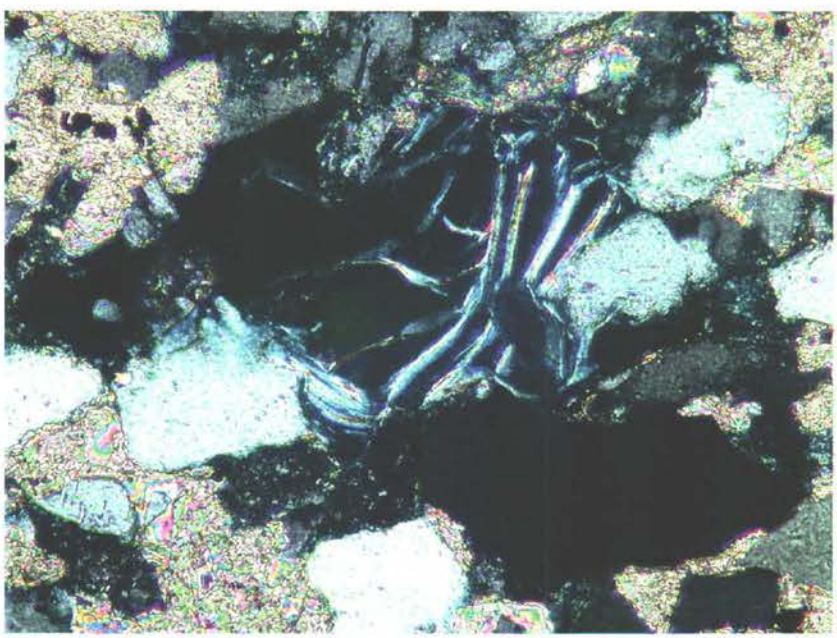

Plate 44. In several secondary pores mica occurs "swollen" as shown here. The individual layers in the mica flake have split from each other, which may be due to precipitation of an unknown mineral between the individual layers. This speculative mineral is now totally dissolved. Field of view 0.5 x 0.3mm, XPL.

Thin section photomicrographs
Well: DIAMANT-1 Depth: 3828.09m

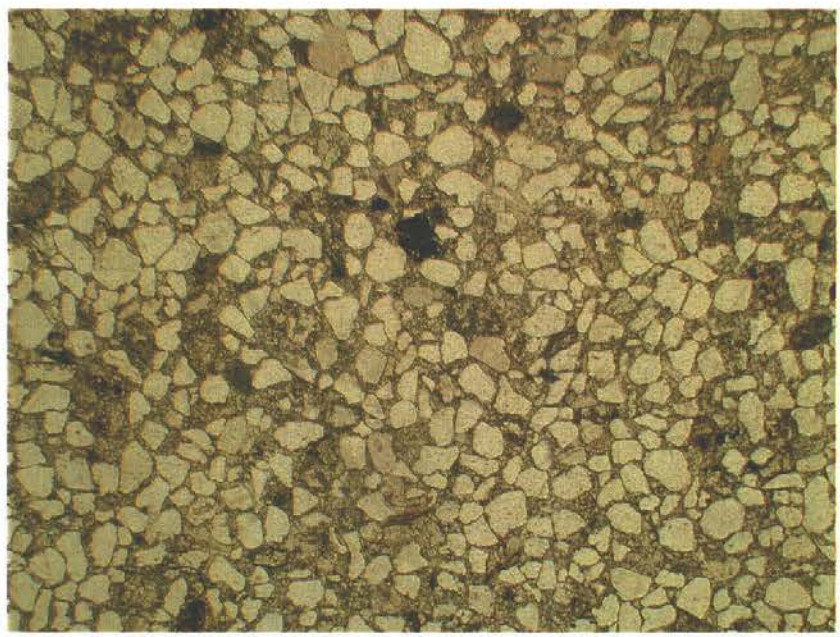

Plate 45. This general view displays a well to moderately sorted fine-grained sublitharenite, showing poikilotopic carbonate cement containing pyrite and mudclasts. Note that the detrital grains are "floating" in the carbonate cement and that some detrital grains has been replaced by the carbonate. Field of view 4.5 x 3.4mm, PPL.

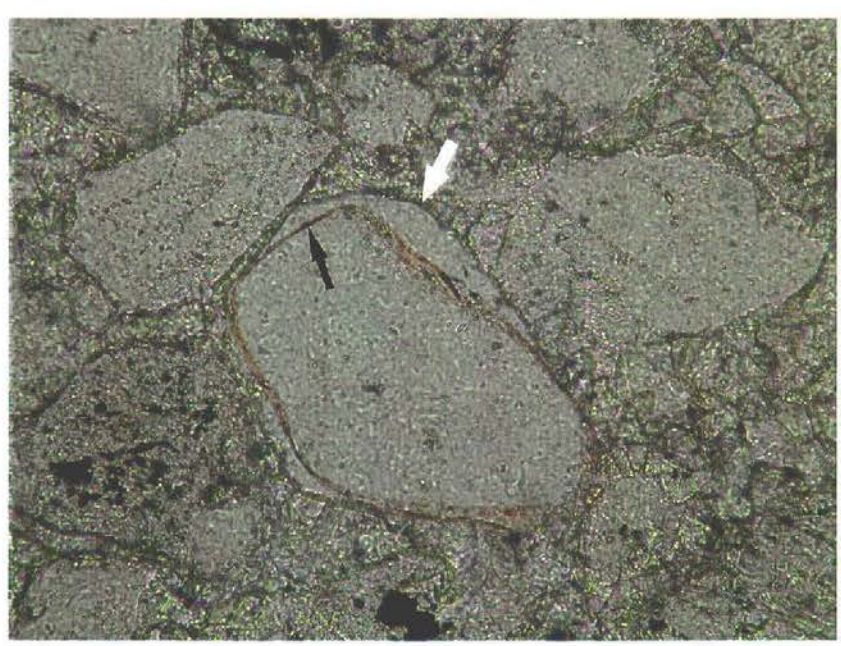

Plate 46. This detailed view shows a quartz grain displaying a conspicuous dust-rim (black arrow) and a rounded overgrowth (white arrow). The rounded nature of the overgrowth indicate that it originate from a former sedimentary cycle. Field of view 0.5 x 0.4mm, PPL.

Thin section photomicrographs
Well: DIAMANT-1 Depth: 3829.60m

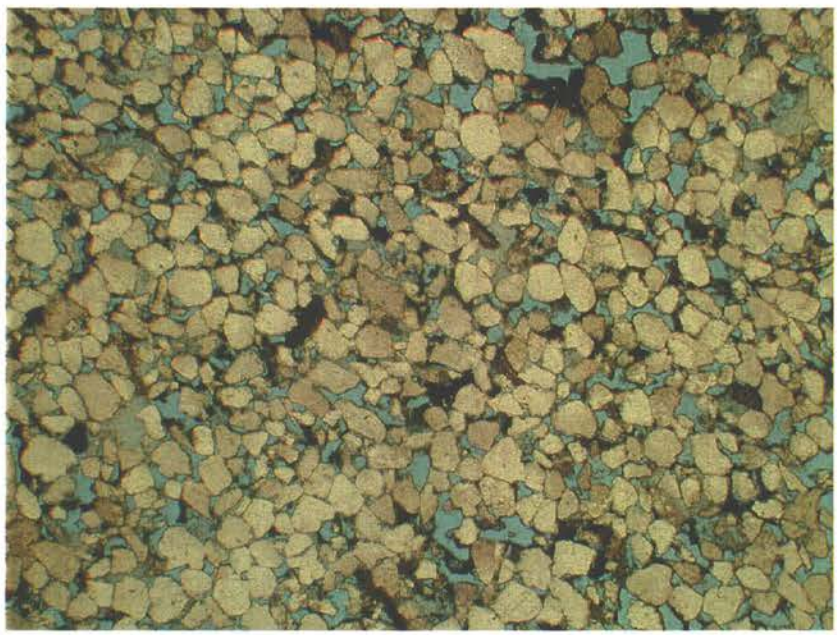

Plate 47. This general view displays a very well to well sorted fine-grained sublitharenite, displaying weak compactional effects. Sporadic carbonate cement, pyrite, kaolinite and mudclasts occur scattered and porosity is enhanced by grain dissolution. The weak compaction, limited authigenic cement, small content of detrital clay and presence of secondary porosity, gives the sandstone an excellent reservoir quality. Field of view 4.5 x 3.4mm, PPL.

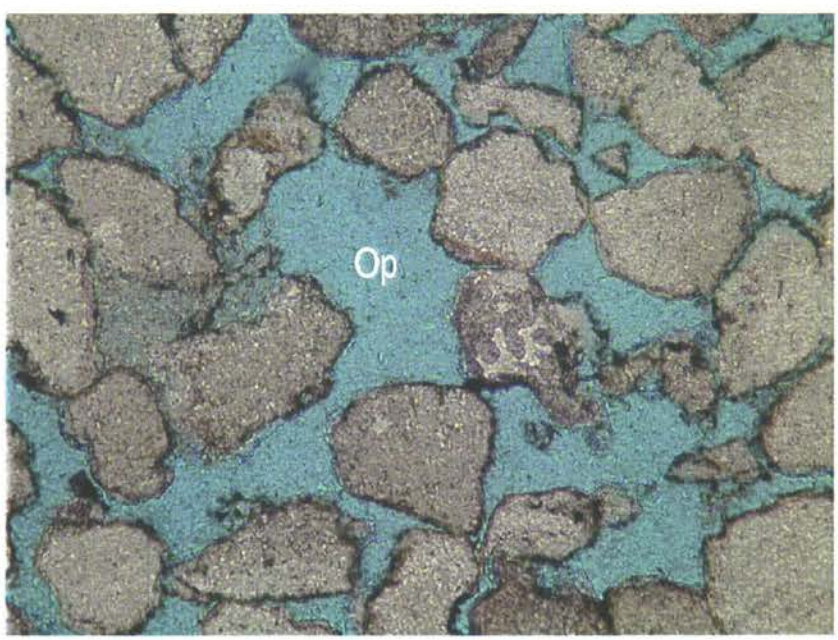

Plate 48. This view illustrates the cement and clay free pores and oversized pores (Op) which result in an extensive pore network with very good interconnectivity. Note that the surfaces of quartz grains occur rough and with pits. Field of view 0.9 x 0.7mm, PPL.

Thin section photomicrographs
Well: DIAMANT-1 Depth: 3833.10m

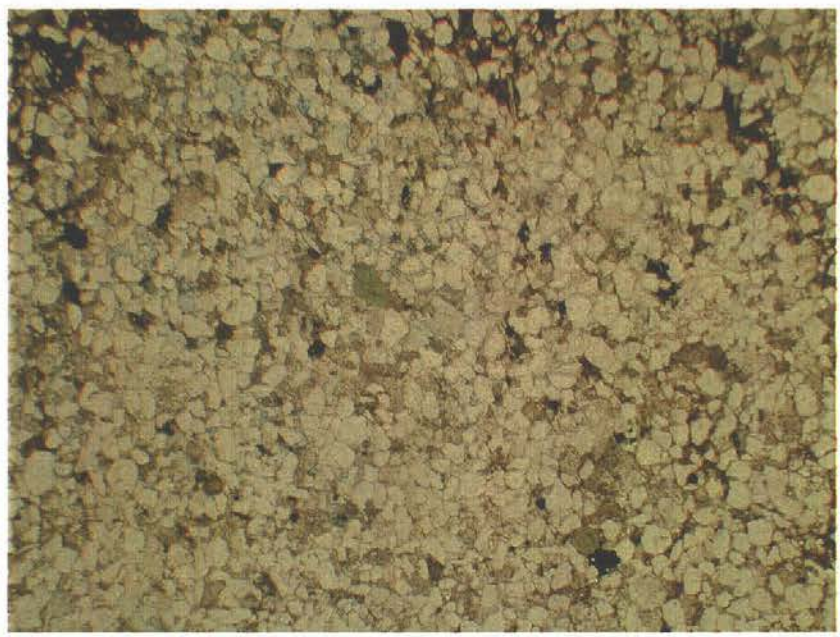

Plate 49. This general view displays a well to moderately sorted very fine-grained sublitharenite, showing patchy carbonate cement, pyrite, organic matter, glauconite pellets and mudclasts. Macro-porosity and permeability is very low. Field of view 5.3 x 4.0mm, PPL.

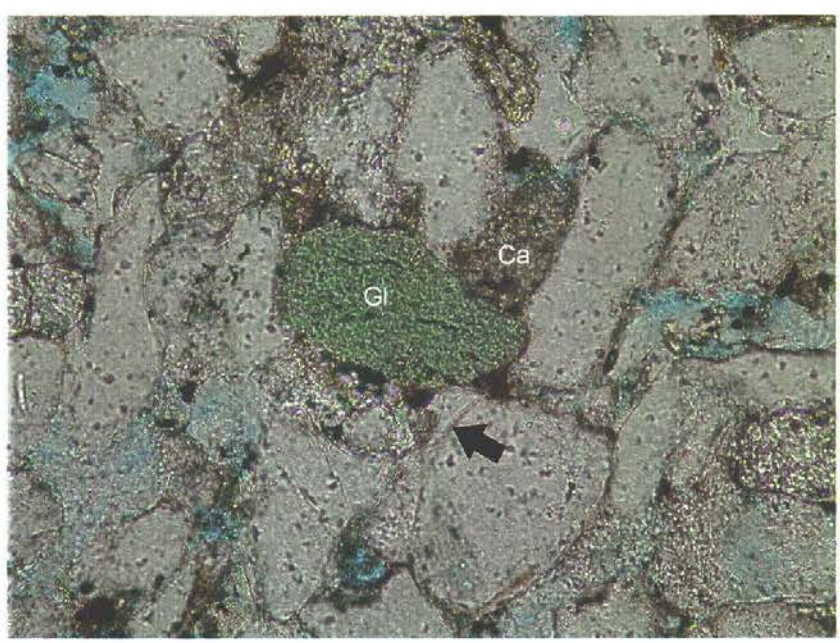

Plate 50. This view shows a weakly deformed glauconite pellet (Gl), carbonate cement (Ca) and a quartz overgrowth clearly defined by a dust-rim (arrowed). Field of view 0.6 x 0.4mm, PPL.

Thin section photomicrographs
Well: DIAMANT-1 Depth: 3835.97m

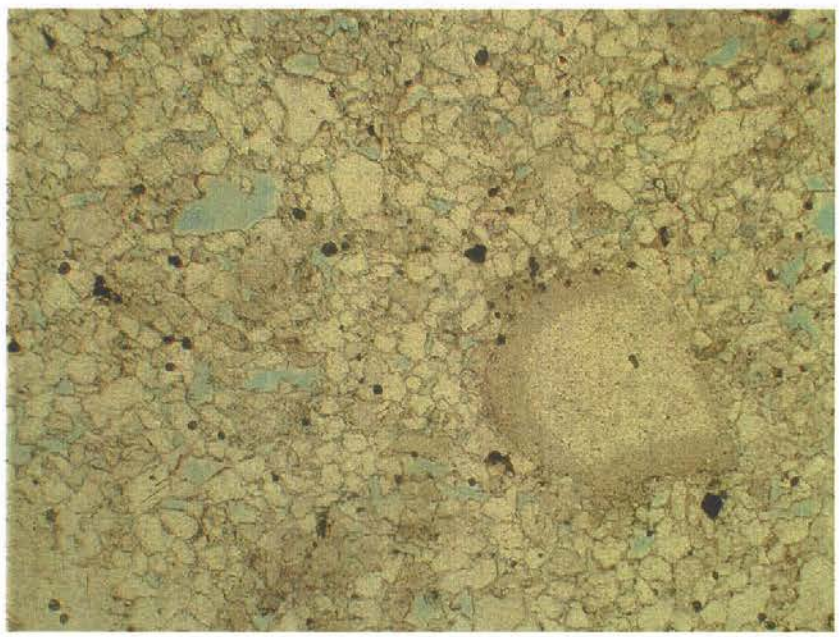

Plate 51. This general view displays a poorly sorted fine-grained sublitharenite, containing widespread quartz cement, scattered pyrite and secondary pores, which enhances porosity. Though quartz cement is widespread, the lack of detrital clay has resulted in the retention of some interconnectivity between pores. Field of view 4.1 x 3.0mm, PPL.

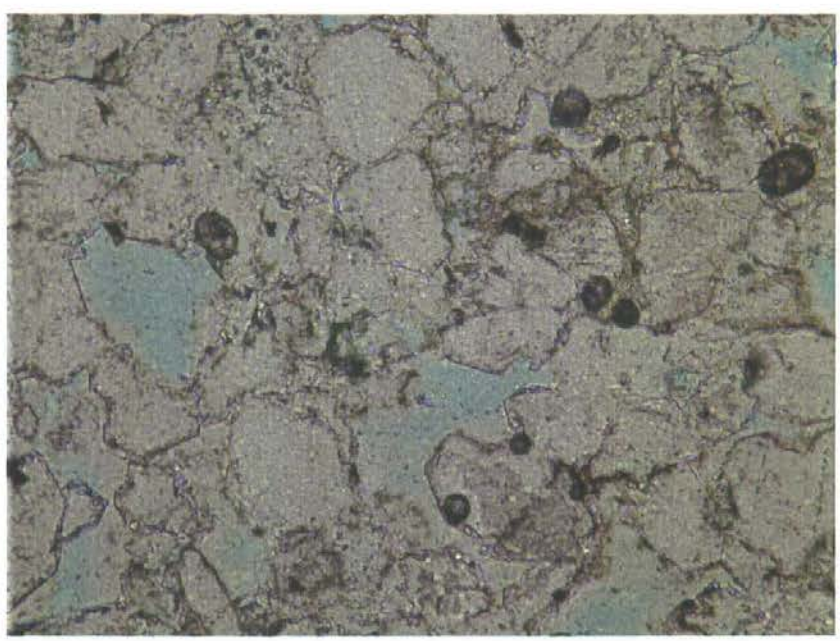

Plate 52. This detailed view illustrates the presence of secondary pores and small eu- and anhedral quartz overgrowths. Field of view 0.9 x 0.7mm, PPL.

Thin section photomicrographs
Well: DIAMANT-1 Depth: 3837.96m

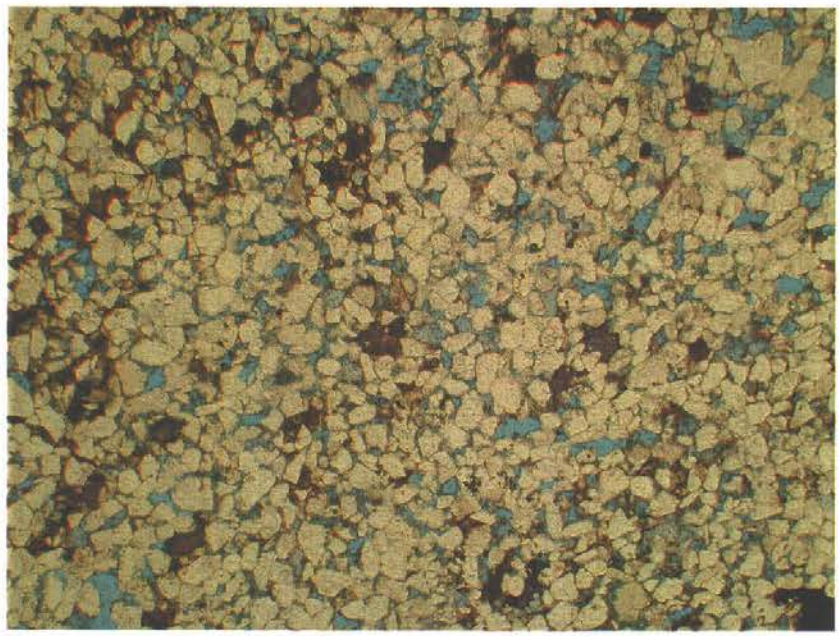

Plate 53. This general view displays a moderately sorted fine-grained sublitharenite, containing carbonate cement (mauve), quartz cement, pyrite, kaolinite booklets, mudclasts and secondary pores. The sandstones is weakly compacted but the present cements has reduced interconnectivity between pores. Field of view 4.8 x 3.6mm, PPL, Alizarin Red S stained.

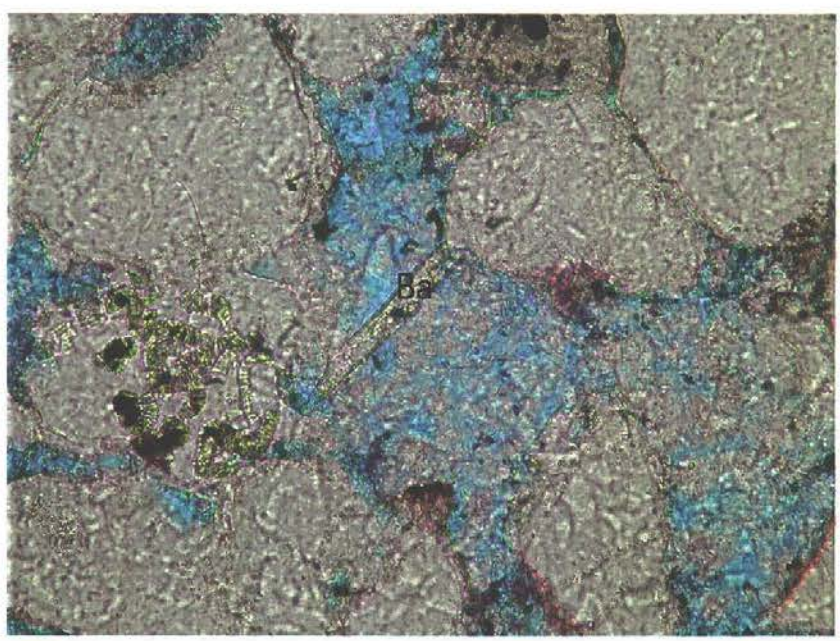

Plate 54. This detailed view shows vermiform kaolinite overgrown by quartz (on the left hand-side) and kaolinite booklets in pore spaces. A baryte needle (Ba) occurs in the pore space. Field of view 0.5 x 0.4mm, PPL, Alizarin Red S stained.

Thin section photomicrographs
Well: RAVN-1 Depth: 4094.25m

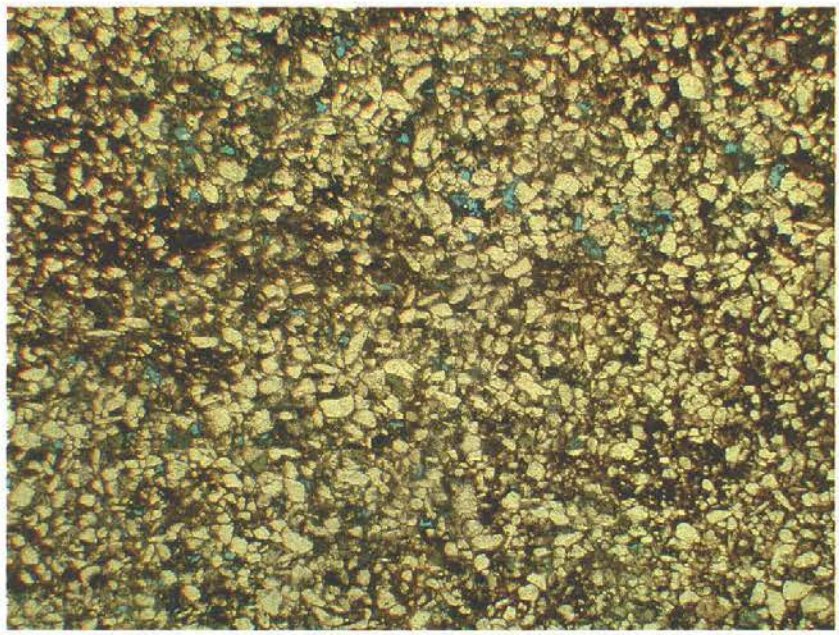

Plate 55. This general view displays a moderately sorted very fine-grained sublitharenite wacke, displaying abundant detrital clay reducing interconnectivity between pores considerably. Also seen are pyrite, organic matter and glauconite pellets. Some secondary porosity occurs. Macro-porosity and permeability is very low. Field of view 4.2 x 3.2mm, PPL.

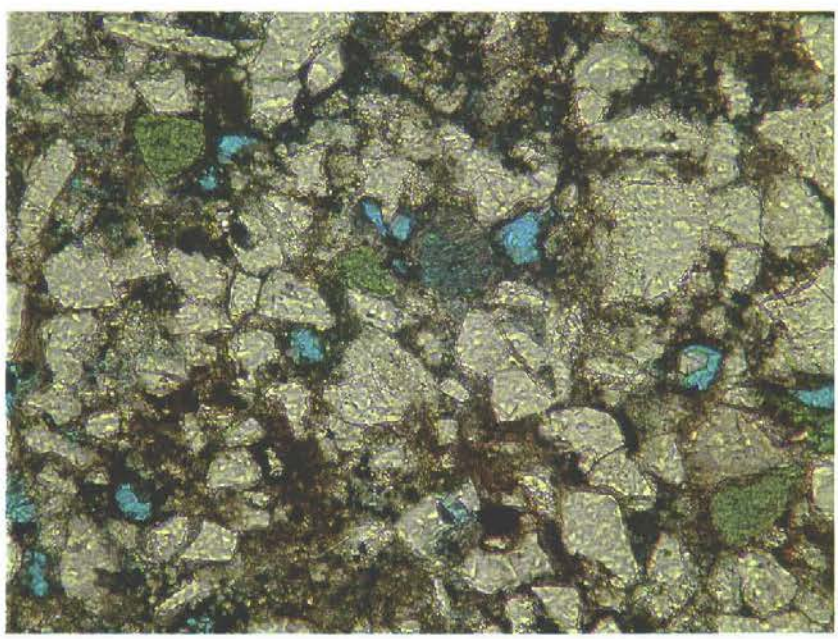

Plate 56. This detailed view shows that glauconite pellets are only weakly effected by compaction. Small secondary pores occur with minute syntaxial quartz crystals (right hand-side). Field of view 0.9 x 0.7mm, PPL.

Thin section photomicrographs
Well: RAVN-1 Depth: 4113.28m

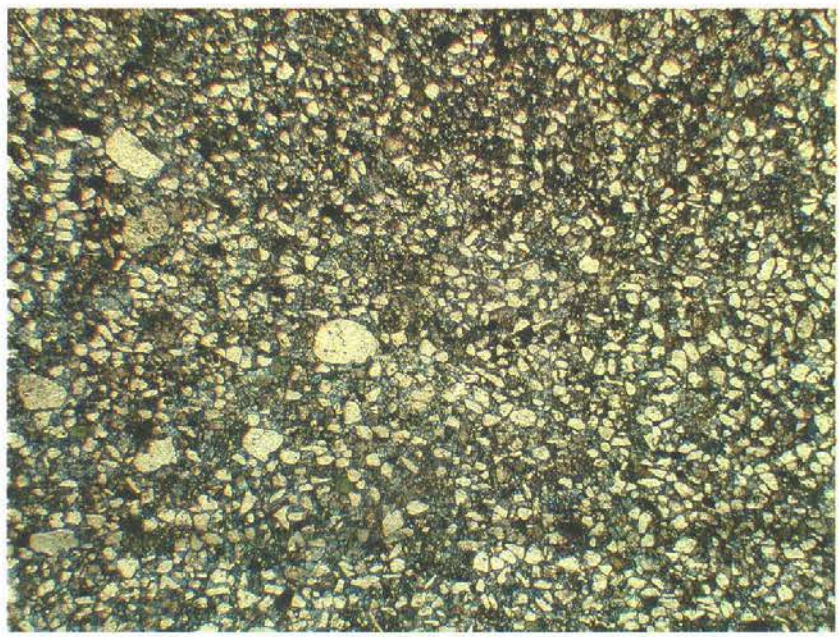

Plate 57. This general view displays a moderately sorted very fine-grained sublitharenite, showing total carbonate cementation (bluish) of the sandstone. Pyrite, mudclasts and glauconite pellets also occur. Note that the detrital grains are "floating" in the carbonate cement. Field of view 4.2 x 3.2mm, PPL, Alizarin Red S stained.

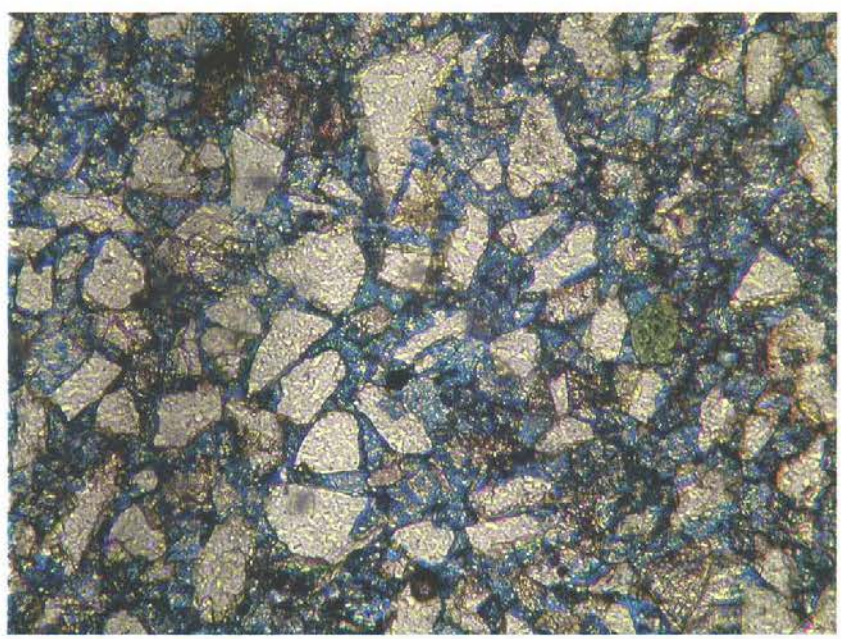

Plate 58. Close up of the pore occluding and grain displacive carbonate cement (blue). Field of view 0.9 x 0.7mm, PPL, Alizarin Red S stained.

Thin section photomicrographs
Well: RAVN-1 Depth: 4114.55m

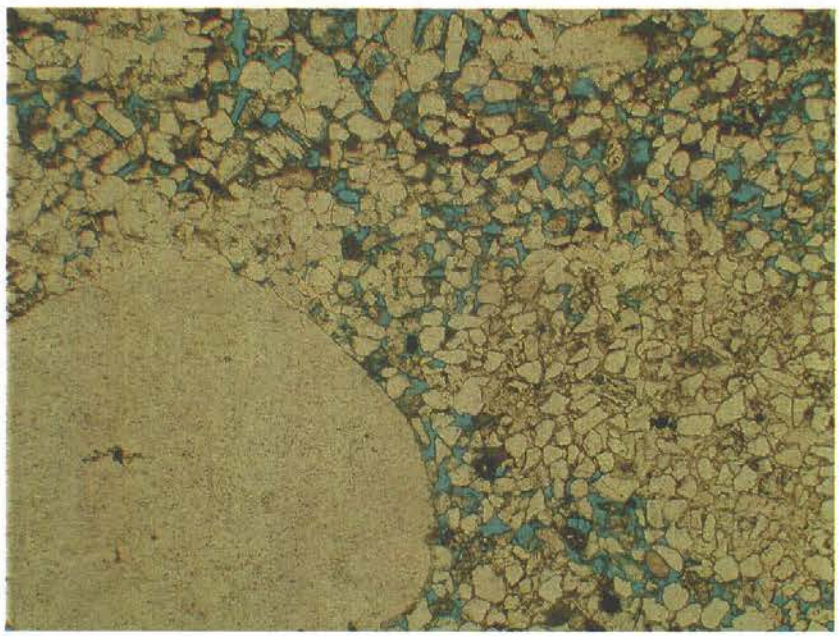

Plate 59. This general view displays a moderately to poorly sorted fine-grained sublitharenite, showing segregated poikilotopic carbonate cement (right hand-side) and quartz cement (above the large well rounded grain). Outside these areas of cement porosity and permeability is relatively high due to lack of detrital clay. Field of view 4.2 x 3.2mm, PPL.

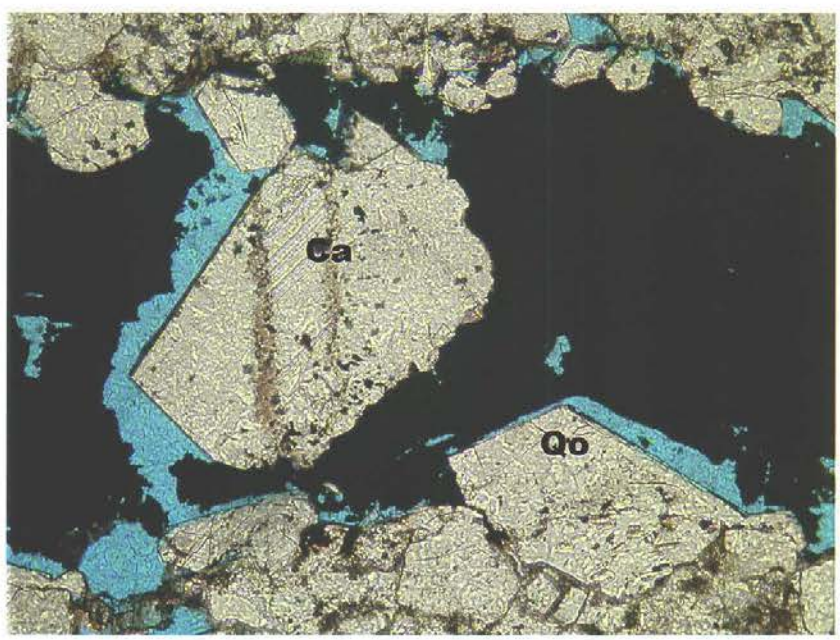

Plate 60. This view shows large carbonate crystals (Ca) and large syntaxial quartz overgrowths (Qo), which have grown displacively and freely into pore spaces in a broken and fractured organic fragment. Field of view 1.1 x 0.8mm, PPL.

Thin section photomicrographs
Well: RAVN-1 Depth: 4125.70m

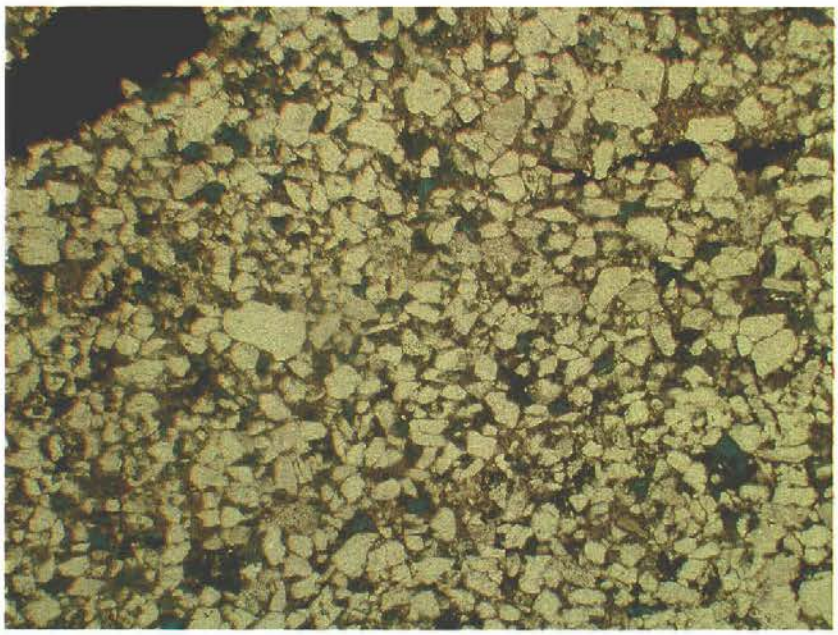

Plate 61. This general view displays a moderately sorted fine-grained sublitharenite, displaying abundant detrital clay reducing interconnectivity between pores considerably. Also seen are pyrite and organic matter. Some secondary porosity occurs. Macro-porosity and permeability is low. Field of view 4.1 x 3.0mm, PPL.

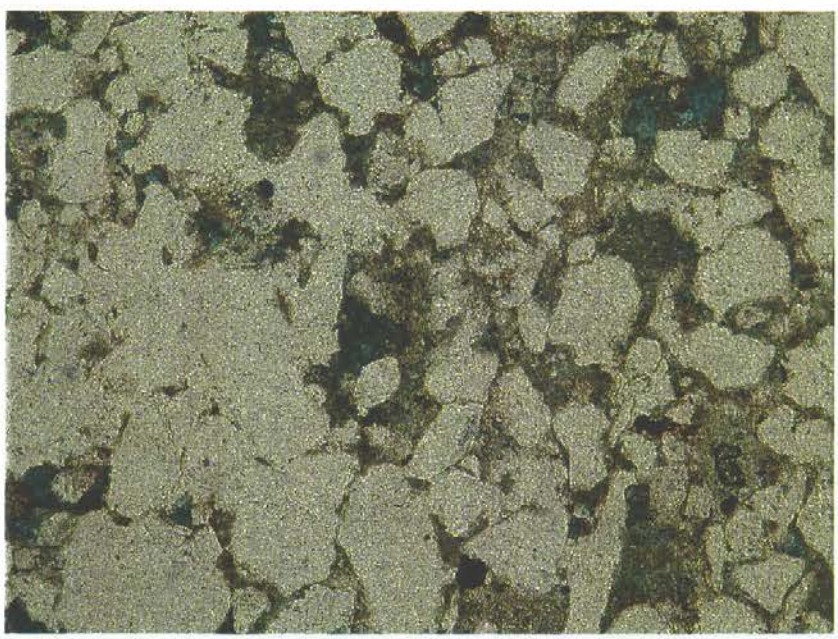

Plate 62. This view shows the reduced interconnectivity between pores due to quartz cement and detrital clay. Note that small secondary pores occur. Field of view 1.3 x 1.0mm, PPL.

Thin section photomicrographs
Well: RAVN-1 Depth: 4136.64m

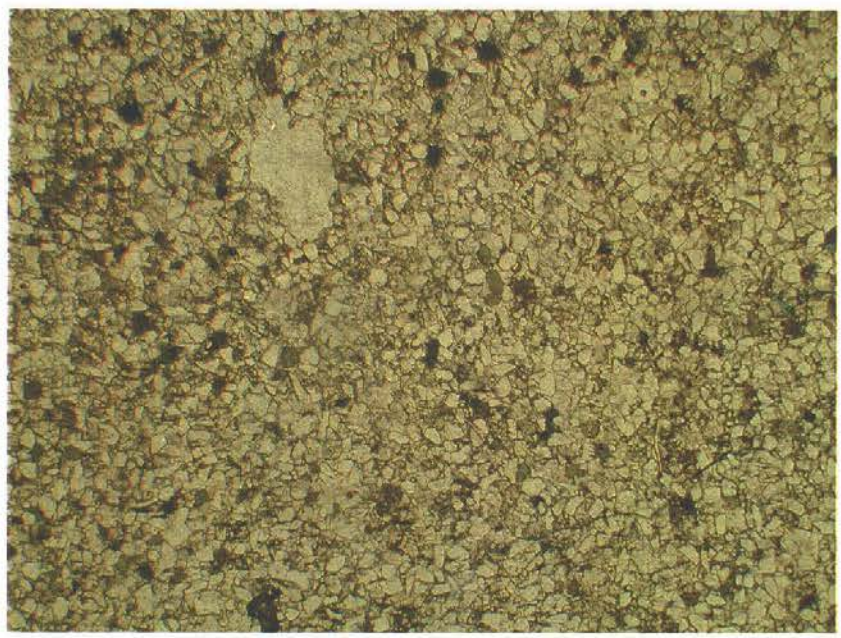

Plate 63. This general view displays a well sorted very fine-grained sublitharenite, showing total carbonate cementation of the sandstone. Glauconite pellets, pyrite and rare mudclasts also occur. Note that the detrital grains are "floating" in the carbonate cement. Field of view 4.2 x 3.2mm, PPL.

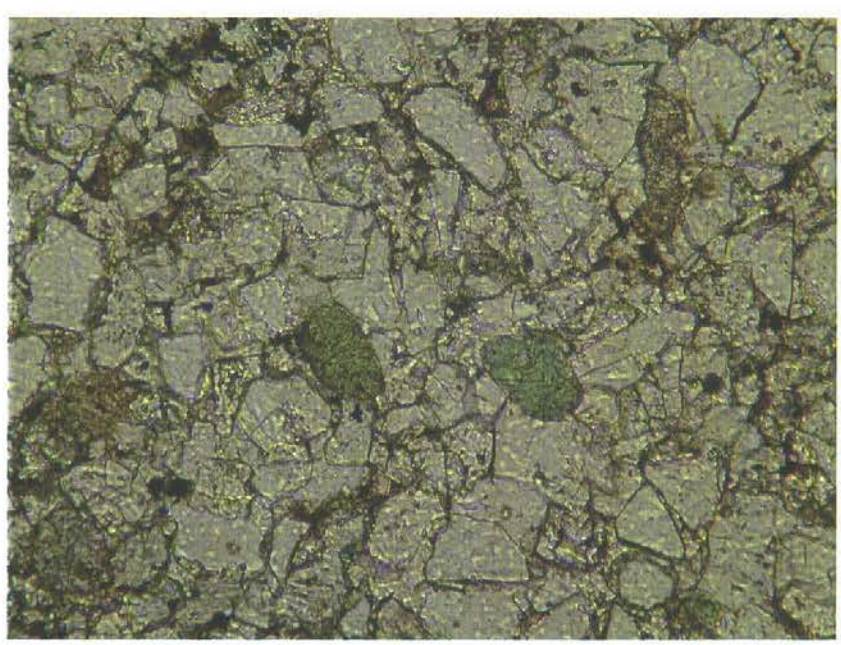

Plate 64. The view shows glauconite pellets in the carbonate cement. The pellets have not been deformed by compaction. Field of view 0.9 x 0.7mm, PPL.

Thin section photomicrographs
Well: RAVN-1 Depth: 4145.04m

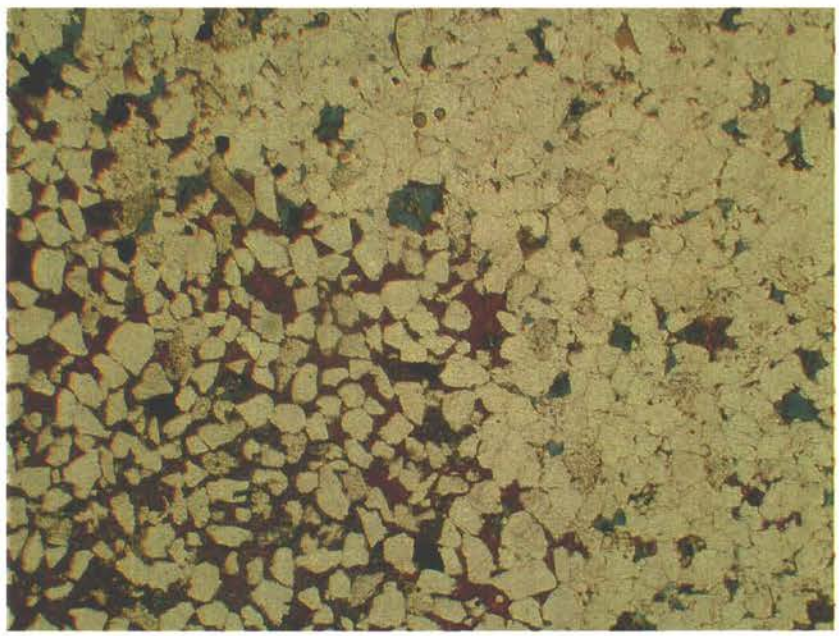

Plate 65. This general view displays a well to moderately sorted fine-grained sublitharenite, showing total carbonate cementation (red) on the left hand-side and occlusion of pore spaces by quartz cement on the right hand-side. The majority of porosity is secondary. Note that the detrital grains are "floating" in the carbonate cement. Field of view 4.4 x 3.3mm, PPL, Alizarin Red S stained.

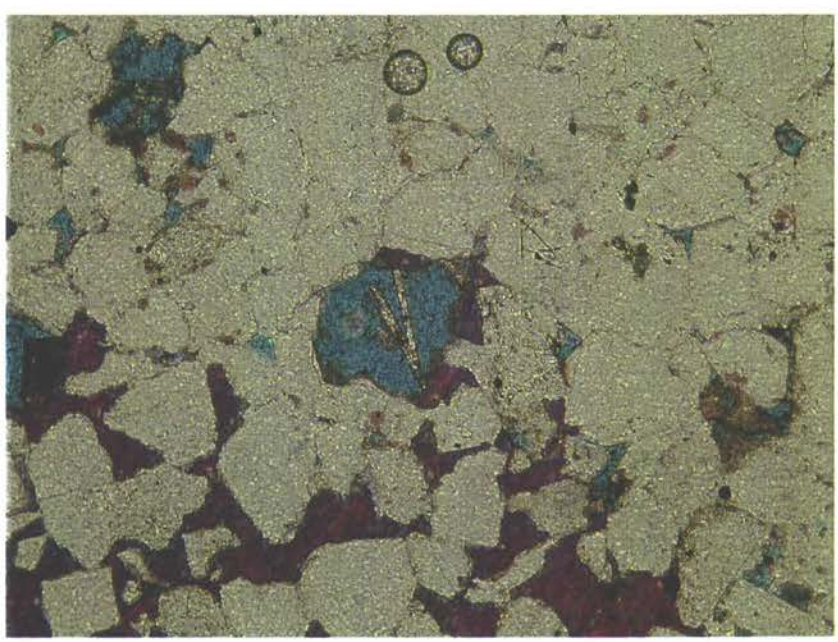

Plate 66. This view shows a close up of the boarder zone between carbonate and quartz cement. In a secondary pore, which post-dates both cement-types, baryte needles have precipitated. Field of view 1.5 x 1.1mm, PPL, Alizarin Red S stained.

Thin section photomicrographs
Well: RAVN-2 Depth: 4262.43m

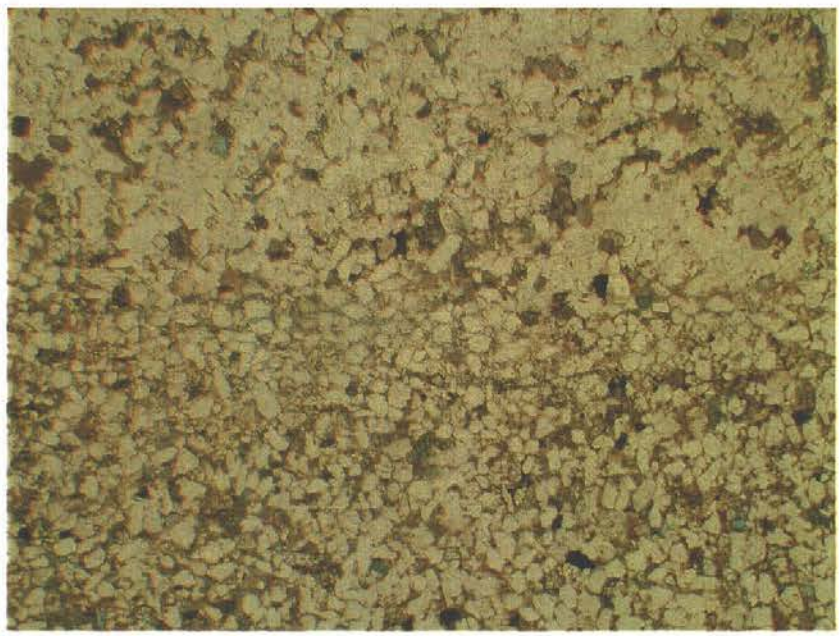

Plate 67. This general view displays a well to moderately sorted fine-grained feldspathic litharenite, displaying abundant detrital clay in the lower part and pore occluding quartz cement in the upper part, which reduce interconnectivity between pores considerably. Few secondary pores occur. Macro-porosity and permeability is very low. Field of view 4.2 x 3.2mm, PPL.

Plate 68. This detailed view shows secondary pores in the area where quartz cement occludes pores. A second quartz cement is seen growing as syntaxial crystals in a secondary pore (white arrow). Later a baryte needle has grown in the same pore (black arrow). Field of view 1.0 x 0.8mm, PPL.

Thin section photomicrographs
Well: RAVN-2 Depth: 4273.81m

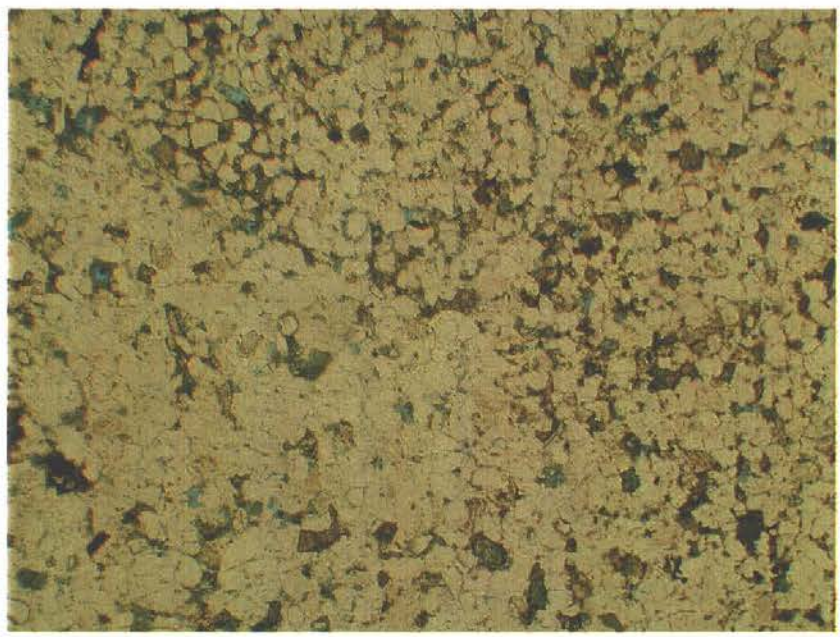

Plate 69. This general view displays a well to moderately sorted fine-grained subarkose, showing cementation by quartz and carbonate resulting of occlusion of pore spaces. The majority of macro-porosity is secondary. Field of view 4.4 x 3.3mm, PPL.

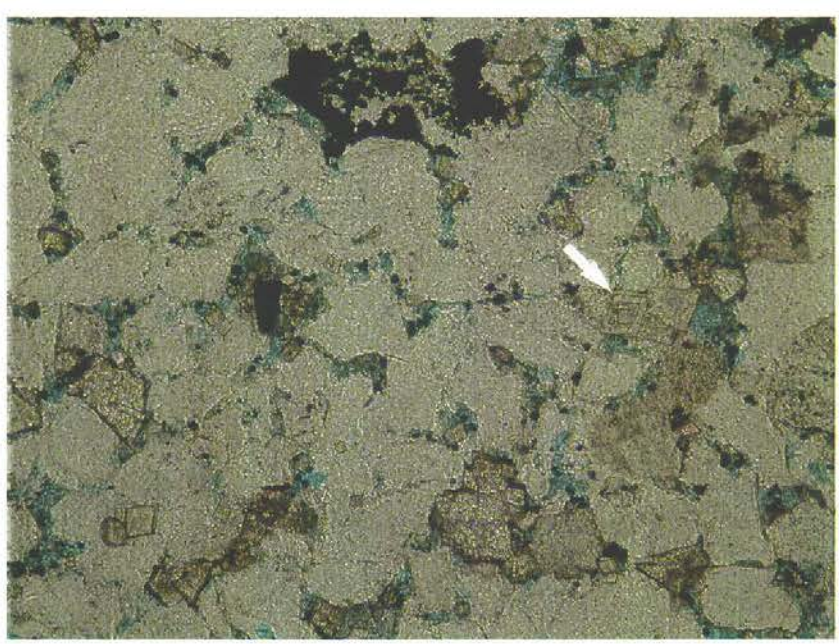

Plate 70. This detailed view shows pore-filling carbonate and dolomite rhombs (some occurring zoned, white arrow). The carbonates are later surrounded by quartz cement. Pyrite in association with organic matter occurs as an early precipitate. Field of view 1.2 x 0.9mm, PPL.

SEM photomicrographs

Well: GERT-1 **Depth: 4928.21m**

Plate 71. The photograph shows a secondary pore with a clay rim on the surfaces of former feldspar. Parts of the clay rim consist of a network of tangled illite threads (see plate 72). Note that the pore space is closely surrounded by well developed quartz cement.

SEM photomicrographs

Well: GERT-1 **Depth: 4928.21m**

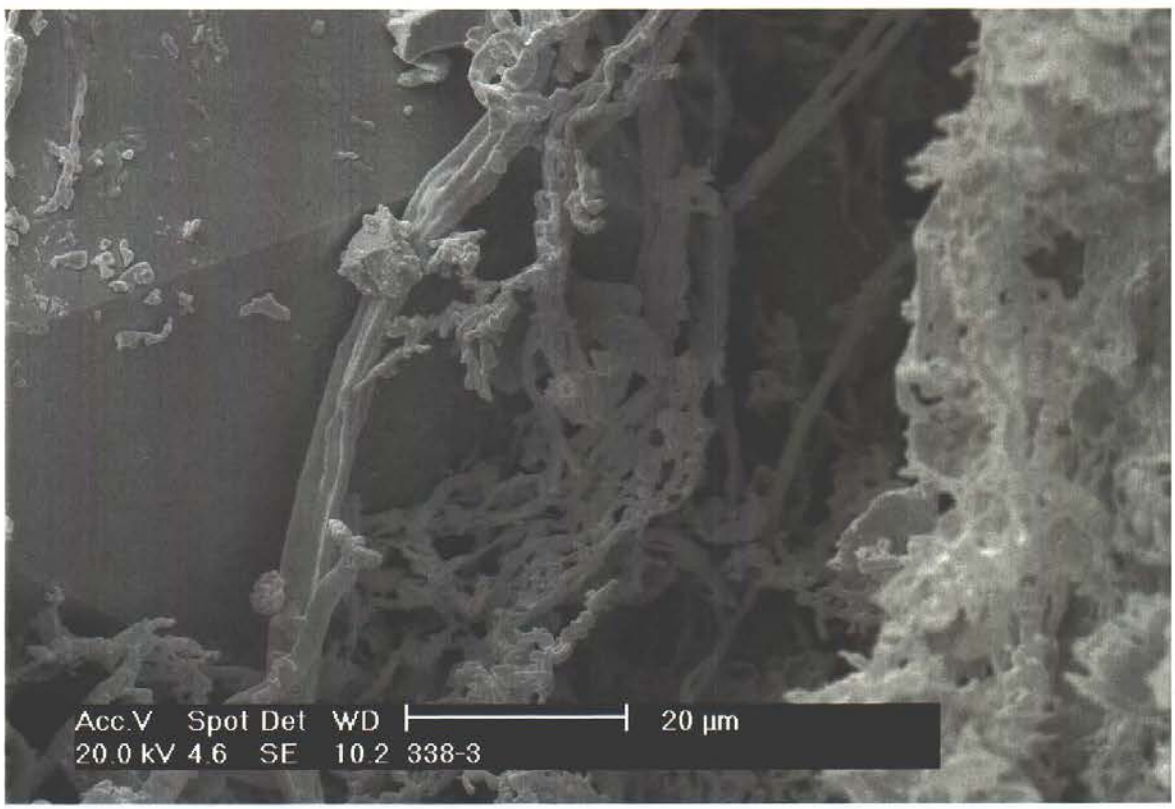

Plate 72. Close up of illitic clay rims showing a network of tangled illite threads.

SEM photomicrographs

Well: GERT-1 **Depth: 4928.21m**

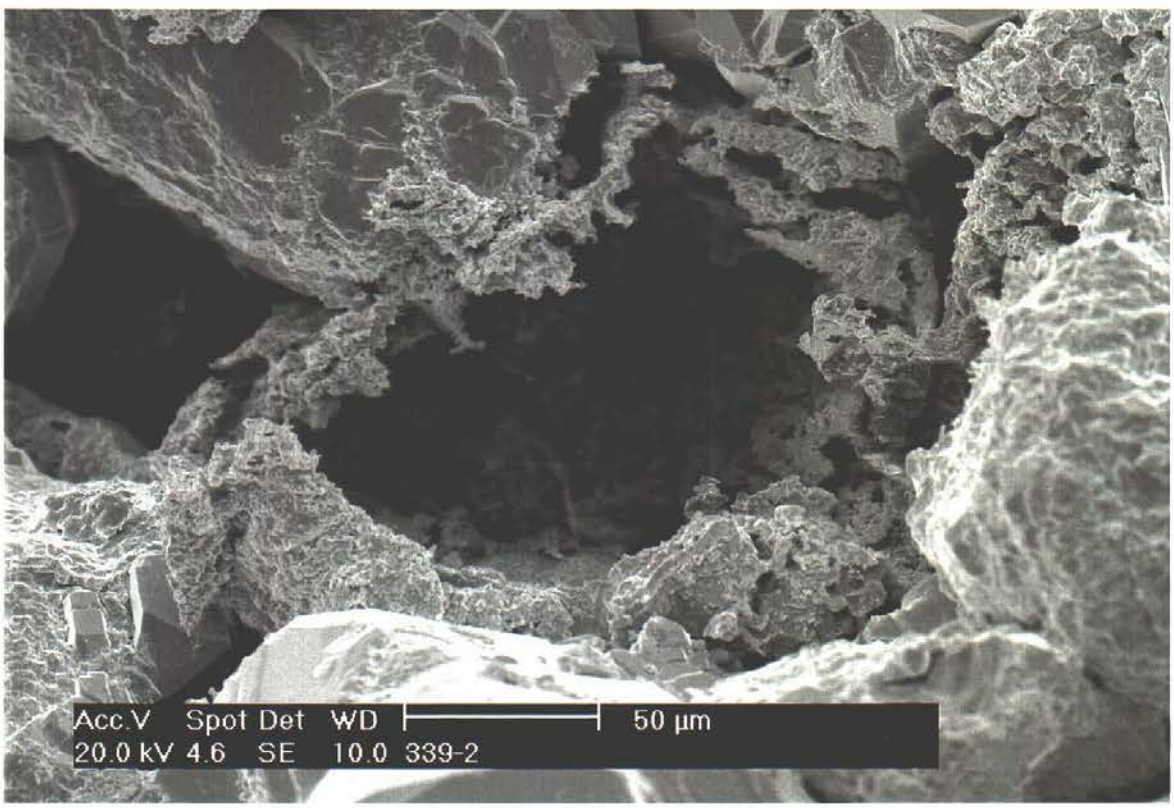

Plate 73. The photograph shows a secondary pore marked by illite, which occur as clay rims on the surfaces of a former feldspar.

SEM photomicrographs

Well: GERT-1 **Depth: 4928.21m**

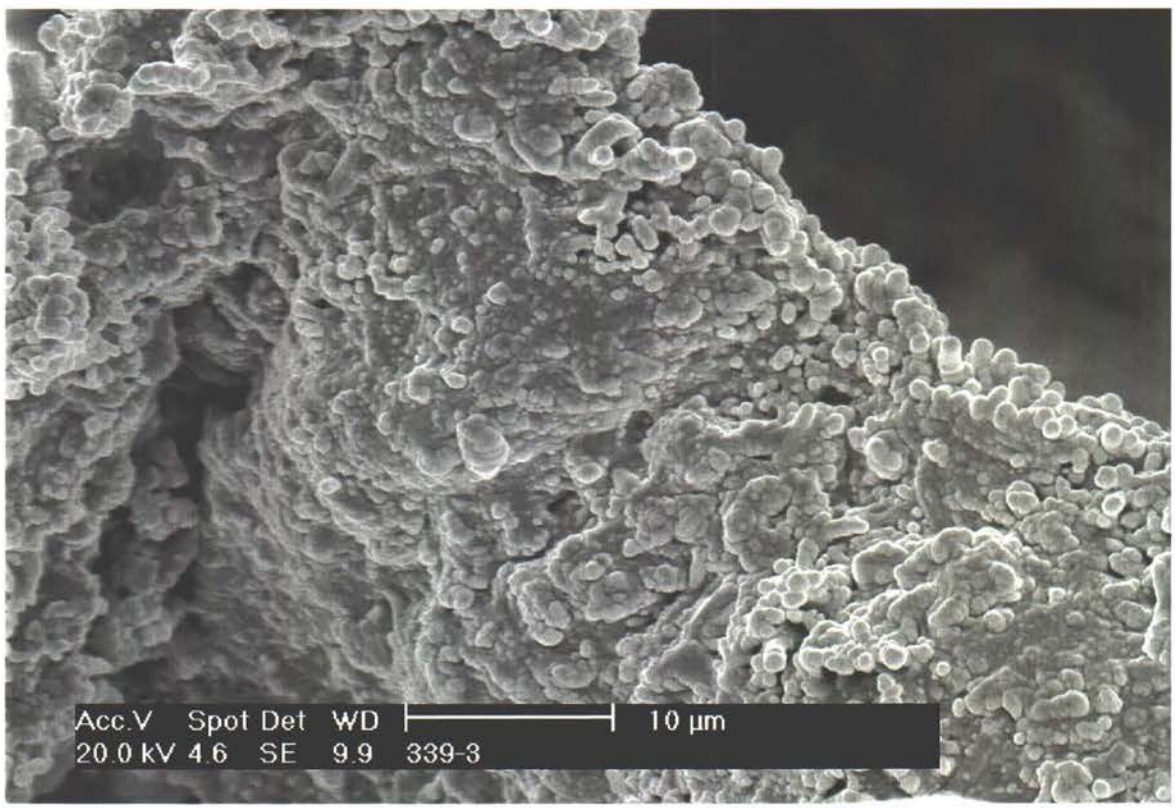

Plate 74. Close up of the illitic clay rims, which here occur as dense amorphous or spherical crystals.

SEM photomicrographs

Well: GERT-2 **Depth: 4817.67m**

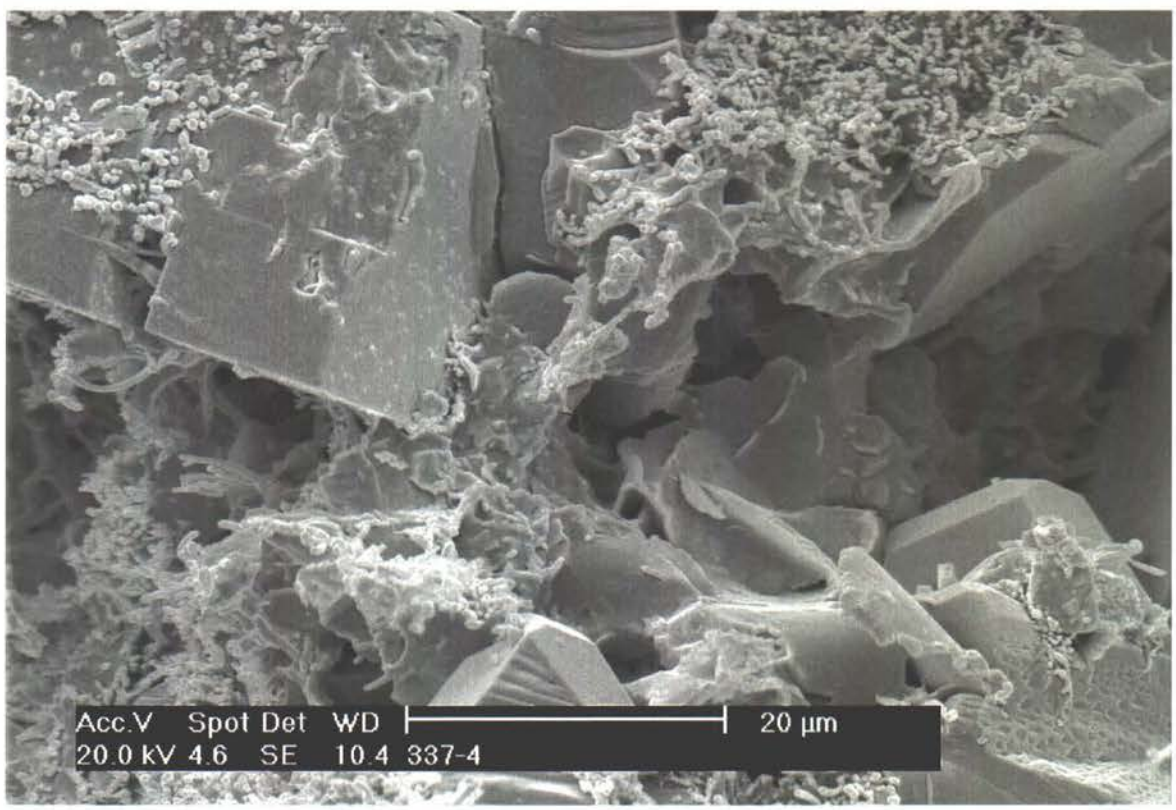

Plate 75. View into pore space where illite occur as flaky illitized smectitic detrital clay and as delicate spheres and worm-like crystals. Note that the illite is partly overgrown by quartz cement.

SEM photomicrographs

Well: GERT-2 **Depth: 4817.67m**

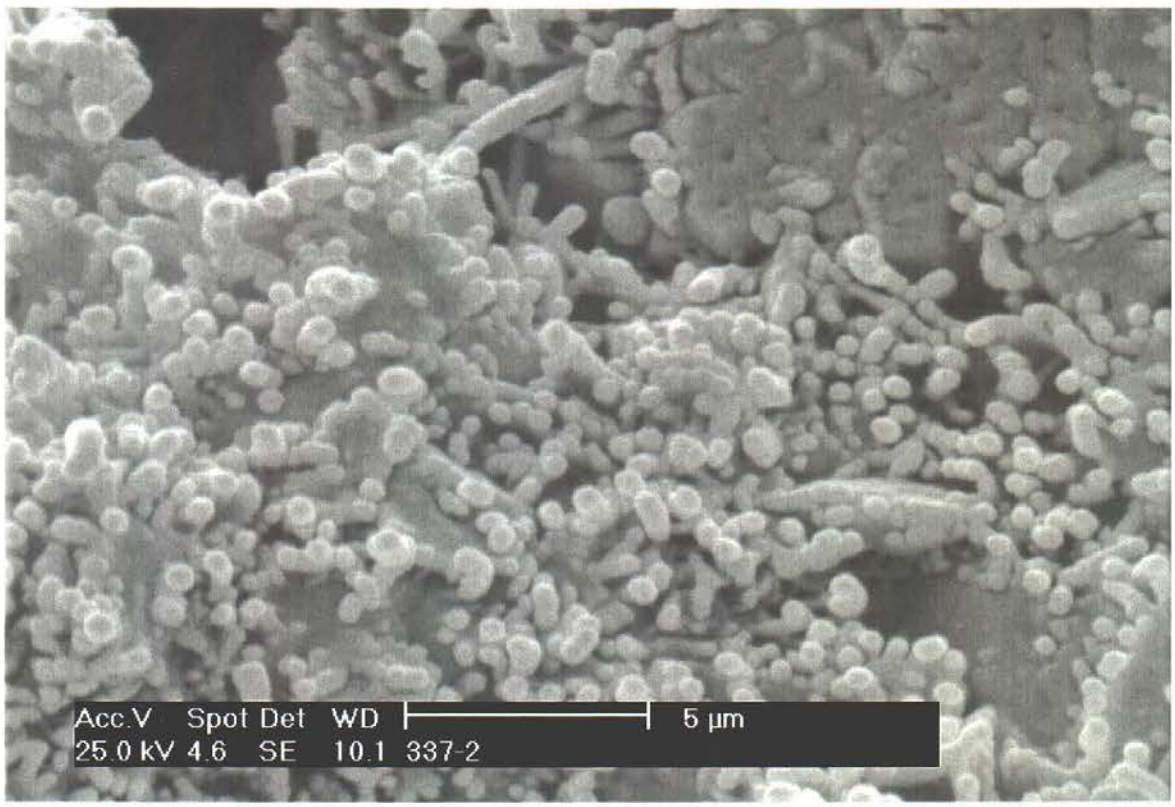

Plate 76. Close up of illite occurring as delicate spheres and worm-like crystals.

SEM photomicrographs

Well: DIAMANT-1 Depth: 3829.30m

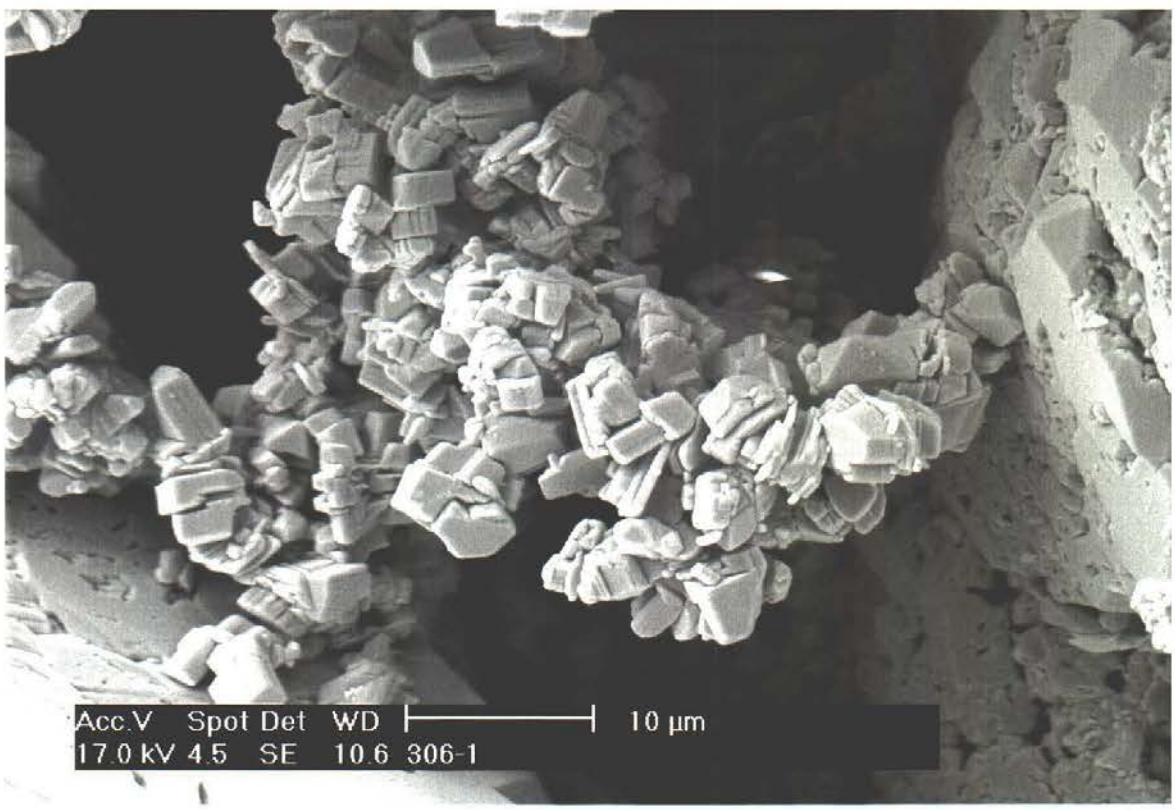

Plate 77. Blocky morphology (dickite) is less common but occurs as thick plates in vermiforms or booklets between the kaolinite plates. The clusters of small booklets are often gathered in secondary pores resulting from dissolved feldspar. Note minor quartz cement on detrital grains.

SEM photomicrographs

Well: DIAMANT-1 Depth: 3833.18m

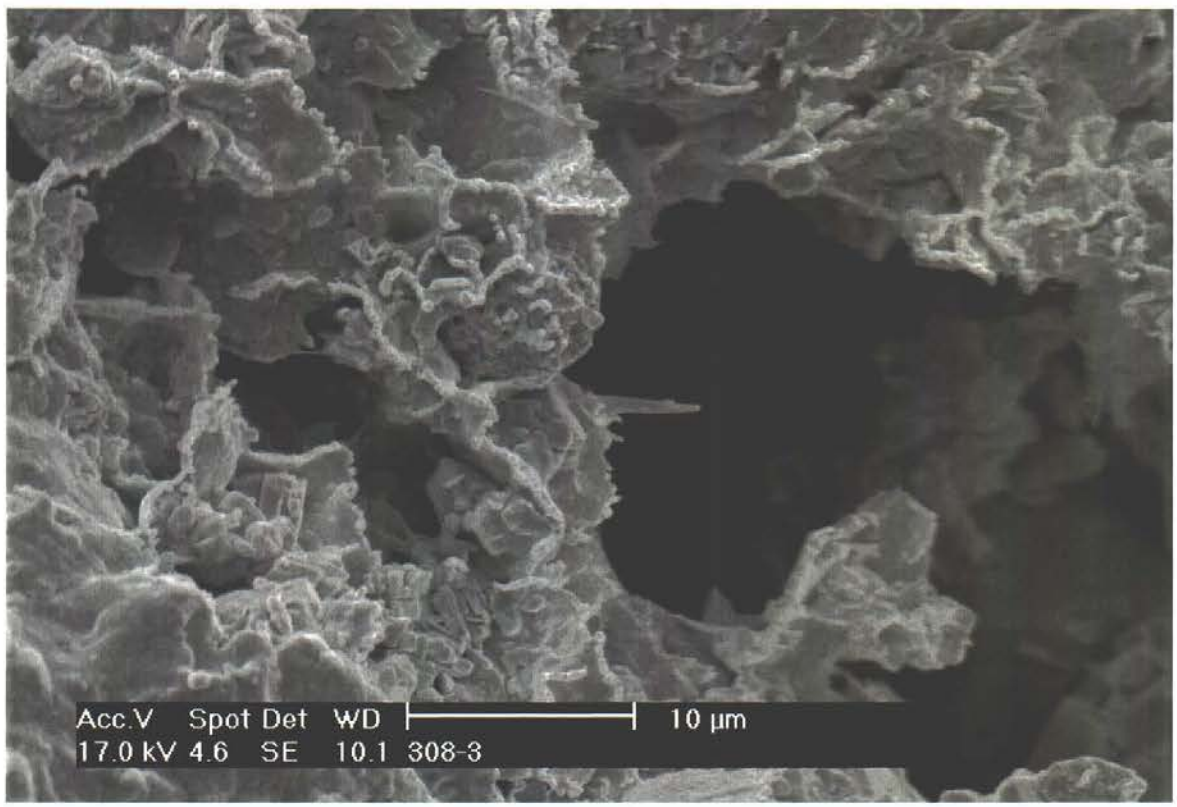

Plate 78. Illite occur as illitized smectite, shown by the typical honeycomb structure, which occur on the grain surfaces. Few delicate neoformed laths of illite has delveloped in association with the illitized smectite (centre of photo).

SEM photomicrographs

Well: RAVN-1 **Depth: 4137.16m**

Plate 79. View into a pore space, where Illite occur primarily as flaky illitized smectitic detrital clay and as neoformed delicate worm-like crystals, which coats pore walls.

SEM photomicrographs

Well: RAVN-1 **Depth: 4137.16m**

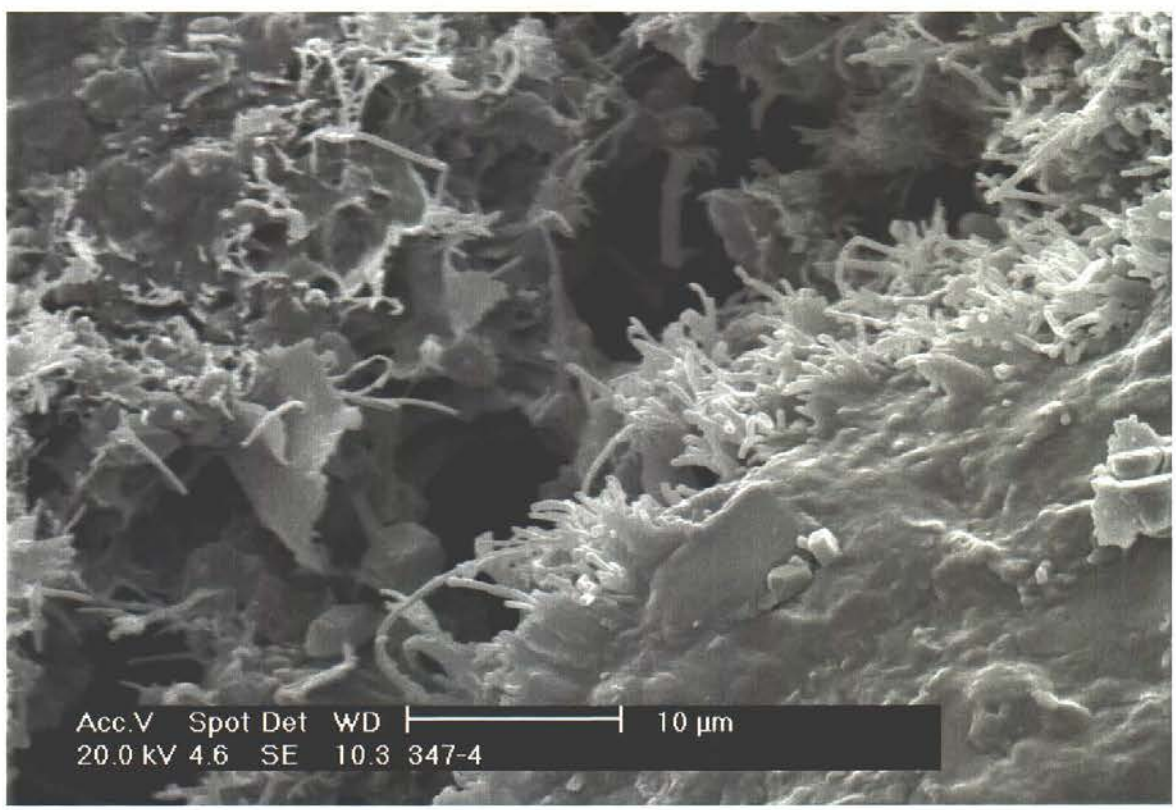

Plate 80. Close up of Illite as neoformed delicate worm-like crystals, which coats pore walls. Few illite flakes are present. The presence of these illite crystals greatly reduce permeability.

top Heno Fm.

JEPPE-1

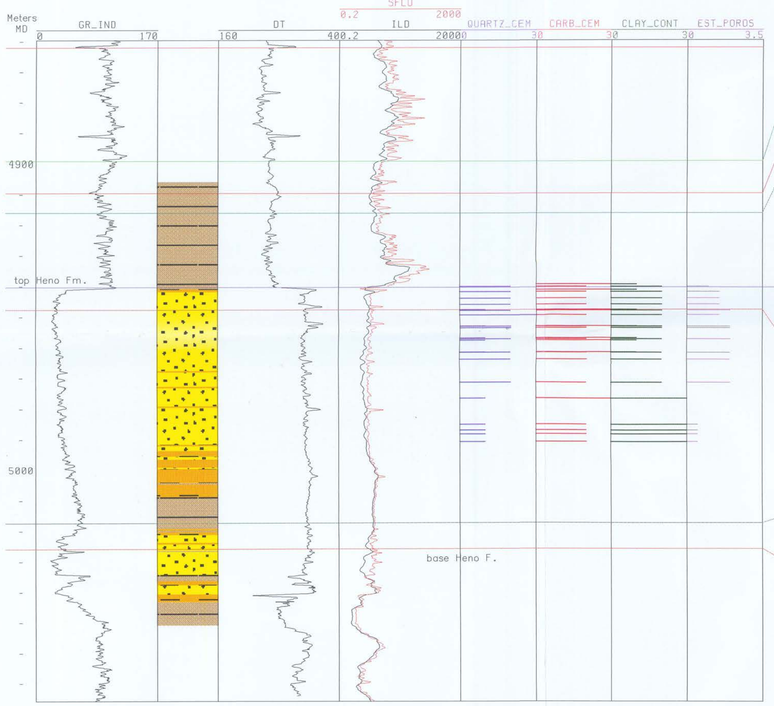

GERT-2

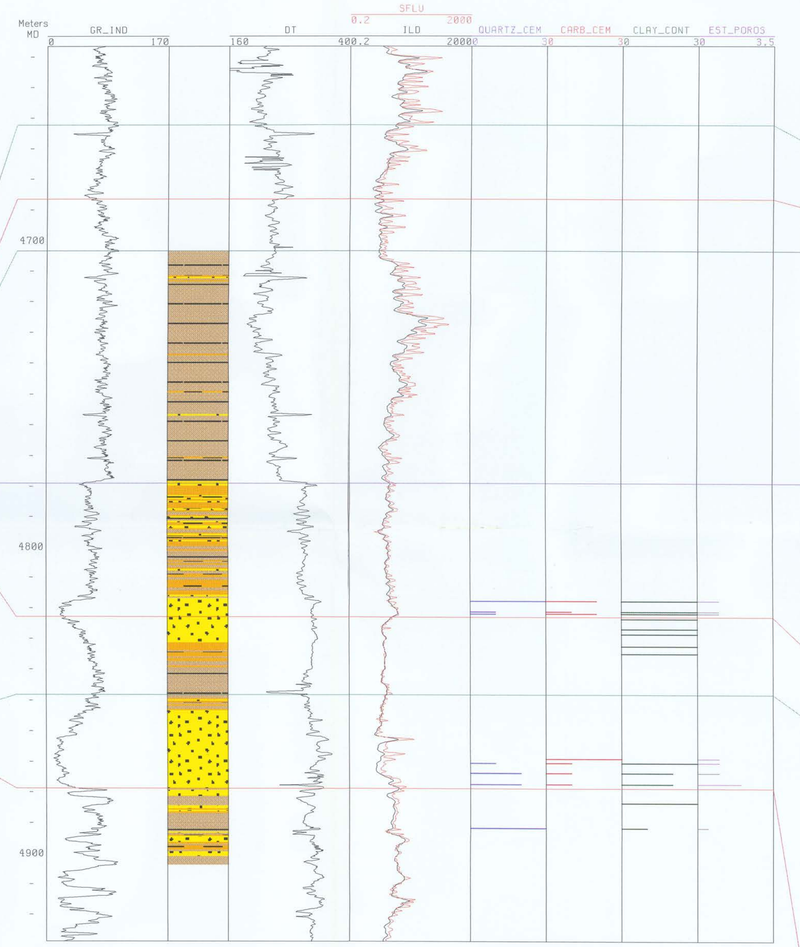

GERT-1

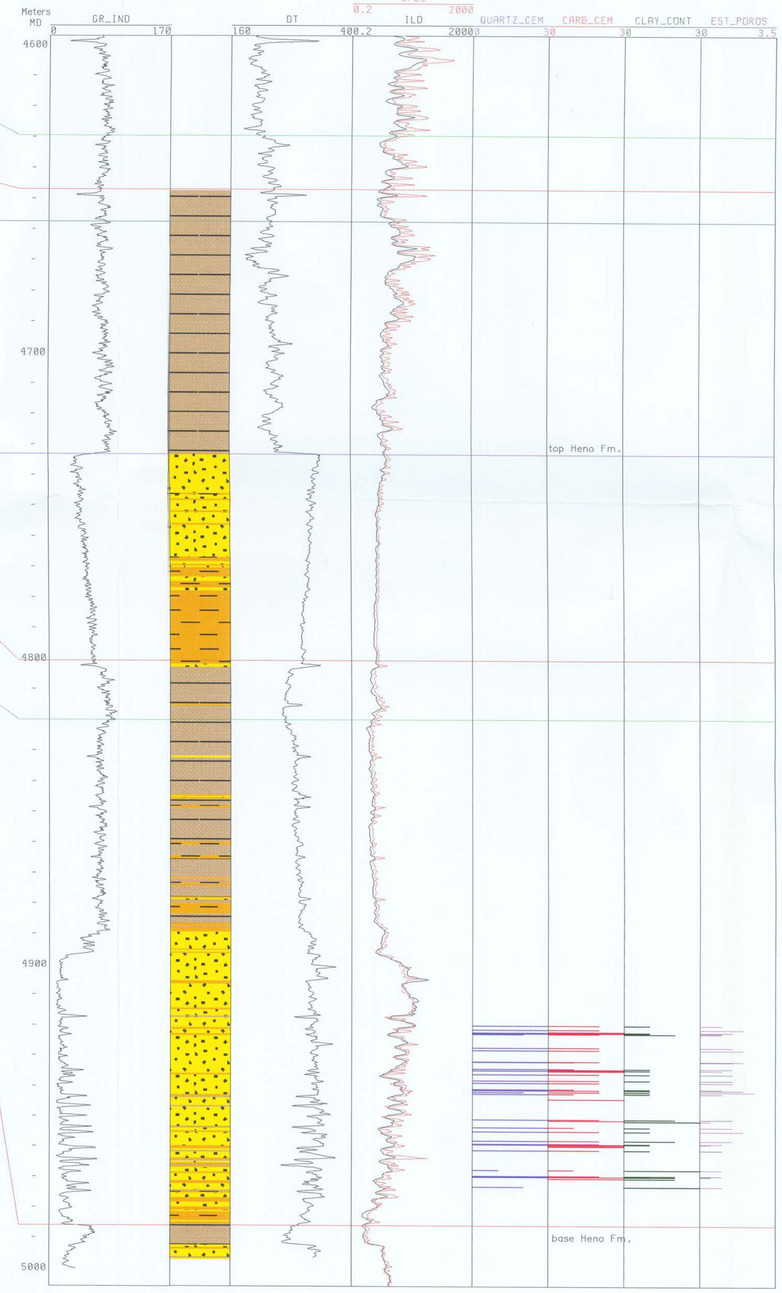

GEUS		
GEOKEMI		
Danish Central Graben		
Vertical Scale: 1:1000	Horizontal Scale: 1:3940	VE = 3.94
Depth Units: METERS	Distance Units: METERS	
Interpreter: JTH,J	Date: 03.01.2002	
ENCLOSURE 1		
Log panel: Jeppe-1, Gert-2, Gert-1		

DIAMANT-1

GWEN-2

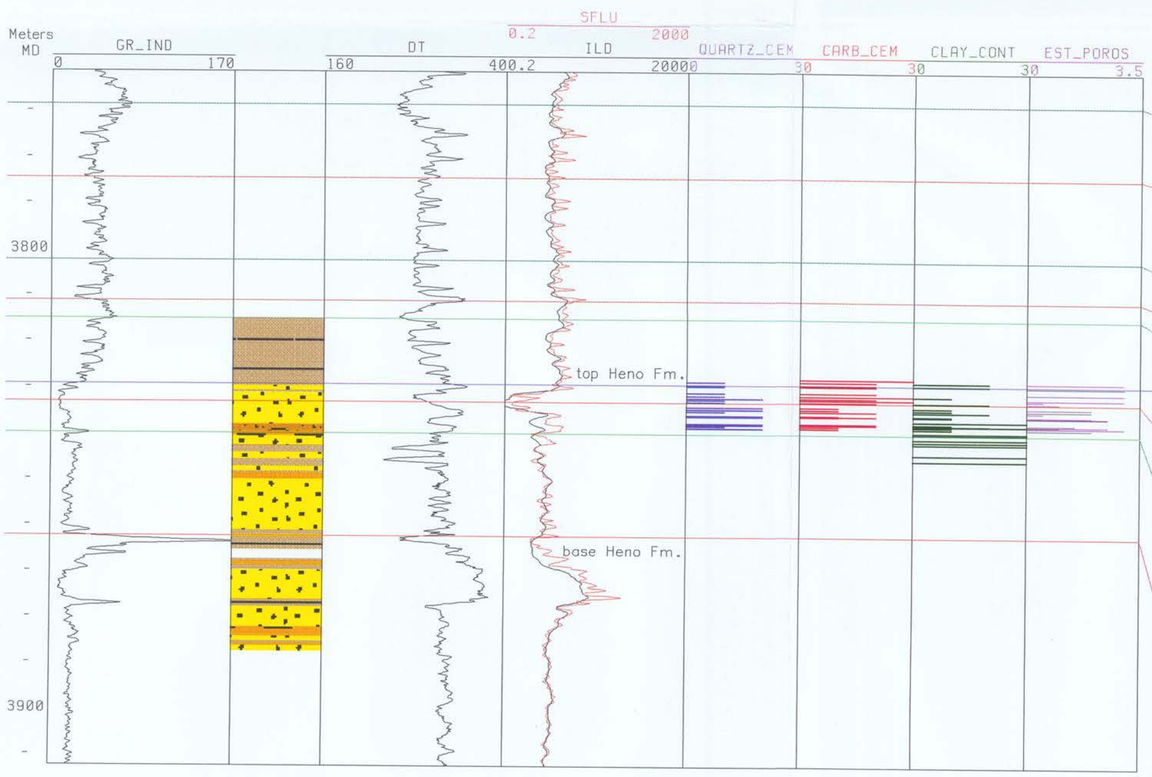

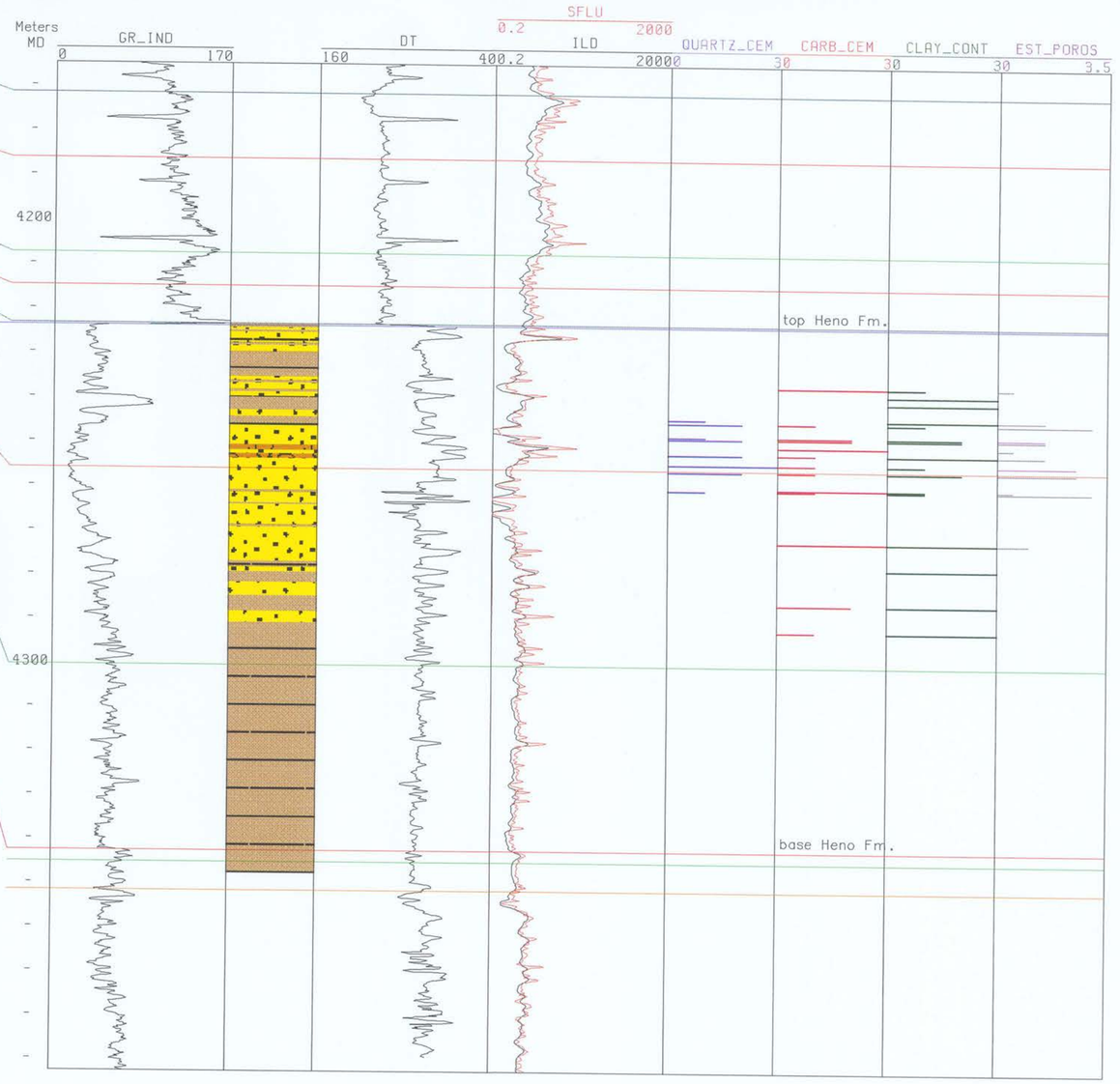

GEUS		
GEOKEMI		
Danish Central Graben		
Vertical Scale: 1:1000	Horizontal Scale: 1:3940	VE = 3.94
Depth Units: METERS	Distance Units: METERS	
Interpreter: JTH,J	Date: 03.01.2002	
ENCLOSURE 2		
Log panel: Diamant-1, Gwen-2		

RAVN-2

RAVN-1

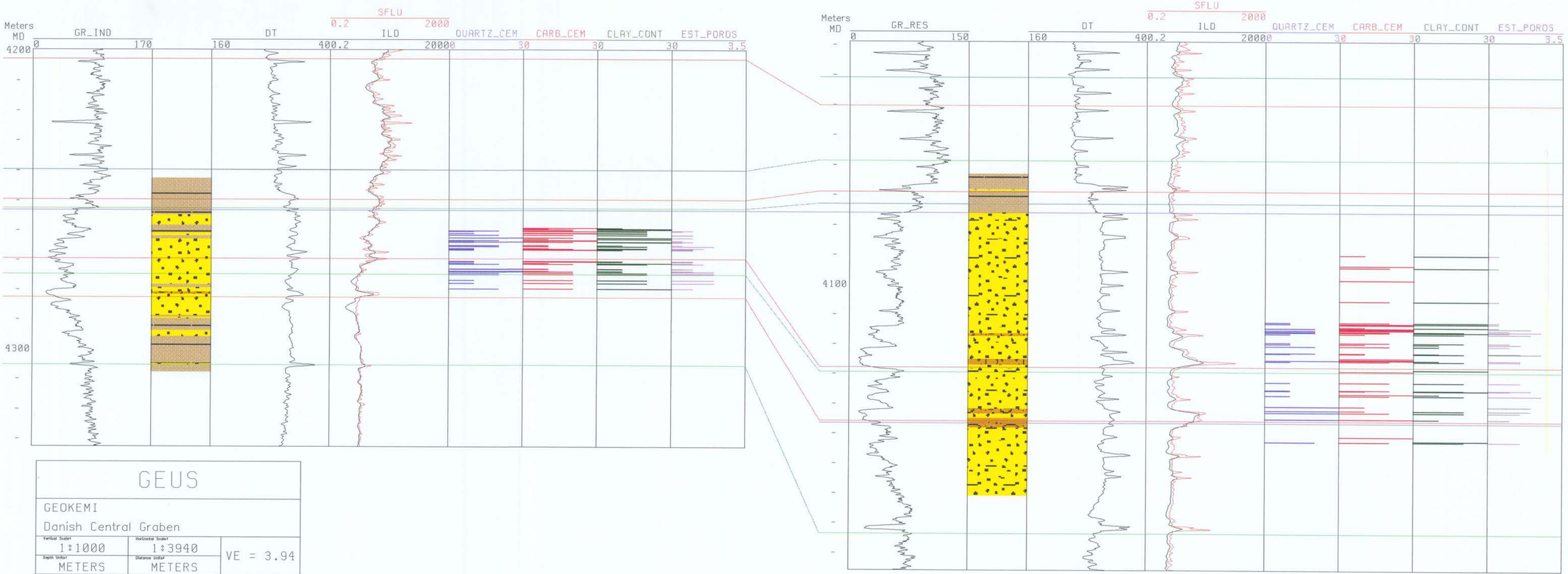

GEUS

GEOKEMI

Danish Central Graben

Vertical Scale:	Horizontal Scale:	
1:1000	1:3940	VE = 3.94
Depth Units:	Distance Units:	
METERS	METERS	
Interpreter:	Date:	
JTH,J	03.01.2002	

ENCLOSURE 3

Log panel: Ravn-2, Ravn-1